BONE HISTOLOGY AND GROWTH OF CHASMOSAURINE CERATOPSID DINOSAURS FROM THE LATE CAMPANIAN KAIPAROWITS FORMATION, SOUTHERN UTAH

by

Carolyn Gale Levitt

A thesis submitted to the faculty of
The University of Utah
in partial fulfillment of the requirements for the degree of

Master of Science

in

Geology

Department of Geology and Geophysics

The University of Utah

May 2013

The University of Utah Graduate School

STATEMENT OF THESIS APPROVAL

The following faculty members served as the supervisory committee chair and members for the thesis of **Carolyn Gale Levitt**.

Dates at right indicate the members' approval of the thesis.

Randall B. Irmis, Chair	**March 8, 2013** Date Approved
Allan A. Ekdale, Member	**March 7, 2013** Date Approved
Scott D. Sampson, Member	**March 11, 2013** Date Approved

The thesis has also been approved by **D. Kip Solomon**, Chair of the Department of **Geology and Geophysics**

and by Donna M. White, Interim Dean of The Graduate School.

ABSTRACT

Ceratopsian dinosaurs are one of the most diverse dinosaur groups in the Cretaceous, and an outstanding question is how growth strategies of this group evolved in relation to their shift from small bipedal basal ceratopsians to larger quadrupedal ceratopsids. Previous bone histology studies have investigated several basal ceratopsians and centrosaurine ceratopsids (e.g., *Centrosaurus*, *Pachyrhinosaurus*, *Einiosaurus*), but no chasmosaurine ceratopsids have been investigated. I conducted histological analysis of humeri, ulnae, femora, tibiae, ribs, and ossified tendons from multiple specimens of two species of chasmosaurine ceratopsid dinosaurs from the late Campanian (Upper Cretaceous) Kaiparowits Formation of southern Utah, *Kosmoceratops richardsoni* and *Utahceratops gettyi*, to examine bone microstructure indicators of growth rate and maturity. I also reexamined the long-bone histology of the ceratopsian dinosaurs *Psittacosaurus mongoliensis*, *Protoceratops andrewsi*, and *Centrosaurus apertus*. All elements of *Utahceratops* and *Kosmoceratops* examined are dominated by densely vascularized tissue, indicative of sustained fast growth. Radially-oriented vascular canals as well as dense osteocytes from throughout ontogeny are further indicators of rapid growth. I identified juvenile (UMNH VP 20444 & UMNH VP 20454), subadult (UMNH VP 16681) and adult (UMNH VP 16860, UMNH VP 16861, UMNH VP 12198) specimens of *Utahceratops*, and two subadult to adult specimens (UMNH VP 17000 & UMNH VP 21339) of *Kosmoceratops*.

I conclude that basal ceratopsians grew more slowly than the large quadrupedal ceratopsids, as evidenced by a generally higher number of definitive growth lines prevalent throughout development. In contrast, the presence of dense osteocytes, and reticular and radially-oriented vascular canals are rapid growth indicators shared by all sampled large ceratopsids, and imply an elevated metabolism for all ceratopsians. Sampled specimens of *Utahceratops* and *Kosmoceratops* do not preserve any evidence of annual lines of arrested growth (LAGs). Placed in context with the number of LAGs observed in Alaskan *Pachyrhinosaurus*, *Centrosaurus* from Alberta, and *Einosaurus* from Montana, these data suggest a latitudinal gradient in the number of LAGs, which suggests that bone growth is reacting to the climate.

TABLE OF CONTENTS

LIST OF TABLES

LIST OF FIGURES

ACKNOWLEDGEMENTS

I would like to first and foremost thank my adviser Dr. Randy Irmis for helping me in developing this idea for my research project and for all of his helpful advice. I would like to thank my committee members Dr. Allan A. Ekdale and Dr. Scott Sampson for all of their advice and encouragement. I would like to thank Mike Getty, Dr. Mark Loewen, Eric Lund, Deanna Brandau, Alan Titus, Brian Switek, and Megan Crocker for all of their helpful discourse throughout this project. I would also like to thank Lab Technicians Quintin Sahratian from the Department of Geology and Geophysics at the University of Utah, Ellen-Thérèse Lamm and Carrie Ancell from the Museum of the Rockies in Bozeman, Montana for teaching me how to mold, cast, cut, and create thin sections of dinosaur bones. Also I would like to thank Lab Preparators Ed Lamb, Sharon Walkington, Fred Lacy, Ann Johnson, and Randy Johnson for cleaning and repairing the dinosaur bones for me to section. I could not have done this masters research project without the help of these wonderful volunteers who are invaluable to the Natural History Museum of Utah and to the scientists who do research on the dinosaurs bones housed within the museum. I would also like to thank Brian Baziak, Sarah Werning, Dawn Renée Farkes Prasad, Sally Potter and Marjorie Chan for all of their technical support with my large images. I would like to thank the following institutions for funding this project: Grand Staircase Escalante Partners, Association of Women Geoscientists, The Geological Society of America, and The Paleontological Society.

I would like to thank my wonderful parents Gloria Evans Levitt and Bart Levitt for all of their love, support and encouragement throughout this project and throughout my whole life. I would like to thank Tim Bussian for his love, support, technical support with Excel and for letting me borrow his Dremel. I would also like to thank Karin Bussian for lending me her external hard drive for this project. She will always be remembered as a sister and a friend.

INTRODUCTION

Ceratopsids, or horned dinosaurs, are large-bodied, quadrupedal, herbivorous ornithischian dinosaurs (Dodson et al., 2004) that belong to the larger clade Ceratopsia, which is diagnosed by characteristics such as parrot-like beaks, dental batteries with shearing dentitions, hypertrophied narial regions, and ornamented parietosquamosal frills (Dodson et al., 2004; Sampson et al., 2010a). Ceratopsians include both small, basal forms like *Psittacosaurus*, and the larger quadrupedal ceratopsids exemplified by *Centrosaurus* and *Triceratops* (Ryan and Russel, 2001; You and Dodson, 2004; Dodson et al., 2004). Ceratopsidae is divided into two clades, the Centrosaurinae and the Chasmosaurinae. Chasmosaurines characteristically have parietosquamosal frills that are typically simply adorned and elongated (Lambe, 1915), whereas centrosaurines generally possess relatively shorter, highly adorned frills (Lambe, 1915; Dodson, 1993; Ryan and Russel, 2001). These clades radiated in a very short amount of time (<5 million years), and were extremely speciose in western North America during the latest Cretaceous (Sampson et al., 2010b). Furthermore, new evidence suggests they were largely endemic, with distinct forms living in each sedimentary basin of western North America (Sampson et al., 2010a).

Ceratopsian dinosaurs were successful herbivores during the Late Cretaceous. In Campanian-Maastrichtian western North American terrestrial ecosystems, ceratopsids remains typically rank second to hadrosaurids in absolute abundance (Lehman, 1997;

Brinkman et al., 1998; White et al., 1998). They played an important role in Late Cretaceous ecosystems as specialized primary consumers possessing dental batteries developed for shearing the plants that they ate (Farlow, 1987).

The evolutionary history of ceratopsians includes several major morphological changes, and an outstanding question is how growth strategies of this group evolved in relation to their shift from small bipedal basal forms to the larger quadrupedal horned ceratopsids, a body size increase of several orders of magnitude (Carrano, 2006). Therefore, comparison of the growth rates and age of maturity among chasmosaurines, centrosaurines, and basal ceratopsids can elucidate how growth strategy changed in concert with locomotion and body size. This question relates more generally to how large animals get so large and the different ways in which they accomplish this, and ceratopsian dinosaurs are an excellent case study.

Growth data can also provide a context for ontogenetic studies demonstrating that horn and frill characters were not fully expressed until individuals approached adult size (Sampson, 1997; Horner and Goodwin, 2008), and inform debates about whether certain species are distinct or different ontogenetic stages of the same taxon (e.g., Scannella and Horner, 2010, 2011; Farke, 2011; Longrich and Field, 2012). Finally, ceratopsids could be ideal for understanding how growth varied across latitude, because Campanian North American taxa range from Alaska to Mexico (e.g., Loewen et al., 2010; Erickson and Drunkenmiller, 2011; Fiorillo and Tykoski, 2012).

Metabolic estimates for large chasmosaurine ceratopsid dinosaurs are not well constrained. A major question has been whether the thermophysiology of dinosaurs was more similar to extant birds and mammals or non-avian reptiles (Lee and Werning,

2008). It is also possible that they developed a thermal physiology that was uniquely their own, operating between 'typical' reptilian and mammalian metabolic rates (de Ricqlés, 1980). Emerging evidence suggests that many dinosaurs had metabolic strategies similar to modern birds and mammals (Horner et al., 2000; Erickson and Tumanova, 2000; Erickson et al., 2001; Padian et al., 2001, 2004; Horner and Padian, 2004; Klein and Sander, 2007; Lee and Werning, 2008; Erickson et al., 2009) therefore, did ceratopsian dinosaurs grow similarly or differently to these other dinosaurs? Specifically, the evolution of increased metabolic rates in dinosaurs is believed to have facilitated the evolution of gigantism by enabling them to build their skeletons swiftly (de Ricqlés, 1980; Chinsamy 1993; Sander 2000); was this also the case for ceratopsian dinosaurs?

Bone Histology

The microstructure of bone can provide answers to the questions of how extinct animals grew, how old they were when they reached sexual maturity, and what the average age was when they died. Numerous studies have been conducted using histology of dinosaur bone and they reveal that the limb bones preserve an excellent record of the life history of the animal being studied (Erickson and Tumanova, 2000; Horner et al., 2000; Padian et al., 2001; Horner et al., 2004; Erickson, 2005; Chinsamy-Turan, 2005; Makovicky et al., 2007; Klein and Sander, 2007; Erickson et al., 2009; Erickson and Druckenmiller, 2011).

Bone histological analysis is the best available method to answer questions regarding ceratopsian growth and physiology, because we cannot observe these taxa in life. The size of the skeleton can provide insight as to the age of the animal, but size does

not always vary with age, so size-independent criteria such as bone histology are better for assessing ontogenetic stages (Johnson, 1977).

Bone deposits lines of arrested growth (or LAGs) that reflect periodicities in growth created by environmental modifications of endogenous rhythms (Francillon-Vieillot et al., 1990; de Ricqlès et al., 1991; Castanet et al., 1993; Castanet et al., 2004). Research on extant animals demonstrates the existence of annual growth lines, which can be used with confidence to determine the ages of the animals, in a number of living species (Castanet et al., 1977; Castanet, 1978; Pascal and Castanet, 1978). LAGs in fossil animals, therefore, are also inferred to be annual (Peabody, 1961). Furthermore, the bone thickness between adjacent LAGs can inform us about these animals' bone growth rate, which allows for direct comparison to growth rates of extant vertebrates (Erickson et al., 2001; Padian et al., 2001; Lee and Werning, 2008).

Unlike growth rings in trees, sampled bones do not always preserve all of the LAGs originally laid down, because they "remodel" themselves through resorption, so the early life history of the animal is often lost. These processes are presumed to be involved in the turnover of calcium and phosphorus in metabolism (Amprino 1967), where remodeling plays a direct and fundamental part in the growth of long bones (de Ricqlés, 1980). The result is that some areas along the length of a bone contain a mosaic of microstructures that have different ontogenetic histories (Enlow, 1963). This remodeling means that a single limb bone lacks a complete life history record (Horner et al., 1999), but successive partial records of limb bones in an ontogenetic series are sufficient to reconstruct the history of bone growth (Chinsamy, 1990, 1993; Curry, 1999; Erickson and Tumanova, 2000; Horner et al., 2000; Sander, 2000; Erickson et al., 2009;

Horner and Padian, 2004; Bybee et al., 2006; Klein and Sander, 2007; Lee, 2007a,b,c; Makovicky et al., 2007; Reizner, 2010; Erickson and Druckenmiller, 2001).

LAGs are not the only osteohistological data available for inferring growth trajectory. Vascular canal orientation and density within the bone cortex also relate to how rapidly animals grow. If the vascularity is dense, it indicates that numerous blood vessels were running through the bone and that the bone tissue was developing rapidly (de Margerie et al., 2002, 2004). Longitudinal canals are usually the most abundant vascular canals seen in a thin section and are circular in cross section (de Margerie et al., 2002). If vascular canals are oriented radially, it is indicative of fast relative growth (de Margerie et al., 2002, 2004). If vascular canals are oriented circumferentially, it is indicative of relative slow growth (de Margerie et al., 2004). The density of osteocyte lacunae (spaces for bone cells) is also useful data, because higher densities of osteocytes indicate faster growth (de Margerie et al., 2002)

Previous Studies

Limb bone histology and inferred growth curves have previously been investigated for smaller, bipedal ceratopsians *Psittacosaurus mongoliensis* (Erickson and Tumanova, 2000) and *Psittacosaurus lujiatunensis* (Erickson et al., 2009), small quadrupedal basal ceratopsians *Protoceratops andrewsi* (Lee, 2007; Makovicky et al., 2007), and the large quadrupedal centrosaurines *Centrosaurus apertus* (Lee, 2007a,b,c), *Pachyrhinosaurus perotorum* (Erickson and Druckenmiller, 2011, Fiorillo and Tykoski, 2012), and *Einosaurus procurvicornis* (Reizner, 2010), but chasmosaurine ceratopsid dinosaurs have yet to be investigated. Small, basal forms (e.g., *Psittacosaurus*

mongoliensis, *Psittacosaurus lujiatunensis*, and *Protoceratops andrewsi*) show moderate rates of growth with a high number of LAGs (Erickson and Tumanova, 2000; Makovicky et al., 2007; Erickson et al., 2009). In contrast, large, quadrupedal centrosaurines (e.g., *Centrosaurus apertus*, *Pachyrhinosaurus perotorum*, and *Einosaurus procurvicornis*) show rapid growth with a small to moderate number of LAGs.

Goals of Present Study

I used osteohistological analysis of the chasmosaurines *Utahceratops gettyi* and *Kosmoceratops richardsoni* to provide insight into how these chasmosaurine ceratopsian dinosaurs grew and how this might relate to their thermal physiology. Placed in context with other previously sampled taxa, these data help evaluate how growth changed during the evolution of ceratopsians, and how these animals grew in comparison with other dinosaurs of similar size. This study analyzes for the first time the limb bone histology of chasmosaurine dinosaurs *Utahceratops* and *Kosmoceratops*, and reevaluate and compare the limb bone histology of *Psittacosaurus mongoliensis*, *Protoceratops andrewsi* and *Centrosaurus apertus* to the Utah forms to gain insight on the physiology, evolution and behavior of these animals. *Utahceratops* and *Kosmoceratops* are ideal for histological analysis because they are ceratopsids from the southern latitudes that provide good comparisons to their northern counterparts in Montana, Canada and Alaska, and are a test of the growth trajectories of co-occurring taxa in a single basin (cf., Fowler, 2011). Furthermore, known specimens of *Utahceratops* range from juvenile to adult, allowing me to reconstruct a nearly complete post-natal ontogenetic record of the species.

GEOLOGIC SETTINGS

Laramidia

For approximately 27 million years of the Late Cretaceous (95–68 Ma), regional tectonics produced the Cretaceous Western Interior Seaway (KWIS), a shallow epeiric sea that flooded the central portion of North America, dividing the continent into eastern and western landmasses known as Appalachia and Laramidia, respectively (Kauffman, 1984; Roberts and Kirschbaum, 1995). The western landmass, Laramidia, was less than 20% the size of present-day North America at its maximum extent (Lehman 1997; Sampson et al., 2010a). Laramidia was occupied by a diverse assemblage of dinosaurs and other nonmarine vertebrate taxa (Gates et al., 2010; Sampson et al., 2010a,b). Among dinosaurs, the same major clades are present in the northern and southern part of Laramidia (e.g., hadrosaurids, ceratopsids, ankylosaurids, tyrannosaurids, ornithomimids), but the assemblages appeared largely distinct at the genus and species levels (Lehman, 1997, 2001; Gates et al., 2010; Sampson et al., 2010a,b). Some of the best information about southern Laramidian dinosaurs has emerged in the past 10 years from late Campanian sediments of southern Utah, including two new chasmosaurine ceratopsid dinosaurs, *Utahceratops* and *Kosmoceratops* (Eaton, 1999; Zanno and Sampson, 2005; Gates and Sampson, 2007; Sampson et al., 2010a,b,c; Gates et al., 2010; Getty et al., 2010).

All specimens of *Utahceratops* and *Kosmoceratops* in this study were discovered in Grand Staircase-Escalante National Monument in southern Utah. Grand Staircase-Escalante National Monument (GSENM) (Fig. 1) encompasses 1.9 million acres of rugged terrain in southern Utah, and was the last major region within the contiguous United States to be mapped topographically (Foster et al., 2001). Formally designated in 1996, the Monument was established in large part to facilitate preservation and study of its diverse natural resources, both living and fossil (Designated by Presidential Proclamation on September 18, 1996, pursuant to the Antiquities Act of 1906). The most fossiliferous terrestrial geologic unit in GSENM is the Upper Cretaceous Kaiparowits Formation, deposited along the eastern margin of Laramidia within 100 km of the seaway (Roberts & Kirschbaum, 1995) in the Kaiparowits Basin, and now exposed on the Kaiparowits Plateau (Eaton, 1991).

The Kaiparowits Formation (Fig. 2) is an unusually thick, ~860 m, package of Upper Cretaceous (late Campanian) strata exposed in Grand Staircase-Escalante National Monument of southern Utah, USA (Roberts, 2007). It is easily recognized by its distinctive, badland-forming blue-gray sandstones and mudstones, which are in stark contrast to the typical tan sandstones of the underlying early Campanian Wahweap and late Turonian-Santonian Straight Cliffs formations, and the overlying maroon conglomerates of the Maastrichtian Canaan Peak Formation (Roberts et al., 2005). This formation is part of a prograding clastic wedge that deposited vast quantities of sediment derived from sources in the Sevier orogenic belt, thrust sheets in southeastern Nevada and southern California, and the Mogollon slope in southwestern Arizona into the syn-evolving Sevier foreland basin (Goldstrand, 1992; Lawton et al., 2003; Roberts, 2007).

Kaiparowits strata represent a muddy-to-sand meandering fluvial system with paleoflow to the east and northeast in a relatively warm, humid paleoclimate (Eaton 1991; Goldstrand 1990, 1991, 1992; Little, 1995; Roberts et al., 2003, 2005, Roberts, 2007). The compositions of the sandstone indicate felsic volcanic, siliciclastic, metamorphic, and plutonic sources (Goldstrand, 1992). Radioisotopic dating of four bentonite horizons (Roberts et al., 2005) produced a late Campanian age of 76.6 – 74.5 Ma for the Kaiparowits Formation (Roberts et al., *in press*). The Kaiparowits Formation has among the highest sediment accumulation rates recorded in the Western Interior Basin (WIB) at 41 cm/ka (Roberts et al., 2005). Using the accumulation rate of 41 cm/ka calculated using these radioisotopic dates, the ca. 860-m-thick Kaiparowits Formation accumulated for ca. 2.1 Ma, from ca. 76.6 – 74.5 Ma (Roberts et al., *in press*).

The Kaiparowits Formation is informally subdivided into three units (lower, middle, upper), based on distinct changes in alluvial architecture (Roberts et al., 2005). Nearly all of the fossils found in this area are found in the lower half of the formation with the age range of ~76.46 +/_014 Ma and ~75.51+/_015 Ma (Roberts et al., 2005; Roberts et al., in press). Many of the most fossiliferous vertebrate-bearing Campanian formations in the WIB are penecontemporaneous with the Kaiparowits Formation (Roberts et al., 2005). Specifically, the Kaiparowits Formation is partially coeval Dinosaur Park Formation, portions of the Judith River, the Two Medicine, Fruitland, and possibly Aguja formations (Goodwin and Deino, 1989; Eberth and Hamblin, 1993; Rogers et al., 1993; Fassett and Steiner, 1997; Rogers, 1994; Roberts et al., 2005; Jinnah et al. 2009).

Localities for specimens in this study

UMNH VP locality 942

This site preserves partial remains of at least three individuals of *Utahceratops*, recognized by distinct size classes of recovered elements (Getty et al., 2010). The specimens were buried in a lag deposit at the base of a sandy channel, in a thin, coarse, pebbly conglomerate. The pebble conglomerate indicates that this material may be reworked from a previous, possibly larger depositional event (Getty et al., 2010). The skeletons were completely disarticulated and demonstrate characteristics consistent with considerable pre-depositional transport, including winnowing of most small elements and breakage and surface abrasion of preserved elements (Getty et al., 2010).

UMNH VP locality 145

This locality preserves the skeletal remains of an individual disarticulated ceratopsian skeleton, the holotype of *Utahceratops* (UMNH VP 12198) (Sampson et al., 2010a). 280 individual elements and associated fragments were discovered spread over an area of approximately 29 square meters (Getty et al., 2010). The majority of missing bones were smaller-sized appendicular and axial elements such as distal phalanges, vertebrae, and chevrons, indicating that these parts of the body were scavenged or hydraulically removed (winnowing) prior to final deposition (Getty et al., 2010). The specimen is preserved in a fine-grained floodplain environment. Very limited evidence of sub-aerial weathering was observed and was only present on axial elements, whereas the prevalence of bone decomposition on the majority of the skeleton is indicative of significant sub-aqueous exposure of the skeleton in a pond environment prior to burial

(Getty et al., 2010). The subaqueous burial interpretation is supported by the influx of fine grained pond sediments, where the grain size decreases from muddy sandstone basally to a muddy siltstone (encasing the bones) and a capping silty claystone stratigraphically up-section (Getty et al., 2010).

UMNH VP locality 945

UMNH VP locality 945 preserves the remains of a nearly completely articulated subadult ceratopsian skeleton (UMNH VP 20444), a partial disarticulated ceratopsian skeleton (UMNH VP 20454), and a partially articulated alligatoroid crocodylian skeleton, about 1 m in length (Irmis et al., *in press*), which appears to have been deposited on top of the articulated ceratopsian carcass prior to burial (Getty et al., 2010). The ceratopsian skeletons are most likely assignable to *Utahceratops* based on available prepared cranial remains from the articulated specimen. UMNH VP 20444 represents the most complete articulated skeleton of any animal found to date in a fine-grained facies (siltstone and mudstone) from the Kaiparowits Fm (Getty et al., 2010). Generally, articulated specimens in the Kaiparowits Fm. are associated with rapid burial in channel sandstone facies (Getty et al., 2010), so this well-preserved specimen in mudstone is unusual.

UMNH VP locality 512

The ceratopsian skeleton at this site was disarticulated, but closely associated, and mostly predepositionally broken. UMNH VP 16865.1 is an unidentified ceratopsian perhaps being *Utahceratops*, but has to be identified with further investigations. "Water-rot" is present on the spongy parts of elements, suggesting a paludal environment. The

surrounding matrix contains degraded plant material, mostly carbonized bits of stems, and leaves. The matrix is gray-green, again supporting a water-logged environment, and is mostly homogenous siltstone and mudstone, with very little sand (only in thin lenses, not very laterally extensive) (E. Lund, personal communication). The sandy siltstone layers include iron concretions, small amounts of organic material and some gastropods (D. Brandau, personal communication).

UMNH VP locality 890

This partial skeleton, UMNH VP 17000, is the holotype of *Kosmoceratops*. The specimen consists of a relatively complete skull, a significant portion of the axial skeleton from neck to tail, including part of the pelvic girdle, and at least part of one limb (Getty et al., 2010; Sampson et al., 2010a). The rest of the limbs and distal tail may have been lost either to scavenging or to rotting of the carcass prior to its deposition (Getty et al., 2010). This specimen was found in a silty sandstone channel facies and appears to represent an individual animal carcass that had been washed into a river channel and buried quickly (Getty et al., 2010).

UMNH VP locality 1323

The ceratopsian material found at this site, UMNH VP 21339, is a single sub-adult to adult disarticulated individual of *Kosmoceratops*. Almost every element shows predepositional breakage. The matrix is stacked siltstones, and mudstones, with minor sandstones (E. Lund, personal communication). The matrix is suggestive of a pond

environment (E. Lund, personal communication). Several varieties of gastropods and bivalves are present, many of which still posses the original aragonite shells.

Figure 1. Map of Grand Staircase-Escalante National Monument. The Kaiparowits Formation is highlighted in green. The localities where the sampled specimens were found are indicated by the labeled black circles. Map modified from Roberts et al. (2005).

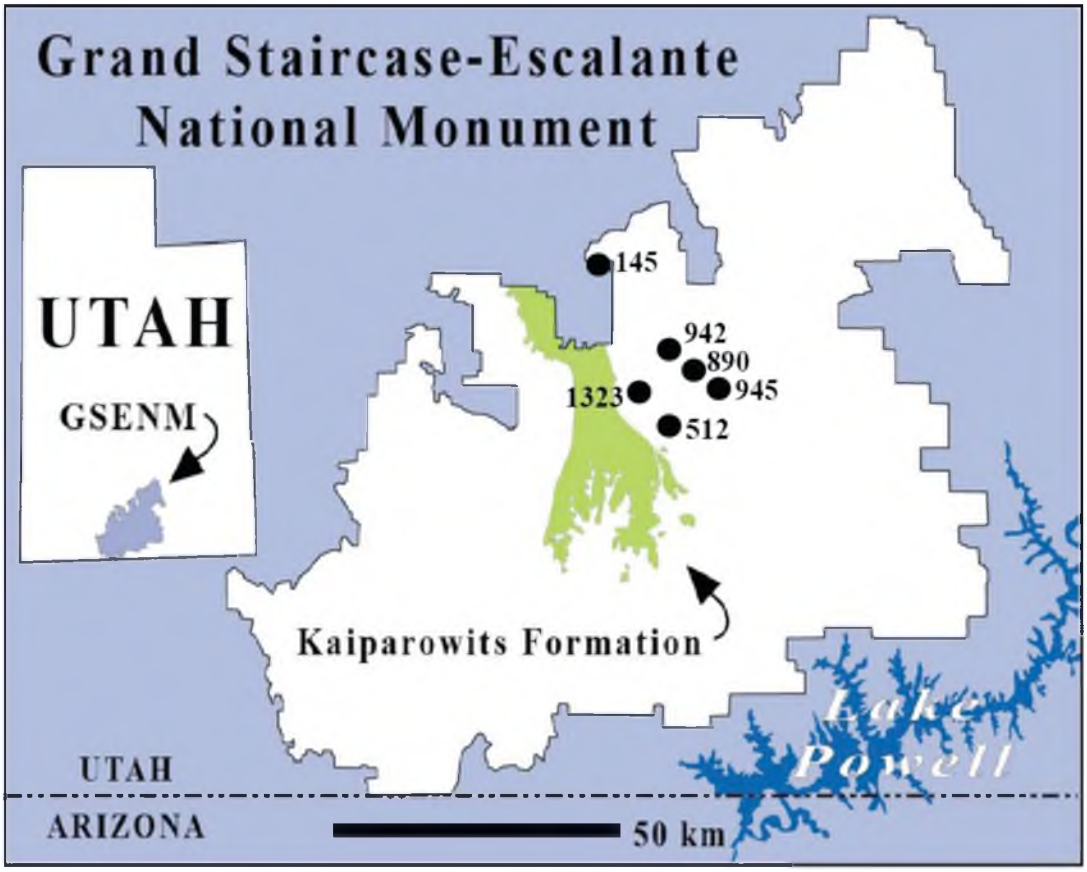
Grand Staircase-Escalante
National Monument
UTAH
GSENM
145
942
890
945
1323
512
Kaiparowits Formation
Lake
Powell
UTAH
ARIZONA
50 km

Figure 2. Stratigraphic column of the Kaiparowits Formation (Modified from Sampson et al., 2010) with sampled specimen localities indicated. The yellow circle indicates an *Utahceratops* specimen, which was not sampled but represents the extent of time in which *Utahceratops* lived. Indeterminant humerus UMNH VP 19490 is excluded from figure because of stratigraphic uncertainty.

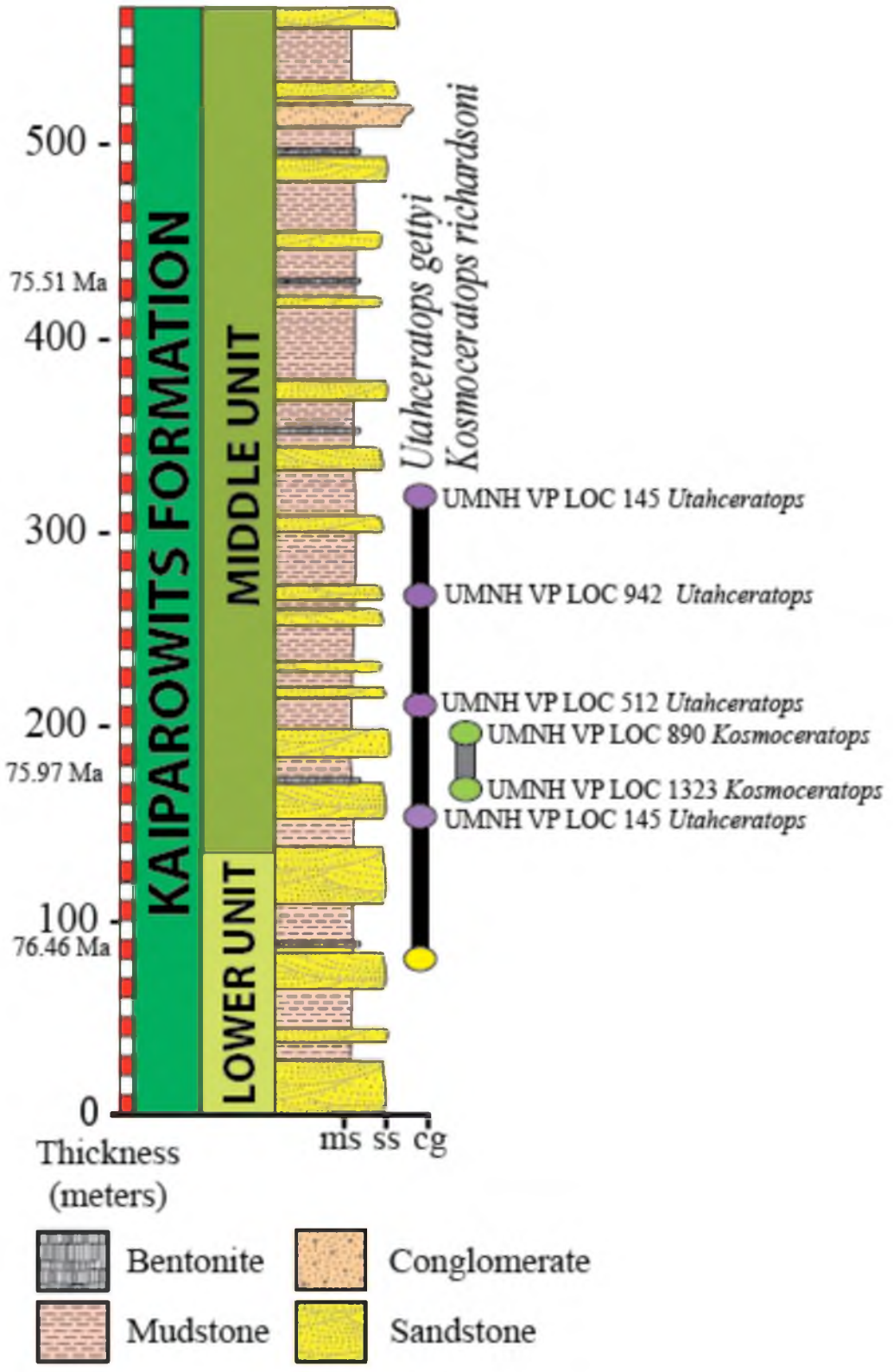
KAIPAROWITS FORMATION
MIDDLE UNIT
LOWER UNIT
500 -
75.51 Ma
400 -
300 -
200 -
75.97 Ma
100 -
76.46 Ma
0
Thickness
(meters)
ms ss cg
Utahceratops gettyi
Kosmoceratops richardsoni
UMNH VP LOC 145 Utahceratops
UMNH VP LOC 942 Utahceratops
UMNH VP LOC 512 Utahceratops
UMNH VP LOC 890 Kosmoceratops
UMNH VP LOC 1323 Kosmoceratops
UMNH VP LOC 145 Utahceratops
Bentonite
Conglomerate
Mudstone
Sandstone

MATERIALS AND METHODS

Specimens

I sampled four individuals from various stages of ontogeny from multiple bonebeds containing *Utahceratops gettyi*. *Utahceratops* is diagnosed as a chasmosaurine ceratopsid dinosaur by possessing the following autapomorphies: nasal horncore caudally positioned, almost entirely behind external naris; supraorbital horncores short, robust, dorsolaterally directed, and oblate in shape with blunt tip; episquamosals on mid portion of lateral frill margin low and extremely elongate and median portion of transverse bar of parietal rostrally curved. *Utahceratops* is further distinguished by mid-frill episquamosals with extremely elongate bases (some > 10 cm) (Sampson et al., 2010a).

The Bluewash Bonebed, UMNH VP LOC 942, preserves partial remains of at least three individuals of *Utahceratops*. For this study, I sectioned three elements, a right tibia (UMNH VP 16681), a right femur (UMNH VP 16860), and a partial shaft from an unidentified limb bone (UMNH VP 16861) from this locality (Fig. 3) (Table 1). Because this is a bonebed filled with disarticulated skeletons, distinguishing which bone came from which individual is difficult. UMNH VP LOC 145 preserves the skeletal remains of an individual disarticulated ceratopsian skeleton of a referred specimen of *Utahceratops* (UMNH VP 12198) (Sampson et al., 2010a).

For this study, I sectioned a left femur, a rib fragment and a tendon fragment. UMNH VP locality 945 preserves the remains of a nearly completely articulated subadult ceratopsid skeleton (UMNH VP 20444) and a partial disarticulated ceratopsid skeleton (UMNH VP 20454), both referable to *Utahceratops*. From the articulated individual, I sectioned a left humerus (UMNH VP 20444.1), a left ulna (UMNH VP 20444.2), a left femur (UMNH VP 20444.4), and a right tibia (UMNH VP 20444.5). From the disarticulated individual, I sectioned a left humerus (UMNH VP 20454.8), a left ulna (UMNH VP 20454.1), a left femur (UMNH VP 20454.5), a right tibia (UMNH VP 20454.3), a rib fragment (UMNH VP 20454.7) and a tendon fragment (UMNH VP 20454.9). Two additional humeri were sectioned from two additional localities. Specimen known as UMNH VP 16865.1 is a left humerus from a single disarticulated individual of an indeterminate ceratopsid, perhaps *Utahceratops*, from UMNH VP locality 512. Specimen UMNH VP 19490 represents an isolated left humerus of an indeterminate ceratopsid.

In addition to sampling *Utahceratops*, I sampled two femora from *Kosmoceratops*. *Kosmoceratops* is diagnosed as a chasmosaurine ceratopsid dinosaur by possessing the following autapomorphies: internal naris rostrocaudally abbreviated and caudodorsally inclined; nasal horncore transversely constricted, long-based, and blade-like, with flattened distal portion; supraorbital horncores dorsolaterally directed proximally, with a ventral curvature distally tapering to a point; parietosquamosal frill relatively short and broad (maximum width ~2 times maximum length), with small, caudally positioned parietal fenestrae; parietosquamosal frill with ten well developed processes on caudal margin composed on each side of three procurved epiparietals (ep1-

3), one procurved process on the parietosquamosal contact (esp), and one laterally to rostrolaterally directed episquamosal (es1) (Sampson et al., 2010a). *Kosmoceratops* is further distinguished by a total of 15 well developed horns or horn-like epiossifications (1 nasal horncore, 2 postorbital horncores, 2 epijugals, and 10 well-developed episquamosals and epiparietals), which makes it one of the most ornate skulls of any known dinosaur (Sampson et al., 2010a).

UMNH VP 17000, a partial skeleton that is the holotype of *Kosmoceratops* from UMNH VP locality 890, consists of a relatively complete skull, a significant portion of the axial skeleton from neck to tail, including part of the pelvic girdle and at least part of one limb (Getty et al., 2010; Sampson et al., 2010a). I sampled the femur from two separate midshaft fragments. I also created a thin section from a femur UMNH VP 21339 (LOC 1323) from a new referred specimen of *Kosmoceratops*. UMNH VP locality 1323 consists of a femur associated with a disarticulated skull.

Preparation of Histological Samples

All specimens were cleaned, repaired, and prepared prior to study. Before creating thin sections, all of the bones were measured, photographed, molded and casted. Research-grade casts were made of each element prior to destruction to ensure all data of each element was preserved. The measurements of each bone sectioned were made using either digital calipers or a cloth metric measuring tape where necessary. The measurements taken include: the preserved length, the width and depth of the proximal end, the width and depth of the distal end, and the width, depth and circumference at the midshaft where the bone was to be sectioned (Fig. 4) (Table 2). Photographs of the bones

prior to sectioning were taken using an Olympus Stylus 1200 12 megapixel digital camera.

Prior to molding, the consolidant "Vinac" (a mixture of acetone and polyvinylacetate beads) was applied to the bones for protection and for easy removal from the putty. To create a mold of small bones such as ribs and tendons, Douglas & Sturgess Silpoxy Putty was used as the molding medium. The putty was placed onto wax paper and then the bone was pressed into the putty. Putty was pressed against the bone to ensure no gaps were present. While the putty was still soft, triangle shaped registration marks were indented in the putty. Vinac was then applied to the bottom part of the mold to act as a separator, and approximately 10 minutes was allowed for the vinac to dry. A ball of putty was placed on top of the bottom mold with the bone still inside, and then pressed all of the way down around the bottom mold all of the way down to the wax paper, creating the top part of the mold. After the putty cured, the two sections were de-molded. The mold is done at this point. The bones I molded using this method were rib UMNH VP 20454.7, tendon UMNH VP 20454.9, rib UMNH VP 12198, and tendon 12198.

The larger molds for this project were done in the following manner. "Klean Klay" of a medium hardness was rolled out until it is about 1 cm thick. The bone was placed on top of the clay and the shape of the bone is outlined with a knife. The clay underneath where the bone is sitting was then removed. The bone was then placed in the hole, and the clay was then pushed up to the bone so that the clay is touching the bone itself. Excess clay was rolled into the shape of a cone and placed at one edge of the clay layout making sure the narrow end of the cone is touching the bone, creating a "pour

spout" for pouring in the eventual casting resin. Using a tool with a thin wire in the shape of a half circle at the end, a moat-like registration groove was cut into the clay all around the bone about a centimeter away.

The desired amount of silicone (Mold Max 20 silicone rubber) was poured into a plastic tub (like a butter tub), mixed, and spread over the bone and on top of the clay. This is the first layer of the silicone. To strengthen the silicone mold, nylon panty hoes were cut up into ~ 5 cm by 5 cm squares and were placed into the wet silicone. At least two hours were allotted for the silicone to dry. Another batch of thin silicone created in the same manner was poured over the nylon pieces. This, too, dried from two hours. A thick layer of silicone was made with the addition of a thickening agent called "Thixotropic". The thick mixture was put on top of the other thin silicone. At least three hours were allotted for this layer to set. A "mother mold" for supporting the silicone mold was made using plaster and fiberglass. First, petroleum jelly was rubbed all over the silicone as a separating agent to ensure that the plaster does not permanently stick to the silicone mold. Pieces of various sizes were cut from closely woven sheets of fiberglass, dipped in wet plaster, and put on top of the silicone. This step was repeated until five layers of fiberglass and plaster were on the mold. When the plaster was dry, the whole mold was flipped over so that the clay was exposed. All of the clay was removed. A rasp was used to smooth out the mold. To create a separator between the silicone halves, "vinac" was used. Once that was dry, the steps for application of silicone and creation of a mother mold were followed again. Once this dried, holes were drilled through both layers of the plaster approximately three centimeters from the edge. The whole mold was knocked on a hard surface to separate the mother mold, and the silicone mold from one

side was carefully peeled away from the bone.

Once the mold was made, a cast of the original bone was created. The mold was sprayed with mold release so that the casting resin did not stick to the silicone rubber. Bolts with washers and wing-nuts were screwed in the drilled holes to secure the mold together. The mold was then positioned vertically with the pour spouts pointing up. Polyester resin (TC-808") was mixed; working time with this resin is short as it cures very rapidly, in about 2 minutes. The mixture was poured into the mold via the pour spout. The whole mold was knocked against a hard surface to release any air bubbles. At least ten minutes was allotted before the newly made cast was removed. Once the cast was removed from the mold, a "Dremel" rotary tool was used to smooth out flashing along the mold seam.

To section the bone, a water-cooled Felker 41-AR tile saw with Norton diamond blades to cut the element in half at the midshaft. A transverse section of bone no thicker than 2.2 cm was then cut from one of the bone halves. All exposed surfaces were then treated with Vinac consolidant and allowed to dry. This transverse section was then embedded in Silmar 95BA-41, a polyester resin. The bone section was placed into a hard plastic container that has been sprayed with mold release. Mixed resin was then poured into in the container with the bone. This container was then placed in an ABBESS Instruments, INC vacuum chamber and brought to the pressure of -72 Kpa (-23 inches of mercury) (with a Fischer High Vacuum Pump LAV-3 vacuum pump). The vacuum pump was then stopped and the chamber was kept at this pressure for three to five minutes; afterwards, the vacuum chamber was slowly released and brought back to room air pressure. The embedded specimen was then removed from the chamber left to fully

harden for twenty-four hours, and finally removed from the container. Initially, the resin block was cut in half with the tile saw, and then a thinner section was cut as thinly as possible from half of the embedded resin block. These sections were dried completely and then a thin cyanoacrylate glue, like PALEOBOND™ Penetrant/Stabilizer, was applied to provide support to the specimen, and allowed to dry again.

Prior to mounting to a slide, this thinner section required 'premount grinding' so that it could be glued onto a glass slide. This grinding was conducted using various coarsenesses of silicone carbide grit powder, water, and a glass plate. The section was successively ground using decreasing coarseness of 120, 320, and 600 grit powders. Each powder was applied to a different glass plate and water was sprayed on for lubrication. The section was placed flat on this water/powder mixture and was moved in an "infinity" symbol to make all sides received the same amount of grinding. Several sections made at the Museum of the Rockies used the same grit powders, but exchanged an Ecomet 4 Grinder-Polisher (Buehler Ltd.) for the glass plate.

Once the specimens had been premount ground, they were mounted onto a glass slide using Devcon™ Two-Ton Epoxy. Two methods were utilized to reduce movement of the specimen during gluing. A weight (a cap filled with pennies embedded in resin) was put on top of the specimen. Alternatively, the section and glued slide were wrapped in wax paper, two extra slides were put on either side to "sandwich" it, and then each side was clamped with wooden clothes pins. The glue was left to dry for 12 hours.

Once the large specimens were mounted, they were further thinned using the water-cooled tile saw. The slide was placed against the metal "bridge vice" about 3 mm away from the blade path, and slowly moved against the blade. The newly exposed bone

was allowed to dry completely, then glued again with cyanoacrylate PALEOBOND™ Penetrant/Stabilizer glue, and left to dry again. 1x2" and 2x3" slides were thinned using the Buehler Petro-Thin Sectioning System, with a 60 grit disk. The attached arm had a vacuum that allowed the slide to stay affixed and be moved against the disk. As the slide was brought closer and closer to the revolving disk, more and more of the specimen was shaved off until the slide reached the desired thickness.

Two methods were used in this study to grind and polish the thin sections. The first, which was used in the Museum of the Rockies Histology Lab, used silicon carbide abrasive papers (Buehler Ltd.) and an Ecomet 4 Grinder-Polisher (Buehler Ltd.) lapidary wheel. The abrasive papers used were grits 60, 120, 180, 320, 600, and 800. I put the desired grit paper on the wheel being sure to secure it with the removable metal ring, turned the motor up to 120 rpm, and turned the water on. The slide was ground using successively finer grit papers as the section got thinner. I was sure to constantly check the thin section thickness with a micrometer. The second method of grinding at the University of Utah was used for most of the sections in this study, and replaced the Ecomet with grinding using glass plates, silicon carbide grit powders (120, 180, 320, 600, and 800), and water, as described above in the "premount grinding" step. As with the Ecomet, I successively ground down each section using decreasing coarsenesses of grit powder.

At the MOR final polishing of each section used a paste on a wet platen consisting of about a tablespoon Buehler 5.0 micron aluminum oxide powder. The thin section was rubbed on the platen in a circular motion or the paste was rubbed onto the slide using a wet micro cloth. After this, a Buehler 1.0 micron aluminum oxide powder

solution was rubbed in a circular motion onto the slide until shiny. At the University of Utah, the slide was ground using very fine 600 and 800 silicon carbide grits until shiny. After polishing, a glass cover slip was permanently glued to each slide with Devcon™ Two-Ton Epoxy.

These finished thin sections were then digitally imaged using a NIKON Optiphot Pol Microscope, PRIOR Optiscan II Automated Stage, a DELL Precision T3400 Computer, a NIKON DS-Fil camera, and NIKON NIS Elements BR 3.0 software. I scanned my slides at 4x magnification, manually focusing every 10 shots.

Analysis of Microstructure

The description of the bone histology of each element begins with large-scale features and works through to smallest-scale features. Large scale features include the nature of the medullary cavity and the extent of trabeculae. Then, because remodeling and secondary osteons were so prevalent, I focused on their extent and location within the thin section. Finally, the small scale features were divided into characters that do and do not change throughout the section. I specifically looked at extent of woven vs. parallel-fibered bone in crossed-polarized light, and how this changed from the medullary cavity to the periosteum. I evaluated the density and direction of vascular canals throughout the section, and described the proportion of simple canals vs. primary osteons vs. secondary osteons. All histological features are described starting from medullary cavity and working my way outwards towards the periosteum. I noted any evidence (or lack of) for Lines of Arrested Growth (LAGs), and External Fundamental System (EFS). If LAGs were present, I measured their circumference, counted how many there were, and

measured their spacing.

I quantitatively calculated the density of both osteocytes and vascular canals (Table 3). In order to calculate the density of both the vascularity and the osteocytes, I focused on a standard column of bone from the anterior part of the midshaft. In Adobe Illustrator CS5.1, I then made uniform boxes of .6009 mm by .6009 mm in size and spaced them 0.5577 mm distance apart from each other. The size and spacing of the box was uniform for every slide analyzed (Fig. 5). I then counted the amount of longitudinal, circumferential, and radial canals (Fig. 6) present within each box for each slide. I did this throughout the sectioned column. I calculated the density of the osteocytes in the same way. I plotted these densities versus the radius of each box from the centroid of the element using Microsoft Excel Mac 2008. I created graphs for all of the femora I analyzed plotting radius vs. vascularity, radius vs. osteocytes, and vascularity vs. osteocytes (Fig. 7). I created graphs for all of the tibiae I analyzed plotting radius vs. vascularity, radius vs. osteocytes, and vascularity vs. osteocytes (Fig. 8). I created graphs for all of the humeri I analyzed plotting radius vs. vascularity, radius vs. osteocytes, and vascularity vs. osteocytes (Fig. 9).

Figure 3. Skeletons of *Utahceratops gettyi* and *Kosmoceratops richardsoni*. Red elements represent the bones sectioned for this study (modified from Sampson et al., 2010a).

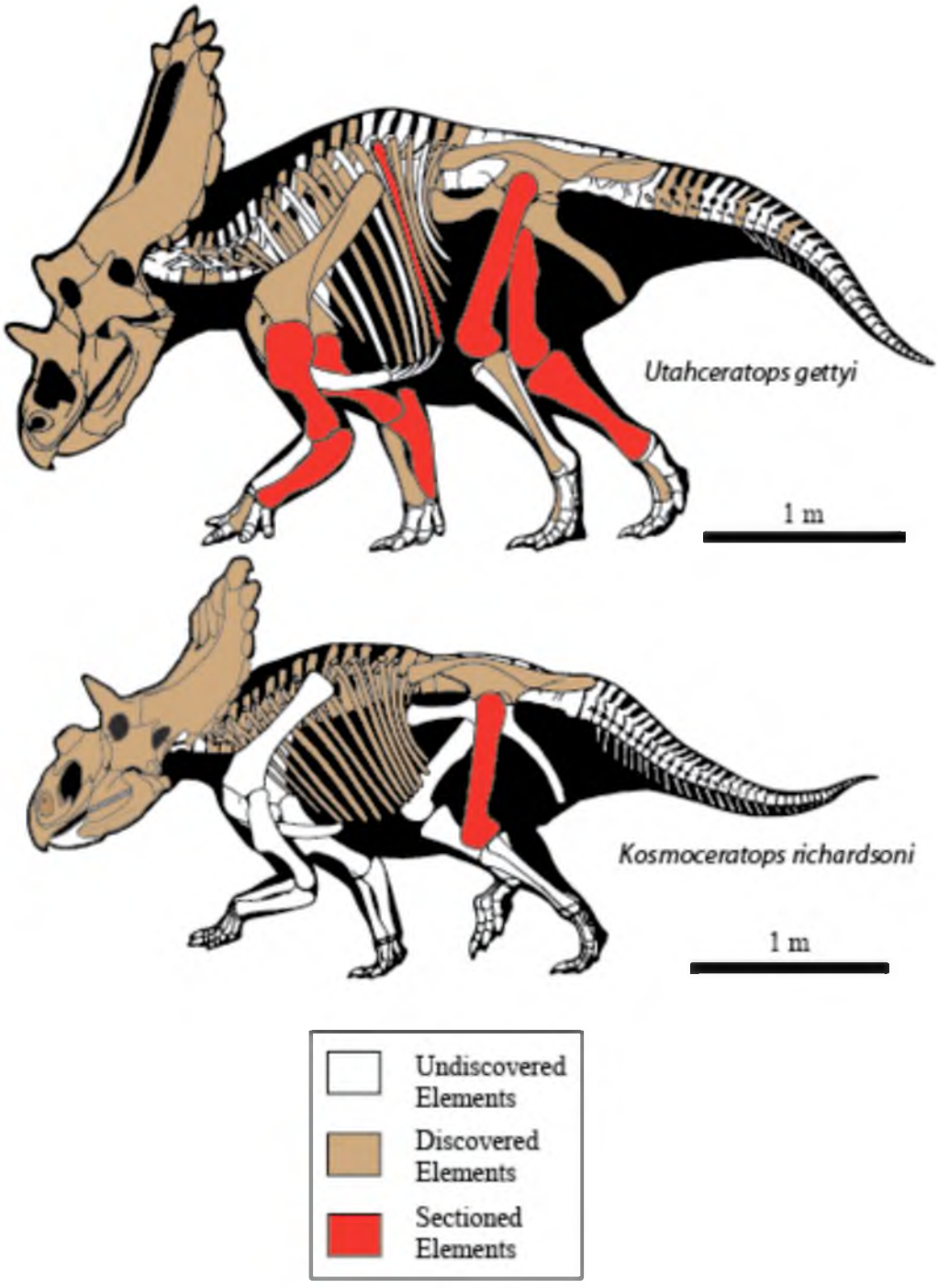
Utahceratops gettyi
1 m
Kosmoceratops richardsoni
1 m
Undiscovered Elements
Discovered Elements
Sectioned Elements

Table 1. Elements sampled in this study.

Specimen	Species	Humerus	Ulna	Femur	Tibia	Rib	Tendon	Limb Shaft
UMNH VP 20444	*Utahceratops*	X	X	X	X			
UMNH VP 20454	*Utahceratops*	X	X	X	X	X	X	
UMNH VP 12198	*Utahceratops*			X		X	X	
UMNH VP 16800	*Utahceratops*			X	X			X
UMNH VP 17000	*Kosmoceratops*			X				
UMNH VP 21339	*Kosmoceratops*			X				
UMNH VP 19490	Indeterminant	X						
UMNH VP 16865	Indeterminant	X						

Figure 4. The outlines of the limb bones that were sampled and the areas where they were measured. A. Outline of a femur; B. Outline of a tibia; C. Outline of an humerus; D. Outline of an ulna. The black line labeled L indicates the full length measurement. The blue line labeled 'pw' indicates the width of the distal end. The red line labeled 'msw' indicates the midshaft width, where the circumference measurement was taken, and where the bone was sectioned. The purple line labeled 'dw' indicates the distal end width measurement. The 'P' arrow indicates the proximal orientation and the 'L' arrow indicates the lateral orientation.

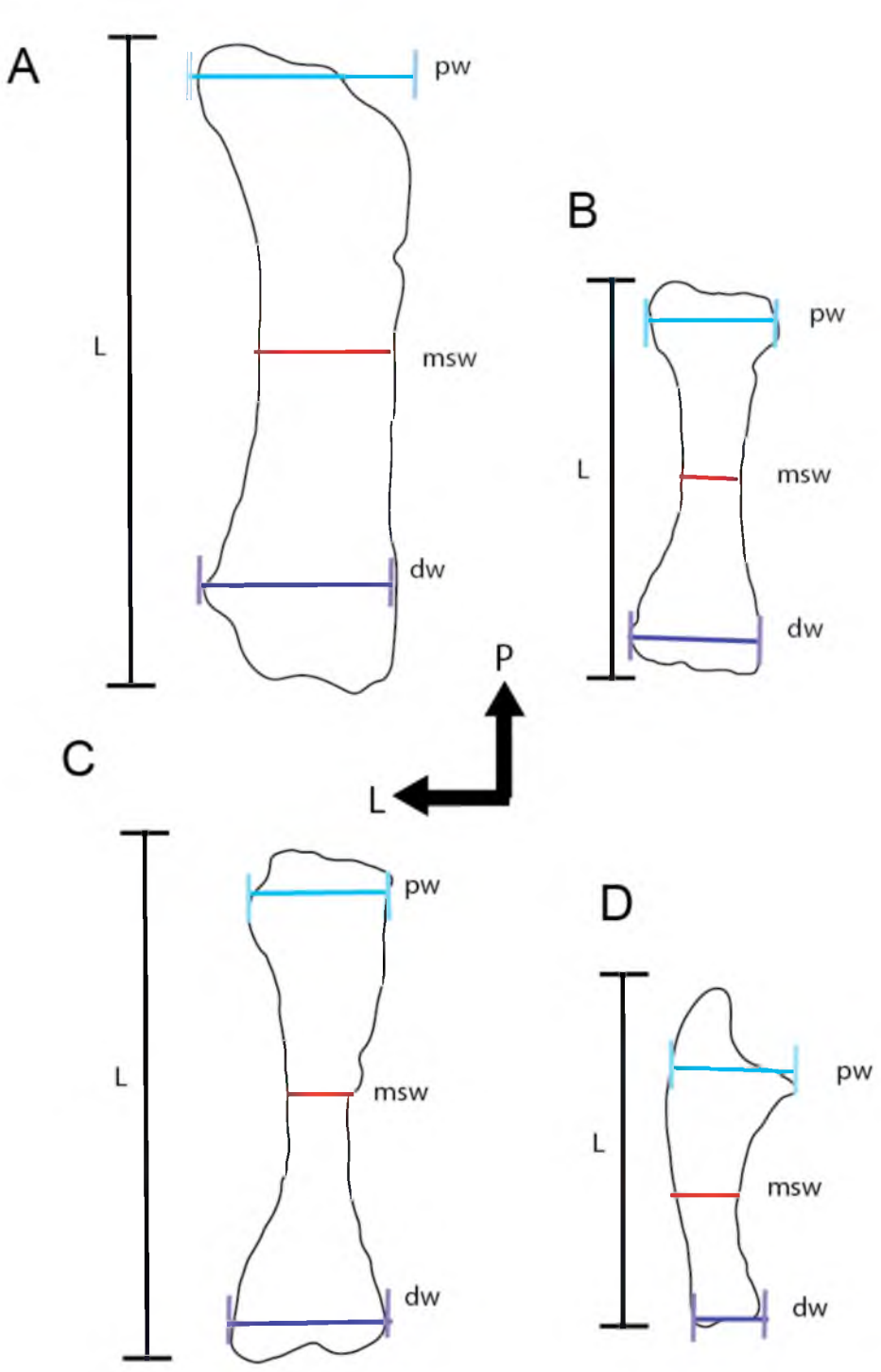
A
pw
L
msw
dw
B
pw
L
msw
dw
P
L
C
pw
L
msw
dw
D
pw
L
msw
dw

Table 2. Bone measurements before sectioning.

SPECIMEN #	LOC #	NAME	SPECIES	ELEMENT	PRESERVED LENGTH mm	PROX WIDTH mm	PROX DEPTH mm	DIST WIDTH mm	DIST DEPTH mm	MIDSHAFT WIDTH mm	MIDSHAFT DEPTH mm	MIDSHAFT CIRCUM mm	DISTANCE FROM DISTAL END mm
UMNH VP 20444.1	945	KC&C	*UTAH*	HUMERUS LF	440.0	144.1 175.0*	44.5	131.9	42.5	55.2	52.3	160.0	150.0
UMNH VP 20444.4	945	KC&C	*UTAH*	FEMUR LF	605.0	---	---	129.1	---	60.0	---	---	245.0
UMNH VP 20444.5	945	KC&C	*UTAH*	TIBIA RT	465.0	136.4*	---	148.6	---	54.4	---	189.0	240.0
UMNH VP 20444.2	945	KC&C	*UTAH*	ULNA LF	322.0	111.4 27.2	46.2	61.1	22.9	55.1	27.9	136.0	120.0
UMNH VP 20454.8	945	KC&C	*UTAH*	HUMERUS LF	210.3	111.1	---	80.2	---	50.5	---	145.1	---
UMNH VP 20454.5	945	KC&C	*UTAH*	FEMUR LF	291.0	97.8*	53.1*	118.8*	55.3*	80.9*	47.5*	230.0	---
UMNH VP 20454.3	945	KC&C	*UTAH*	TIBIA RT	231.0	56.4*	73.9*	87.8	38.5	50.6	55.5	167.0	---
UMNH VP 20454.1	945	KC&C	*UTAH*	ULNA LF	321.0	93.1	34.7	64.6	25.4	50.5	22.7	121.0	110.0
UMNH VP 20454.7	945	KC&C	*UTAH*	RIB FRAG	104.4	31.9	---	27.4	---	31.4	---	75.0	---
UMNH VP 20454.9	945	KC&C	*UTAH*	TENDON FRAG	92.8	17.0	---	14.9	---	14.1	---	40.0	---
UMNH VP 12198	145	THE BLUES	*UTAH*	FEMUR LF	874.0	173.9*	90.0*	248.9*	96.4*	80.9*	73.2*	437.0	550.0
UMNH VP 12198	145	THE BLUES	*UTAH*	RIB FRAG	114.4	23.1	---	22.6	---	23.0	---	58.0	---
UMNH VP 12198	145	THE BLUES	*UTAH*	TENDON FRAG	68.9	17.0	---	12.7	---	14.9	---	44.0	---
UMNH VP 16681	942	BLUEWASH	*UTAH*	TIBIA RT	450.0	159.2	56.7	149.7	40.1	69.8	55.4	205.0	222.0
UMNH VP 16860	942	BLUEWASH	*UTAH*	FEMUR RT	488.0	390.3*	56.7	---	---	95.4	58.5*	250.0	324.0 PROX
UMNH VP 16861	942	BLUEWASH	*UTAH*	LIMB SHAFT	180.0	---	---	---	---	---	---	180.0	---
UMNH VP 19490		VARIOUS	*UTAH*	HUMERUS LF	167.6*	---	---	---	---	54.3	68.5	204.0	---
UMNH VP 16865.1	512	KAC	*UTAH*	HUMERUS LF	545.0	131.0	83.6	152.4	47.1	61.9	56.7	189.0	182.0
UMNH VP 17000	890	KOSMO	*KOSMO*	FEMUR FRAG A	118.8	68.5	---	66.0	---	72.2	---	211.0	---
UMNH VP 17000	890	KOSMO	*KOSMO*	FEMUR FRAG B	80.9*	---	---	---	---	70.0	72.6	223.0	---
UMNH VP 21339	1323	HEC 11-3	*KOSMO*	FEMUR FRAG A	670.0*	315.0	---	---	---	155.0	---	---	440.0 PROX
UMNH VP 21339	1323	HEC 11-3	*KOSMO*	FEMUR FRAG B	---	---	---	---	---	---	---	---	440.0 PROX

Table 3. Data from the analysis of the thin sections. This table includes the number and type of vascular canals seen in each element, and the change in vascular densities and osteocytes densities for each bone.

Specimen #	Box #	Total	Longitudinal	Radial	Circumferential	Osteocytes	Ratio L:R	Radius	Vascularity /mm^2	Osteocytes /mm^2
UMNH VP 16860A	1	14	14	0	0	633	-	5.15	38.77	1753.07
femur *Utahceratops*	2	3	3	0	0	423	-	6.31	8.31	1171.48
gettyi	3	7	7	0	0	653	-	7.46	19.39	1808.46
	4	8	8	0	0	544	-	8.62	22.16	1506.59
	5	12	11	1	0	800	11.00	9.78	33.23	2215.57
	6	7	7	0	0	800	-	10.94	19.39	2215.57
	7	13	11	0	2	868	-	12.10	36.00	2403.89
	8	11	10	1	0	674	10.00	13.26	30.46	1866.62
	9	10	10	0	0	600	-	14.42	27.69	1661.68
	10	12	10	2	0	744	5.00	15.57	33.23	2060.48
UMNH VP 20444.4	1	3	3	0	0	127	-	18.27	8.31	351.72
femur *Utahceratops*	2	3	3	0	0	358	-	19.43	8.31	991.47
gettyi	3	3	3	0	0	450	-	20.59	8.31	1246.26
	4	3	3	0	0	375	-	21.75	8.31	1038.55
	5	5	5	0	0	344	-	22.91	13.85	952.70
	6	3	3	0	0	400	-	24.07	8.31	1107.79
	7	3	3	0	0	400	-	25.23	8.31	1107.79
	8	3	3	0	0	451	-	26.38	8.31	1249.03
	9	2	1	1	0	400	1.00	27.54	5.54	1107.79
	10	4	4	0	0	400	-	28.70	11.08	1107.79
	11	5	3	2	0	432	1.50	29.86	13.85	1196.41
	12	7	7	0	0	357	-	31.02	19.39	988.70
	13	5	5	0	0	400	-	32.18	13.85	1107.79
	14	4	4	0	0	400	-	33.34	11.08	1107.79

Table 3 Continued.

Specimen #	Box #	Total	Longitudinal	Radial	Circumferential	Osteocytes	Ratio L:R	Radius	Vascularity /mm^2	Osteocytes /mm^2
	15	4	4	0	0	548	-	34.49	11.08	1517.67
	16	2	2	0	0	500	-	35.65	5.54	1384.73
	17	3	3	0	0	570	-	36.81	8.31	1578.59
UMNH VP 20454.5	1	5	5	0	0	500	-	13.06	13.85	1384.73
femur *Utahceratops*	2	16	16	0	0	490	-	14.22	44.31	1357.04
gettyi	3	6	6	0	0	400	-	15.38	16.62	1107.79
	4	6	6	0	0	433	-	16.54	16.62	1199.18
	5	13	13	0	0	460	-	17.70	36.00	1273.95
	6	4	4	0	0	361	-	18.86	11.08	999.78
	7	15	15	0	0	400	-	20.01	41.54	1107.79
	8	15	15	0	0	400	-	21.17	41.54	1107.79
	9	11	11	0	0	367	-	22.33	30.46	1016.39
	10	18	18	0	0	458	-	23.49	49.85	1268.41
UMNH VP 12198 femur	1	2	2	0	0	346	-	24.28	6.78	1172.62
Utahceratops gettyi	2	3	3	0	0	500	-	25.36	10.17	1694.53
	3	2	2	0	1	550	-	26.45	6.78	1863.99
	4	3	3	0	0	470	-	27.54	10.17	1592.86
	5	3	3	0	0	400	-	28.62	10.17	1355.63
	6	4	4	0	0	420	-	29.71	13.56	1423.41
	7	3	3	0	0	500	-	30.80	10.17	1694.53
	8	3	3	0	0	500	-	31.88	10.17	1694.53
	9	5	5	0	0	600	-	32.97	16.95	2033.44
	10	9	8	0	1	600	-	34.06	30.50	2033.44
	11	7	7	0	0	770	-	35.14	23.72	2609.58
	12	7	7	0	0	485	-	36.23	23.72	1643.70
UMNH VP 20444.5 tibia	1	3	3	0	0	500	-	12.19	8.31	1384.73
Utahceratops gettyi	2	3	3	0	0	500	-	13.35	8.31	1384.73

Table 3 Continued.

Specimen #	Box #	Total	Longitudinal	Radial	Circumferential	Osteocytes	Ratio L:R	Radius	Vascularity /mm^2	Osteocytes /mm^2
	3	7	7	0	0	500	-	14.51	19.39	1384.73
	4	3	3	0	0	700	-	15.67	8.31	1938.62
	5	7	7	0	0	500	-	16.82	19.39	1384.73
	6	0	0	0	0	500	-	17.98	0.00	1384.73
	7	1	1	0	0	900	-	19.14	2.77	2492.52
	8	8	8	0	0	900	-	20.30	22.16	2492.52
	9	9	9	0	0	700	-	21.46	24.93	1938.62
	10	3	3	0	0	700	-	22.62	8.31	1938.62
	11	7	7	0	0	800	-	23.78	19.39	2215.57
	12	5	5	0	0	700	-	24.94	13.85	1938.62
	13	3	3	0	0	700	-	26.09	8.31	1938.62
	14	0	0	0	0	730	-	27.25	0.00	2021.71
	15	4	4	0	0	700	-	28.41	11.08	1938.62
	16	0	0	0	0	800	-	29.57	0.00	2215.57
UMNH VP 20454.3 tibia	1	6	6	0	0	600	-	11.82	16.62	1661.68
Utahceratops gettyi	2	16	16	0	0	600	-	12.98	44.31	1661.68
	3	7	7	0	0	567	-	14.14	19.39	1570.29
	4	11	11	0	0	740	-	15.29	30.46	2049.40
	5	11	11	0	0	638	-	16.45	30.46	1766.92
	6	11	11	0	0	700	-	17.61	30.46	1938.62
	7	9	9	0	0	600	-	18.77	24.93	1661.68
	8	9	9	0	0	600	-	19.93	24.93	1661.68
	9	9	6	0	3	770	-	21.09	24.93	2132.49
	10	11	8	0	3	750	-	22.25	30.46	2077.10
	11	7	7	0	0	600	-	23.40	19.39	1661.68

Table 3 Continued.

Specimen #	Box #	Total	Longitudinal	Radial	Circumferential	Osteocytes	Ratio L:R	Radius	Vascularity /mm^2	Osteocytes /mm^2
	12	9	9	0	0	673	-	24.56	24.93	1863.85
	13	0	0	0	0	600	-	25.72	0.00	1661.68
	14	4	4	0	0	700	-	26.88	11.08	1938.62
UMNH VP 16681 tibia	1	3	3	0	0	82	-	11.82	8.31	227.10
Utahceratops gettyi	2	5	5	0	0	183	-	12.98	13.85	506.81
	3	12	12	0	0	325	-	14.14	33.23	900.08
	4	12	12	0	0	320	-	15.29	33.23	886.23
	5	15	15	0	0	574	-	16.45	41.54	1589.67
	6	13	13	0	0	660	-	17.61	36.00	1827.85
	7	13	12	0	1	660	-	18.77	36.00	1827.85
	8	16	16	0	0	570	-	19.93	44.31	1578.59
	9	20	20	0	0	500	-	21.09	55.39	1384.73
	10	12	12	0	0	500	-	22.25	33.23	1384.73
	11	20	20	0	0	470	-	23.40	55.39	1301.65
	12	16	16	0	0	600	-	24.56	44.31	1661.68
	13	14	14	0	0	500	-	25.72	38.77	1384.73
	14	21	21	0	0	700	-	26.88	58.16	1938.62
	15	13	13	0	0	700	-	28.04	36.00	1938.62
	16	12	12	0	0	700	-	29.20	33.23	1938.62
	17	4	4	0	0	650	-	30.36	11.08	1800.15
	18	6	6	0	0	581	-	31.51	16.62	1609.06
UMNH VP 16865.1B	1	3	3	0	0	130	-	18.71	8.31	360.03
humerus Indeterminant	2	6	6	0	0	92	-	19.87	16.62	254.79
ceratopsian	3	3	3	0	0	240	-	21.02	8.31	664.67
	4	5	5	0	0	829	-	22.18	13.85	2295.88

Table 3 Continued.

Specimen #	Box #	Total	Longitudinal	Radial	Circumferential	Osteocytes	Ratio L:R	Radius	Vascularity /mm^2	Osteocytes /mm^2
	5	7	7	0	0	655	-	23.34	19.39	1814.00
	6	4	4	0	0	587	-	24.50	11.08	1625.67
	7	3	3	0	0	473	-	25.66	8.31	1309.96
	8	5	5	0	0	526	-	26.82	13.85	1456.74
	9	4	4	0	0	724	-	27.98	11.08	2005.09
	10	6	6	0	0	724	-	29.14	16.62	2005.09
	11	10	10	0	0	767	-	30.29	27.69	2124.18
	12	11	11	0	0	627	-	31.45	30.46	1736.45
	13	12	12	0	0	600	-	32.61	33.23	1661.68
	14	7	7	0	0	723	-	33.77	19.39	2002.32
UMNH VP 20454.8	1	8	8	0	0	500	-	15.70	22.16	1384.73
humerus *Utahceratops*	2	8	8	0	0	600	-	16.86	22.16	1661.68
gettyi	3	12	12	0	0	582	-	18.02	33.23	1611.83
	4	12	12	0	0	670	-	19.18	33.23	1855.54
	5	9	9	0	0	660	-	20.33	24.93	1827.85
	6	13	13	0	0	700	-	21.49	36.00	1938.62
	7	13	13	0	0	623	-	22.65	36.00	1725.38
	8	18	18	0	0	600	-	23.81	49.85	1661.68
	9	20	20	0	0	600	-	24.97	55.39	1661.68
	10	14	6	3	5	500	2.00	26.13	38.77	1384.73
UMNH VP 19490	1	8	8	0	0	500	-	11.22	22.16	1384.73
Humerus indeterminant	2	7	7	0	0	544	-	12.38	19.39	1506.59
ceratopsian	3	10	10	0	0	376	-	13.54	27.69	1041.32
	4	8	8	0	0	631	-	14.70	22.16	1747.53
	5	14	14	0	0	521	-	15.86	38.77	1442.89
	6	13	13	0	0	655	-	17.02	36.00	1814.00

Table 3 Continued.

Specimen #	Box #	Total	Longitudinal	Radial	Circumferential	Osteocytes	Ratio L:R	Radius	Vascularity /mm^2	Osteocytes /mm^2
	7	17	17	0	0	600	-	18.17	47.08	1661.68
	8	18	18	0	0	700	-	19.33	49.85	1938.62
	9	12	10	2	0	700	5.00	20.49	33.23	1938.62
	10	19	16	3	0	600	5.33	21.65	52.62	1661.68
	1	9	7	2	0	517	3.50	17.70	24.93	1431.81
UMNH VP 17000 femur	2	6	5	1	0	475	5.00	18.86	16.62	1315.49
Kosmosaurus richardsoni	3	17	17	0	0	700	-	20.02	47.08	1938.62
	4	10	10	0	0	565	-	21.17	27.69	1564.75
	5	9	9	0	0	730	-	22.33	24.93	2021.71
	6	9	8	1	0	670	8.00	23.49	24.93	1855.54
	7	9	9	0	0	663	-	24.65	24.93	1836.15
UMNH VP 21339B	1	6	6	0	0	252	-	4.03	16.62	697.90
femur *Kosmoceratops*	2	8	8	0	0	482	-	5.18	22.16	1334.88
richardsoni	3	4	4	0	0	500	-	6.34	11.08	1384.73
	4	6	6	0	0	700	-	7.50	16.62	1938.62
	5	8	8	0	0	566	-	8.66	22.16	1567.52
	6	2	2	0	0	480	-	9.82	5.54	1329.34
	7	5	5	0	0	730	-	10.98	13.85	2021.71
	8	6	6	0	0	500	-	12.14	16.62	1384.73
	9	7	7	0	0	741	-	13.30	19.39	2052.17
	10	7	7	0	0	781	-	14.45	19.39	2162.95
	11	4	4	0	0	746	-	15.61	11.08	2066.02
	12	2	2	0	0	668	-	16.77	5.54	1850.00
	13	1	1	0	0	456	-	17.93	2.77	1262.88
TMP 66.10.36 tibia	1	14	10	4	0	602	2.50	14.08	38.77	1667.22
Centrosaurus apertus	2	13	11	2	0	613	5.50	15.23	36.00	1697.68

Table 3 Continued.

Specimen #	Box #	Total	Longitudinal	Radial	Circumferential	Osteocytes	Ratio L:R	Radius	Vascularity /mm^2	Osteocytes /mm^2
	3	13	10	3	0	673	3.33	16.39	36.00	1863.85
	4	13	11	2	0	579	5.50	17.55	36.00	1603.52
	5	14	10	4	0	845	2.50	18.71	38.77	2340.20
	6	11	10	1	0	588	10.00	19.87	30.46	1628.44
	7	14	13	1	0	671	13.00	21.03	38.77	1858.31
	8	21	19	2	0	950	9.50	22.19	58.16	2630.99
	9	22	19	3	0	901	6.33	23.35	60.93	2495.29
	10	21	17	4	0	610	4.25	24.50	58.16	1689.37
	11	23	22	1	0	626	22.00	25.66	63.70	1733.68
	12	15	15	0	0	670	-	26.82	41.54	1855.54
	13	8	3	5	0	400	0.60	27.98	22.16	1107.79
TMP 79.11.56 tibia	1	9	9	0	0	395	-	7.82	24.93	1093.94
Centrosaurus apertus	2	12	11	1	0	514	11.00	8.98	33.23	1423.50
	3	9	9	0	0	465	-	10.14	24.93	1287.80
	4	14	12	2	0	500	6.00	11.30	38.77	1384.73
	5	14	13	1	0	499	13.00	12.46	38.77	1381.96
	6	12	12	0	0	458	-	13.61	33.23	1268.41
	7	6	6	0	0	530	-	14.77	16.62	1467.82
	8	14	14	0	0	570	-	15.93	38.77	1578.59
	9	18	18	0	0	500	-	17.09	49.85	1384.73
	10	16	16	0	0	448	-	18.25	44.31	1240.72
	11	14	12	2	0	565	6.00	19.41	38.77	1564.75
	12	19	19	0	0	456	-	20.57	52.62	1262.88
	13	13	10	3	0	394	3.33	21.73	36.00	1091.17
	14	12	11	1	0	300	11.00	22.88	33.23	830.84

Table 3 Continued.

Specimen #	Box #	Total	Longitudinal	Radial	Circumferential	Osteocytes	Ratio L:R	Radius	Vascularity /mm^2	Osteocytes /mm^2
	15	11	9	0	2	200	-	24.04	30.46	553.89
	16	16	14	2	0	740	7.00	25.20	44.31	2049.40
	17	14	12	2	0	480	6.00	26.36	38.77	1329.34
femur F-2 *Protoceratops*	1	10	10	0	0	500	-	8.49	27.69	1384.73
andrewsi	2	11	11	0	0	534	-	9.29	30.46	1478.89
	3	15	15	0	0	800	-	10.09	41.54	2215.57
	4	14	14	0	0	700	-	10.89	38.77	1938.62
	5	18	18	0	0	821	-	11.69	49.85	2273.73
	6	15	15	0	0	1000	-	12.49	41.54	2769.46
MPC-D100/530 femur	1	8	8	0	0	566	-	19.04	22.16	1567.52
Protoceratops andrewsi	2	8	8	0	0	700	-	20.01	22.16	1938.62
	3	9	9	0	0	800	-	20.97	24.93	2215.57
	4	17	17	0	0	779	-	21.94	47.08	2157.41
	5	13	12	1	0	700	12.00	22.90	36.00	1938.62
	6	7	7	0	0	128	-	23.87	19.39	354.49
MPC-D100/530 humerus	1	7	7	0	0	465	-	6.03	19.39	1287.80
Protoceratops andrewsi	2	18	18	0	0	474	-	7.03	49.85	1312.73
	3	27	27	0	0	555	-	8.02	74.78	1537.05
	4	12	11	0	1	558	-	9.01	33.23	1545.36
	5	11	11	0	0	763	-	10.00	30.46	2113.10
	6	9	5	4	0	638	1.25	10.99	24.93	1766.92
	7	21	18	3	0	843	6.00	11.98	58.16	2334.66
PIN 698/1977 femur	1	11	4	7	0	900	0.57	-	30.46	2492.52
Psittacosaurus	2	19	13	6	0	800	2.17	-	52.62	2215.57
mongoliensis	3	20	4	16	0	851	0.25	-	55.39	2356.81
	4	9	8	1	0	566	8.00	-	24.93	1567.52

Figure 5. UMNH VP 16860 femur illustrating how vascular canal density and osteocytes density were calculated. The blue circles indicate vascular canals. The white dots indicated osteocytes. The A arrow is pointing in the direction of the anterior side of the bone. The L arrow is pointing the direction of the lateral side of the bone.

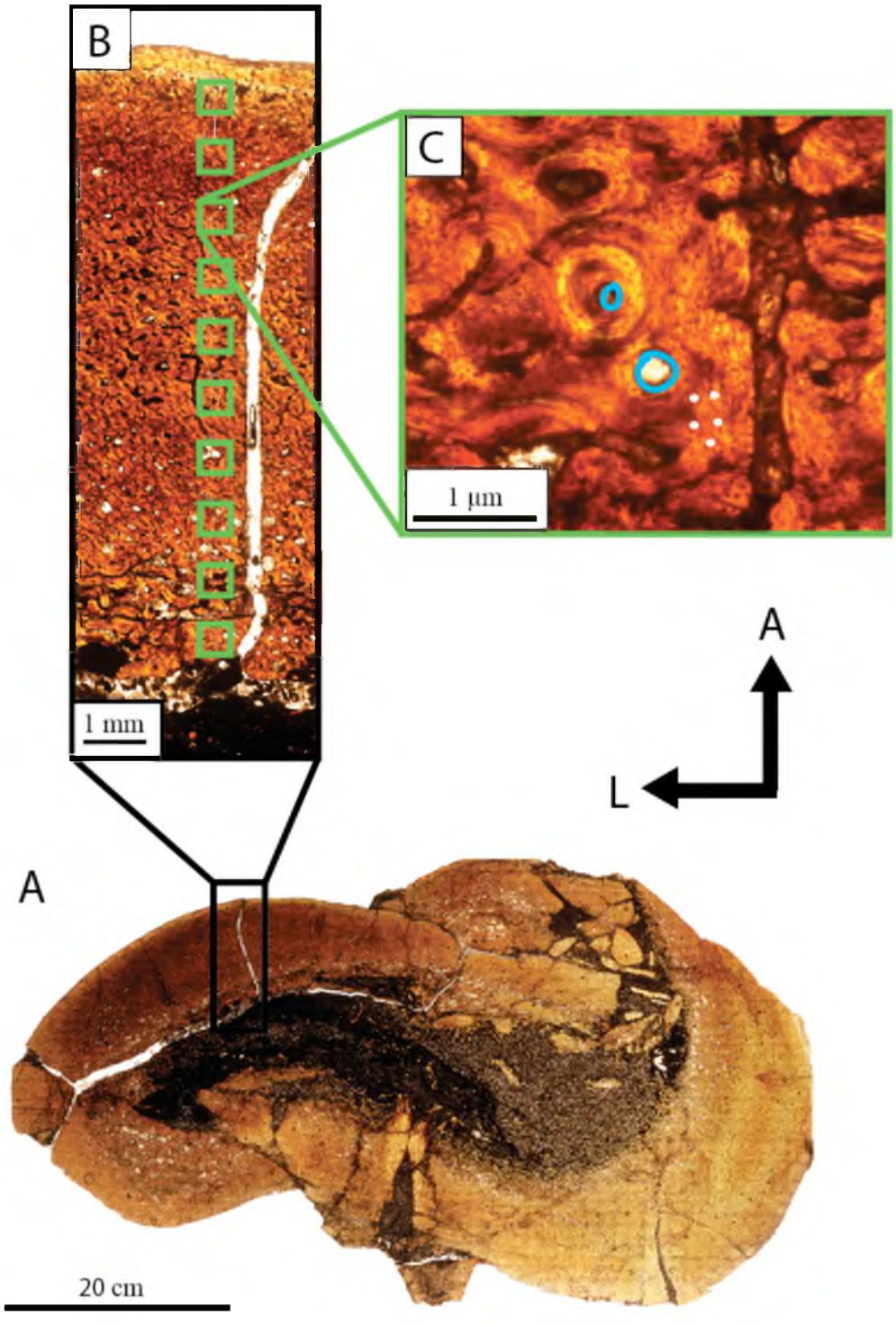
B
C
1 µm
1 mm
A
L
A
20 cm

Figure 6. This humerus, (UMNH VP 20454.8), illustrating the different types of vascular canals. The vascular canal outlined in yellow is a radial canal. The red horizontal lines represent the circumferential canals. The blue dots indicated longitudinal vascular canals.

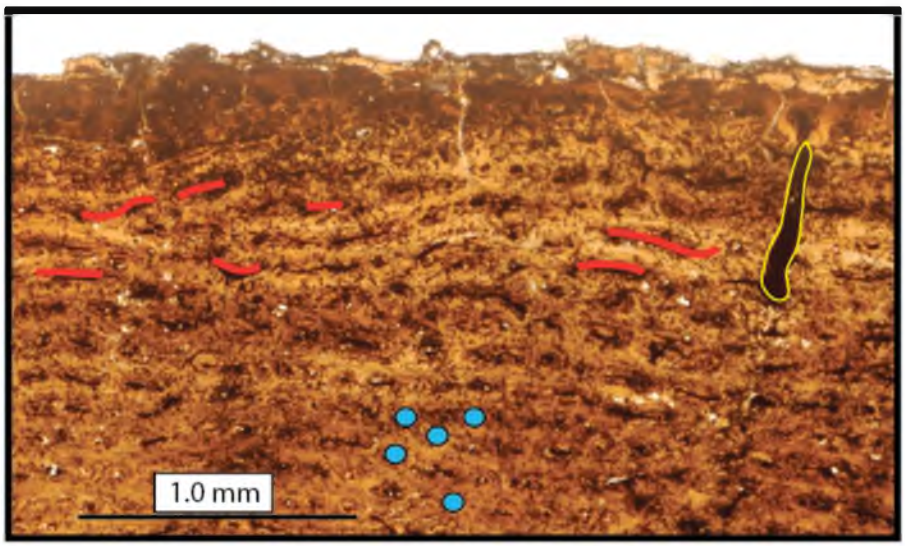
1.0 mm

Figure 7. Graphs that represent the data collected in the femora analysis of the different taxa of ceratopsians. A. The radius of the element plotted against the osteocytes densities. B. The densities of the vascularity seen plotted against the osteocyte densities. C. The radius of the element plotted against the vascular densities.

A

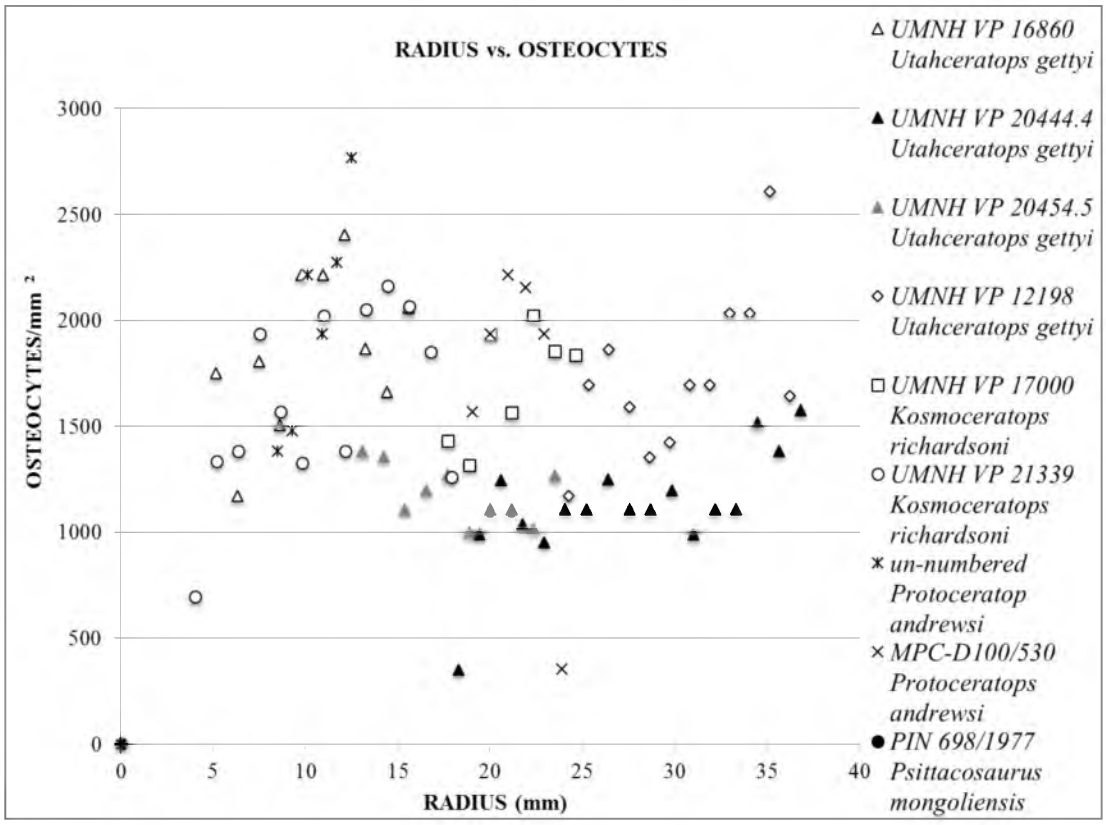
RADIUS vs. OSTEOCYTES
OSTEOCYTES/mm ²
RADIUS (mm)
0
500
1000
1500
2000
2500
3000
0
5
10
15
20
25
30
35
40
UMNH VP 16860 Utahceratops gettyi
UMNH VP 20444.4 Utahceratops gettyi
UMNH VP 20454.5 Utahceratops gettyi
UMNH VP 12198 Utahceratops gettyi
UMNH VP 17000 Kosmoceratops richardsoni
UMNH VP 21339 Kosmoceratops richardsoni
un-numbered Protoceratop andrewsi
MPC-D100/530 Protoceratops andrewsi
PIN 698/1977 Psittacosaurus mongoliensis

B

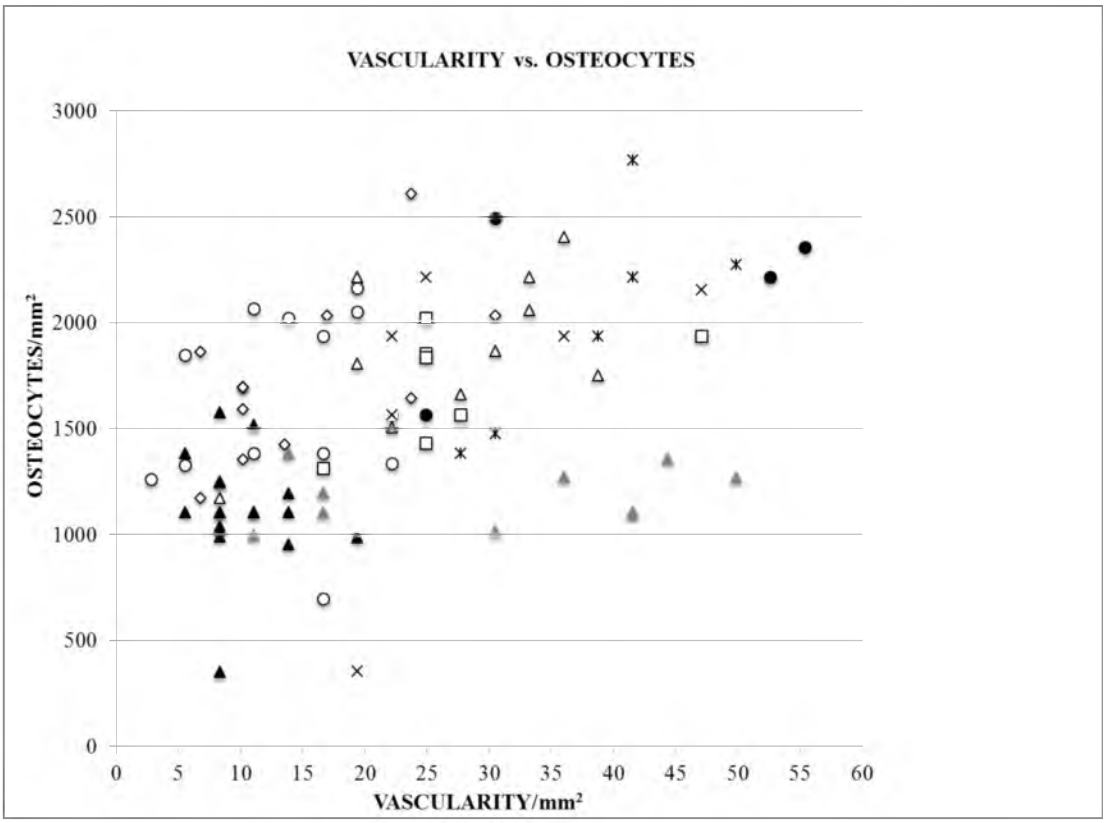

Figure 7 Continued.

C 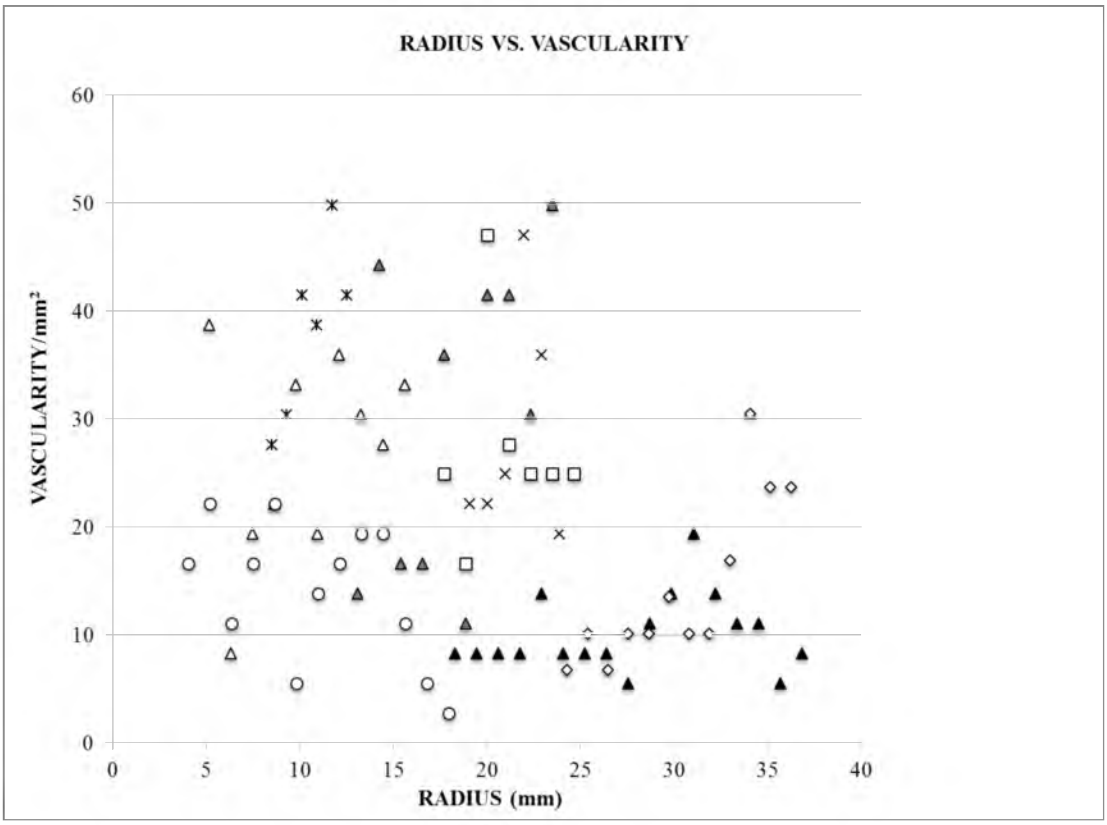

Figure 7 Continued.

Figure 8. Graphs that represent the data collected in the tibiae analysis of the different taxa of ceratopsians. A. The radius of the element plotted against the osteocytes densities. B. The densities of the vascularity seen plotted against the osteocyte densities. C. The radius of the element plotted against the vascular densities.

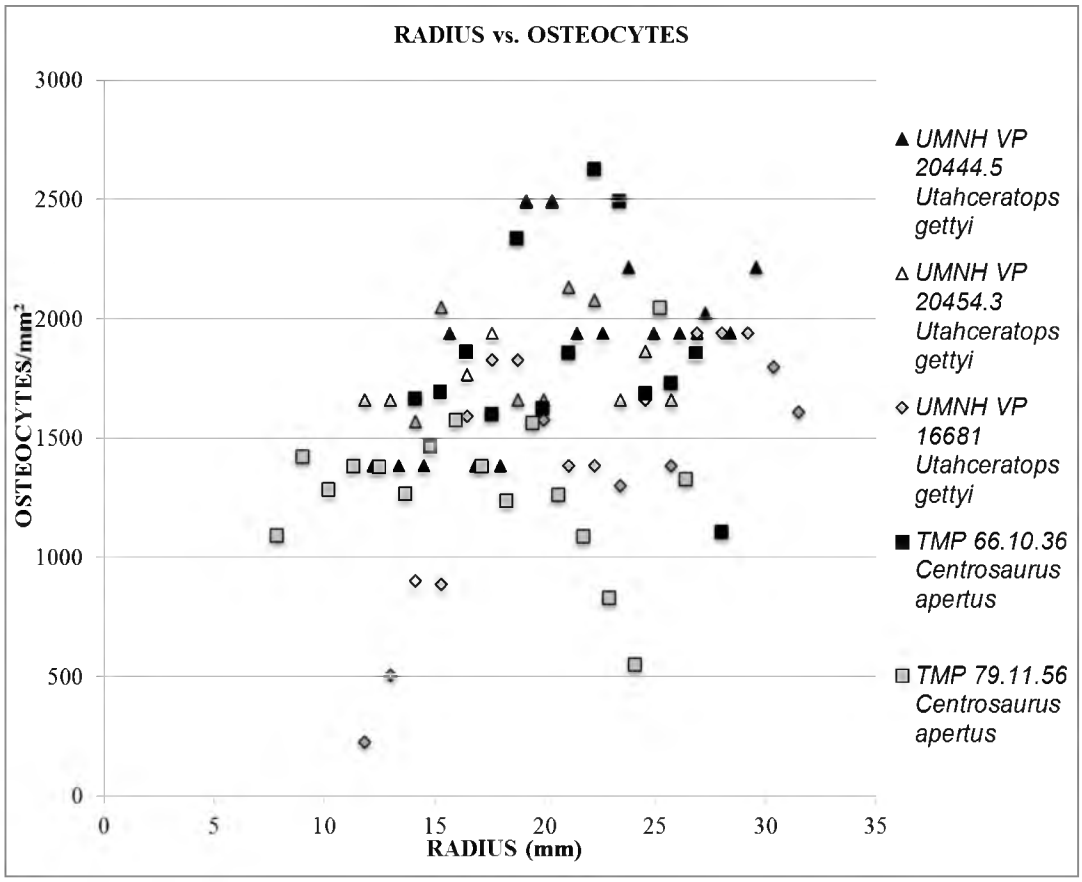
RADIUS vs. OSTEOCYTES
OSTEOCYTES/mm²
3000
2500
2000
1500
1000
500
0
0
5
10
15
20
25
30
35
RADIUS (mm)
UMNH VP 20444.5 Utahceratops gettyi
UMNH VP 20454.3 Utahceratops gettyi
UMNH VP 16681 Utahceratops gettyi
TMP 66.10.36 Centrosaurus apertus
TMP 79.11.56 Centrosaurus apertus

A

B

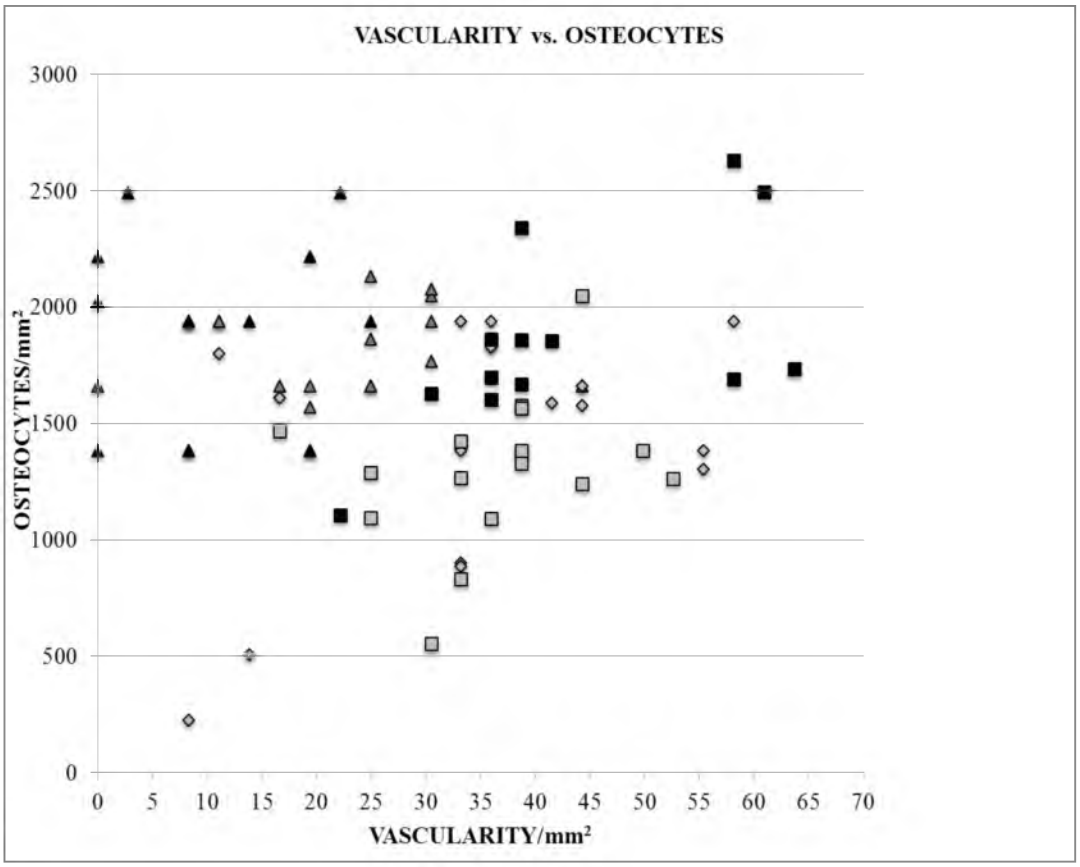

Figure 8 Continued.

C

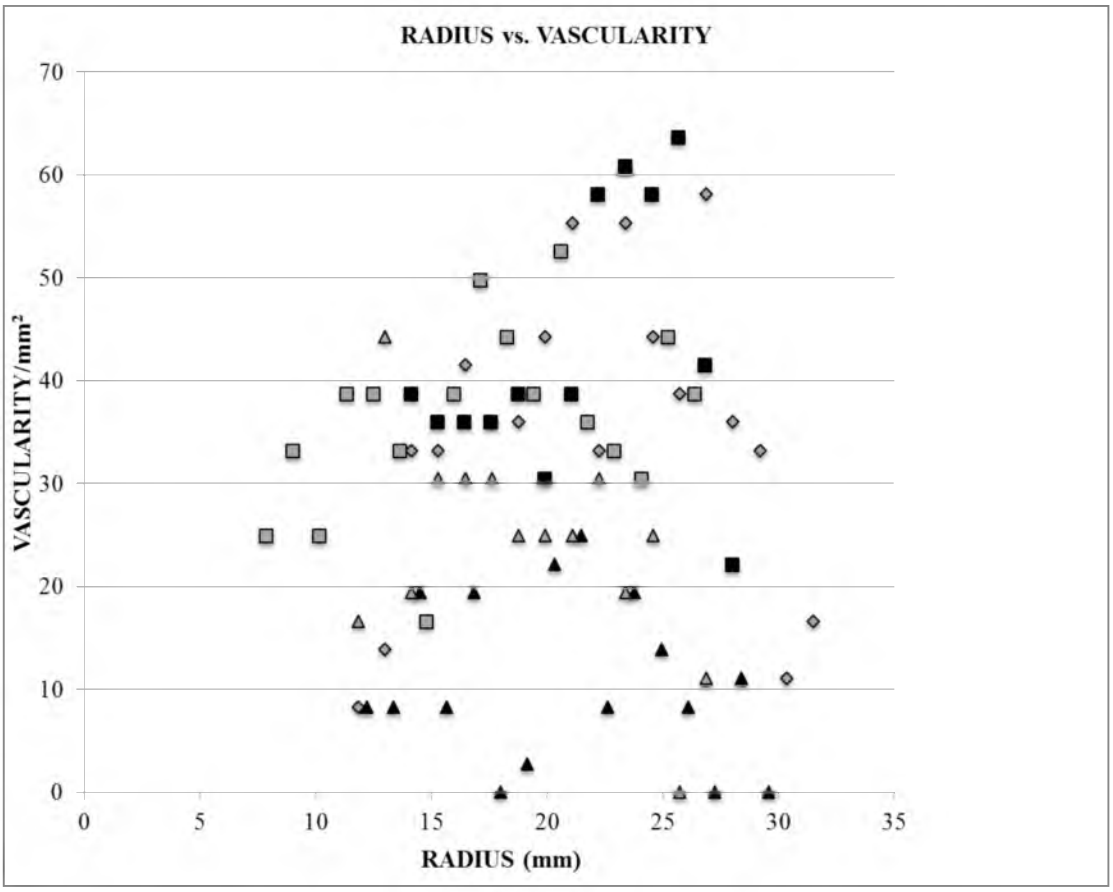

Figure 8 Continued.

Figure 9. Graphs that represent the data collected in the humeri analysis of the different taxa of ceratopsians. A. The radius of the element plotted against the osteocytes densities. B. The densities of the vascularity seen plotted against the osteocyte densities. C. The radius of the element plotted against the vascular densities.

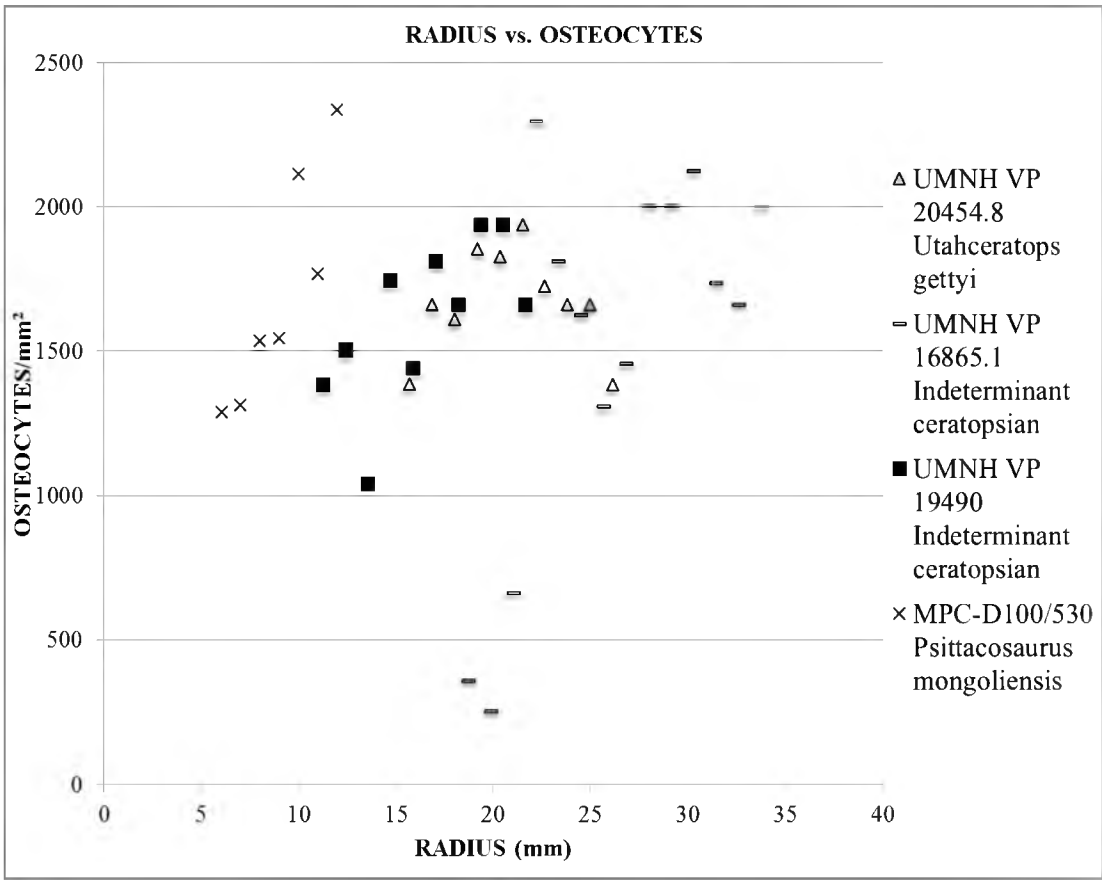
RADIUS vs. OSTEOCYTES
OSTEOCYTES/mm²
RADIUS (mm)
0
500
1000
1500
2000
2500
0
5
10
15
20
25
30
35
40
UMNH VP 20454.8 Utahceratops gettyi
UMNH VP 16865.1 Indeterminant ceratopsian
UMNH VP 19490 Indeterminant ceratopsian
MPC-D100/530 Psittacosaurus mongoliensis

A

B

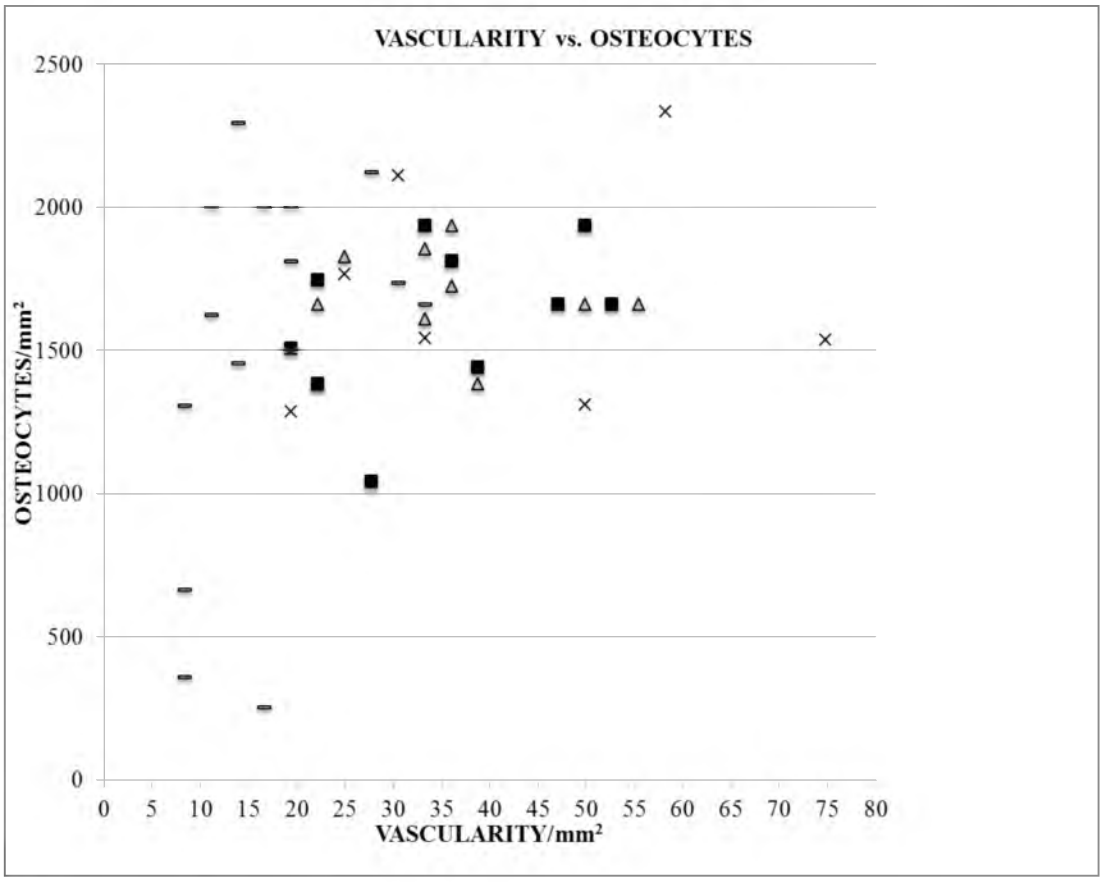

Figure 9 Continued.

C

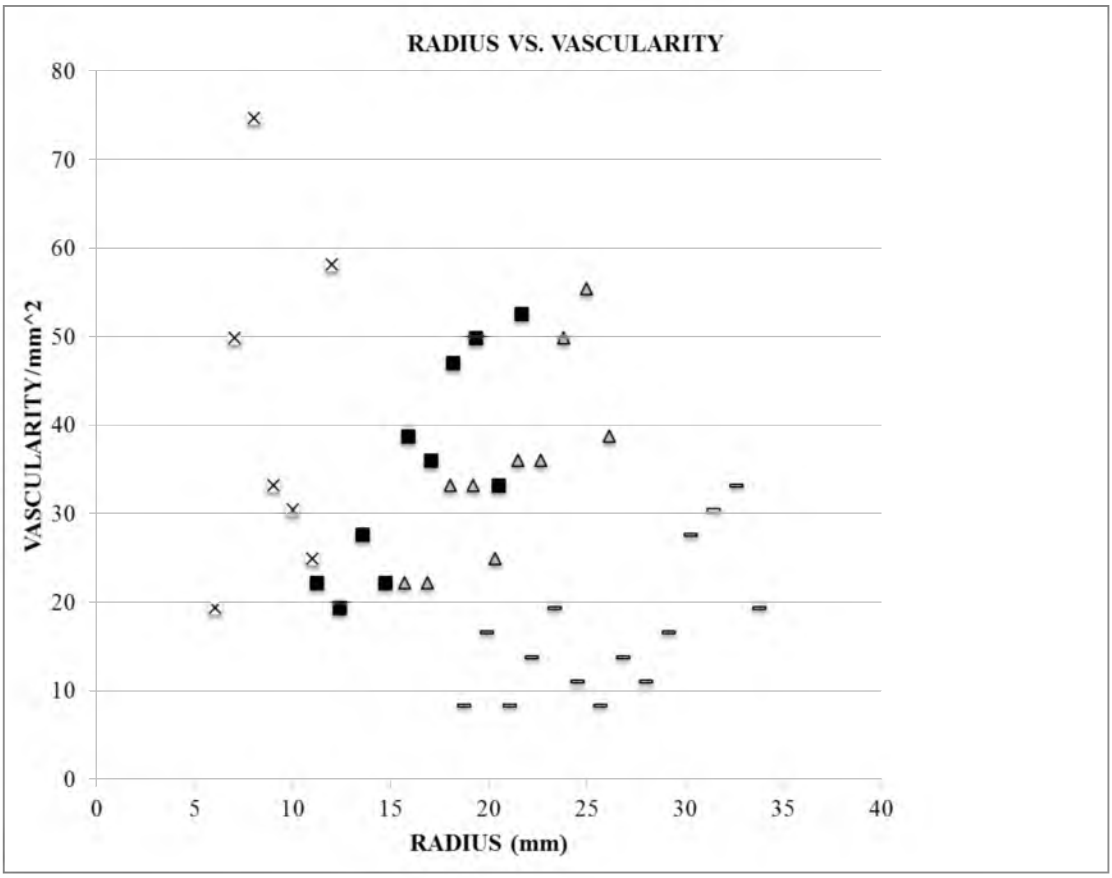

Figure 9 Continued.

RESULTS

Utahceratops gettyi Bone Histology

Humerus

UMNH VP 20444.1. This bone (Fig. 10) has a mid-diaphyseal circumference of 160 mm and has a complete length of 440 mm. It was sectioned at the midshaft, 150 mm from the distal end. The medullary cavity is 21.16 mm by 17.91 mm (long axis medial-laterally oriented) and is not crushed. A post-mortem fungal alteration (which is described in Trueman and Martill, 2002) dominates this bone and all sampled elements from UMNH VP locality 945 (Brandau and Irmis, 2011, 2012). This gives the microstructure a gritty or dirty appearance and obscures some of its detail. The fungal alteration is pervasive enough that it is not possible to observe osteocytes continuously throughout the cross section. There were trabeculae present at one time but I cannot identify the extent of them; there is an abrupt transition between the matrix infilling the medullary cavity and the bone tissue of the cortex. The bone tissue is dominated by woven collagen fiber orientation, although this was difficult to assess due to the fungal alteration. Secondary osteons encircle the medullary cavity and are evenly distributed. Where this occurs, observed collagen fiber orientation reflects the orientation of the fibers of the secondary bone tissue. Longitudinal canals, circular or elliptical in shape, make up the majority of the vascular canals, but some radial canals are present near the periosteum. The canals do not exhibit any orderly change in density. The ratio of simple

canals to primary and secondary osteons is 0:90:10, respectively. Histological details do not appear to change circumferentially, but they do change vertically from the medullary cavity to the periosteum. Evenly distributed secondary osteons are restricted to a narrow region encircling the medullary cavity. The bone does not preserve any LAGs. It does have a pronounced color change 2.5 mm from the periosteum (13 mm from the edge of the medullary cavity, and 22.2 mm from the middle of the medullary cavity), but this does not appear to be associated with any histological differences.

UMNH VP 20454.8. This bone (Fig. 10) possesses a mid-diaphyseal circumference of 145.1 mm and a preserved length of 210.3 mm. I sectioned this humerus at the approximate midshaft (neither distal nor complete proximal end is preserved). The medullary cavity internal to the cortex is 24.37 mm by 15.21 mm (long axis medial-laterally oriented) and shows no evidence of crushing. Fungal alteration is present, but the microstructure can be observed clearly. Trabeculae are not abundant, but those present near the medullary cavity comprise primary bone and are oriented at right angles to the medullary cavity rim. There is an abrupt transition between the cortical bone tissue and the infilled medullary cavity. No remodeling is apparent in the cortex of the bone. Under cross-polarized light the entire cortex displays woven collagen fiber orientation. The proportion of simple canals versus primary osteons and secondary osteons is 10:90:0 respectively, where the simple canals are restricted to the periosteum and the primary osteons make up the majority of the cortex. Simple canals are restricted to the periosteum, and no secondary osteons are present. The vascular canals are predominantly longitudinal, except at the periosteum, where the ratio of longitudinal to circumferential to radial canals is 16:14:8 canals per mm^2. From the edge of the

medullary cavity to the periosteum, there is a gradual increase in vascular canal density from 22 canals per mm^2 to 55 canals per mm^2. The vascular canals also change in size and shape, starting out fairly large encircling the medullary cavity, 0.111 mm by 0.049 mm, to more circumferential squat ellipses measuring 0.163 mm circumferentially and 0.018 radially. Osteocyte density is fairly uniform throughout the entire bone ranging from 1384 osteocytes per mm^2 to 1938 osteocytes per mm^2. A change of tissue characterized by elliptical, more reticular vascularity and more dense osteocytes is seen starting 2.5 mm internal from the periosteum (11 mm from the edge of the medullary cavity, 19 mm from the center of the medullary cavity). The matrix of the bone is mostly unchanged circumferentially except for some large vascular cavities, which are present on the anterior side of the bone and on both lateral sides, but not on the posterior side. They range in diameter from 3 μm to 3 mm. No LAGs are present.

Ulna

UMNH VP 20444.2. This ulna (Fig. 11) has a mid-diaphyseal circumference of 136 mm and has a complete length of 322 mm. This element was sectioned at the midshaft, 12.0 cm from the distal end. The medullary cavity internal to the cortex is 25.0 mm by 5.09 mm (medio-lateral axis and antero-posterior axis). Fungal alteration is pervasive in this bone, which makes some of the microstructure difficult to observe. Trabeculae are present but are so fractured and altered by the fungal invasion that further histological details could not be determined. There is a gradual transition between the compact bone tissue of the cortex and the trabeculae infilled medullary cavity. The cortex is woven-fibered bone throughout, but this is difficult to ascertain because of the

fungal alteration. The approximate proportion of simple canals versus primary osteons versus secondary osteons is 20:80:0, respectively, with predominantly primary osteons through the inner cortex and simple canals restricted to near the periosteum. The vascular canals are predominantly longitudinal and uniformly circular in shape, becoming smaller in diameter as they approach the periosteum. This vascular canal size change is associated with a color change at 4.0 mm from the periosteum, easily visible as a line on the polished section. The fungal alteration is so severe in this bone that osteocytes cannot be observed. This makes the color and vascularity change harder to see. There is no evidence of LAGs.

UMNH VP 20454.1. This element (Fig. 11) has a mid-diaphyseal circumference of 110 mm and has a complete length of 321 mm. This ulna was sectioned at the midshaft, 110 mm from the distal end. The bone is crushed antero-posteriorly into the medullary cavity, making accurate measurement of the cavity difficult. Like other specimens from this locality, fungal alteration is severe, making some of the microstructure difficult to observe. Neither cancellous bone nor trabeculae are present. There is an abrupt transition between the bone tissue of the inner cortex and the matrix infilling the medullary cavity. The collagen fiber orientation is dominated by woven fibered bone throughout the thin section. Vascular canals are predominantly longitudinal, comprised exclusively of primary osteons. The shape, size, and density of the vascular canals change throughout the section. Near the medullary cavity, canals are larger, more oblong and oriented radially. Approximately 3 mm away from the medullary cavity, the vascular canals become smaller, more circular, and more dense in a zone that is ~2 mm thick. For the final 2.5 mm adjacent to the periosteum, the vascular canals are more

circumferential and infilled with a black, opaque mineral. The fungal alteration is so severe that osteocytes are not clearly observable. No LAGs are present.

Femur

UMNH VP 16860. This femur (Fig. 12) has a mid-diaphyseal circumference of 250 mm, with a preserved femur length of 488 mm (the distal end is not preserved). The bone is antero-posteriorly crushed, which makes the medullary cavity a sigmodal shape instead of ovoid or circular. A small amount of cancellous bone is present, circumferentially outlining the medullary cavity. Preserved trabeculae comprise woven-fibered primary bone, and are arranged in an unordered web. The transition between the bone tissue of the cortex and the matrix-infilled medullary cavity is gradual because of the presence of trabeculae. Excluding the trabecular bone tissue, the majority of the tissue comprises secondary osteons, seen best in cross-polarized light. These secondary canals make the fiber orientation difficult to observe because the remodeling has obscured most primary bone tissue. No simple canals or primary osteons are visible. Longitudinal canals dominate, but radial canals are present sporadically between 9-16 mm away from the center of the medullary cavity. The density of the vascular canals does not seem to vary in an orderly fashion (Table 3). There are larger vascular canals, about 1 mm in diameter, which outline the medullary cavity and are deformed by the crushing. The density of the osteocytes generally increases towards the periosteum with osteocytes counts ranging from 1171 osteocytes per mm^2 to 2200 osteocytes per mm^2 moving nearer to the periosteum, but because the bone is primarily made up of secondary osteons, this density increase does not reflect the density of osteocytes of primary bone

tissue. No LAGs are present.

UMNH VP 12198. The mid-diaphyseal circumference of this element (Fig. 12) is 437 mm, with a preserved femur length of 874 mm (the distal end is incomplete). Because of its substantial size, a complete cross section was not made. Instead an 18 mm wide core was removed from the anterior surface of the mid-diaphysis of the bone. As a result, the full extent of the medullary cavity is unknown. The trabeculae present are composed of secondary osteons. Woven collagen fibers dominate, but this represents mostly secondary bone tissue in the form of secondary osteons, which are present throughout the cortex all the way to the periosteum. They are concentrated towards the medullary cavity, but form approximately 75% of vascular canals throughout the cortex in comparison to primary osteons, and no simple canals are observed. The vascular canals are primarily longitudinal in orientation with a few radial canals at the periosteum. The vascular canals near the medullary cavity are larger, approximately 0.5 mm in diameter, becoming progressively smaller towards the periosteum. Osteocytes are consistently dense through the section. No LAGs are apparent.

UMNH VP 20444.4. The complete femur length of this individual is 605 mm; I took the section (Fig. 12) from a location 245 mm from the distal end of the bone. The majority of the posterior side, however, is missing therefore a full circumference measurement was not possible, but it can be estimated at around ~200 mm. The medullary cavity is approximately 47 mm by 26 mm, although the second measurement was estimated because of incompleteness of the element. Minimal cancellous bone is present and no trabeculae are apparent. There is an abrupt transition between the cortical bone tissue and the matrix-infilled medullary cavity. The entire bone comprises woven

collagen fibers. Vascular canals are all primary osteons except outlining the medullary cavity where a few (10% of the total matrix) secondary osteons are present. Simple canals are rare if present. Vascular density remains consistent throughout the section, from the medullary cavity towards the periosteum, and the vascular canals are predominantly longitudinal in orientation, with a few radial canals in the inner cortex. Longitudinal canals are larger (about 0.19 mm in diameter) nearer to the medullary cavity and become progressively smaller (0.08 mm) and more uniform moving from the medullary cavity outward to the periosteum. The density of the canals ranges from 8 canals/mm^2 to 19 canals/mm^2, and average around 8 canals/mm^2 throughout the section. Osteocyte density does not vary drastically, ranging from just under 1000 osteocytes per mm^2 to 1578 osteocytes per mm^2. Moving closer to the periosteum, 34.5 mm from the medullary cavity, average osteocyte density is higher so that it ranges from 1384 to 1578 per mm^2.

A change in tissue or a pause in growth may be present because both the thin section and polished section display at least two concentric color changes, one 10.72 mm from the periosteum, and the second 18.57 mm away. These color changes are linked with an alignment and size increase of vascular canals. Until this point, the vascular canals were unordered and not arranged in a certain way. At these color changes, the vascular canals organize and align themselves along the color band. These canals also become slightly larger near the color changes. The two bands are not diagnostic of a LAG because they do not birefringe under cross-polarized light or show any momentary cessation of growth (cf. Chinsamy, 1994).

UMNH VP 20454.5. The femur has a mid-diaphyseal circumference of 230 mm

and a preserved length of 291 mm (as both the distal end and the proximal end are incomplete). The medullary cavity internal to the cortex is 61.55 mm (along the long axis of the cross section) by 28.16 mm and there is no evidence for crushing. Trabecular bone is extensive and circumferentially lines the exterior of the medullary cavity. The trabeculae comprise primary bone tissue and are arranged in a reticular pattern. There is an abrupt shift between the end of the trabeculae and the infilled medullary cavity. Fungal invasion is also present but does not obscure fine details such as osteocytes. The bone tissue possesses a woven collagen fiber orientation (Fig. 13). The extent of simple canals versus primary canals versus secondary canals is 5:65:30, respectively, with simple canals occurring predominantly near the periosteum, primary osteons making up the bulk of the cortex, and secondary osteons uniformly distributed around the circumference of the medullary cavity. Vascular canal density and orientation do not change throughout the section. Four zones unique in color, size and shape of vascular canals, and mineral infilling can be observed. Zone one is nearest the medullary cavity and is ~2.4 mm thick. Here, the vascular canals are primary longitudinal, vary in shape from circular to elliptical, and have a density ranging from 13-44 vascular canals/mm^2. Zone two is lighter colored, ~3 mm thick, and is dominated by longitudinal canals that are ovoid in cross-section. The vascular density ranges from 16-36 canals/mm^2. Zone three is darker, consisting of larger, denser longitudinal vascular canals, possessing an elliptical shape with the long axis of the ellipse oriented medio-laterally. This zone is 4.2 mm thick, with vascular densities varying from 11-41 canals/mm^2. The exterior-most zone has a distinct appearance. In contrast to the aforementioned vascular canals, which are infilled with quartz, the canals in this zone are filled with some type of opaque black

mineral. The longitudinal vascular canals range from circular to elliptical in cross-section; a reticular organization is prominent, with the highest vascular canal density being ~50 canals per mm^2. This zone is approximately 0.6 mm wide, and ends at the periosteum. Osteocyte density does not change through the entirety of the thin section (Table 3). There is no evidence of radial canals or LAGs. The cessation of zone one and the beginning of zone four can be observed on the surface of the polished section, but this does not exhibit the histological characteristics that define a true LAG.

Tibia

UMNH VP 16681. This element has a mid-diaphyseal circumference of 102 mm and a complete length of 450 mm. This tibia (Fig. 14) was sectioned at the midshaft, 22.2 cm from the distal end. The medullary cavity dimensions are 34.62 mm (long axis) by 14.34 mm. There is some posterio-medial crushing. This makes the medullary cavity subcircular and means the posterior edge of the bone is crushed, which makes the histology difficult to follow circumferentially. The trabeculae that are still attached to the lining of the medullary cavity are arranged in an unordered web. Preserved trabeculae are abundant, infill the entire medullary cavity, and are composed mainly of primary bone tissue. Osteocytes appear to have a consistent density throughout the cortex. Vascular canal density also does not seem to change through the section. Longitudinal canals dominate, although a few radial canals are present throughout the cortex, particularly in the vicinity of the periosteum. Reticular canals are also present but not dominant. The bone tissue is dominated by well defined secondary osteons, which rim the spaces between the trabeculae. Because the cortical bone is composed primarily of

secondary osteons, observing the collagen fiber orientation primary bone tissue is impossible. The ratio of simple to primary to secondary osteons is 10:0:85 respectively, with secondary osteons making up the majority of the bone extending circumferentially around the medullary cavity, and simple canals restricted to the periosteum. No LAGs or abrupt color changes were observed.

UMNH VP 20444.5. This tibia (Fig. 14) has a mid-diaphyseal circumference of 189 mm, a complete length of 465 mm and shows no evidence of crushing. The element was sectioned at the midshaft, 24.0 cm from the distal end. The medullary cavity internal to the cortex is 26.30 mm (along the long axis) by 19.40 mm. Trabeculae are absent and the transition from the bone tissue of the cortex and the matrix-infilled medullary cavity is abrupt. Fungal invasion is present throughout the whole cross-section of this element, making some of the microstructure, specifically osteocytes, difficult to see. The collagen fiber orientation is extremely difficult to observe because of the fungal degradation, but it appears the bone is composed of woven collagen fibers. This histology is uniform circumferentially. The bone is almost completely composed of primary osteons and only a few secondary osteons are observed at the periosteum, making a thin rim outlining the edge of the bone. The ratio of primary to secondary osteons throughout the cortex is 95:5. The density of vascular canals changes across the radius of the bone, but not in any increasing or decreasing order. The vascular canal density ranges from less than 1 to 24 canals/mm^2, with the cross-sectional shape of the longitudinal vascular canals being primarily circular in cross section. Moreover, the osteocytes do not exhibit an orderly transition in density, ranging from 1384 to 2492 osteocytes/mm^2.

Three circumferential color changes are present that were initially interpreted as

LAGs (Levitt, 2011). However, upon further investigation, these color changes do not exhibit the characteristics that define a LAG; that is, they do not show a distinct cessation in growth that is birefringent under cross-polarized light and can be observed around most or all of the bone's circumference. These color changes may reflect heterogeneities in preservation mode, but they do seem to be linked to growth, because the nature of vascularity changes slightly across the boundaries. The first zone of distinct color is approximate 3 mm thick and lies closest to the medullary cavity. The vascular canals are larger than the canals closer to the periosteum, ~0.009 mm in diameter, therefore there are fewer canals per mm^2 (about 8 canals/mm^2, located 12 mm from the center of the medullary cavity). Zone two, beginning at 15 mm from the center of the medullary cavity, is 9 mm thick, and has highly variable vascular canal density, from less than 1 to 25 canals/mm^2. Zone three, starting 24 mm from the center of the bone, is slightly darker in color, approximately 2.5 mm thick, and has a vascular density of 8-19 canals/mm^2. Zone four, starting at 26.5 mm from the center, is even darker, with larger vascular canals that are more elliptical in cross section, ranging from less than 1 to 11 canals/mm^2. Finally, a rim of different colored bone tissue, composed mostly of secondary osteons, outlines the periosteum. Some radial canals are present in this area.

UMNH VP 20454.3. This element (Fig. 14) has a mid-diaphyseal circumference of 167 mm and a preserved length of 231 mm. Both proximal and distal ends are missing. This tibia was sectioned at the midshaft, 167 mm from the distal end. The medullary cavity internal to the cortex is 19.34 mm in diameter and the cross section is circular in shape. Trabeculae are absent and there is an abrupt change between the bone tissue of the cortex and the matrix-infilled medullary cavity. This element shows

evidence of fungal effects but not so extensively as to obscure the microstructure. This tibia is composed entirely of woven collagen fibers. The density of osteocytes is fairly consistent throughout the whole bone, averaging 1760 per mm^2, varying from 1570 per mm^2 at a distance of 14 mm from the center, to 2132 osteocytes per mm^2 at a distance of 21 mm from the center of the medullary cavity. Vascular canals are dominantly primary osteons. The vascular canal density is consistent through the inner cortex averaging ~ 24 canals per mm^2, but then decreases to ~11 canals per mm^2 in density near the periosteum. Vascular canal orientation is predominantly longitudinal, but circumferential vascular canals are also present between 1.92 mm and 4.81 mm from the edge of the periosteum. A change in color is present 1.74 mm from the edge of the periosteum. This is not associated with a change in the density or orientation of vascular canals, but there is a slight change in osteocyte density (from 1661 to1938 osteocytes per mm^2) towards the periosteum. This dark brown color may be due to the high density of osteocytes or may represent a larger concentration of fungal invasion. The histology is not uniform circumferentially. On the anterior and right lateral side near the medullary cavity are large cavities ranging in size from 3 microns to 3 mm in diameter. Also, the density and size of the vascular canals decreases on the lateral posterior side of the element. No LAGs are present.

Indeterminate limb shaft

UMNH VP 16861. This element, recovered from UMNH VP locality 942, is crushed and broken to the extent that precise identification is impossible, but it is obviously some sort of limb bone shaft. This bone has a circumference of 180 mm where

it was sectioned and has a preserved length of 180 mm. The medullary cavity internal to the cortex is completely crushed, and anatomical orientation of the crushing cannot be determined. The trabeculae comprise largely primary bone tissue with occasional secondary osteons. No order can be seen in the orientation of the trabeculae because of the crushing. In crossed-polarized light, the bone tissue is entirely woven-fibered bone; however, the bone tissue is primarily secondary osteons, so the collagen fiber orientation of primary bone tissue is unknown. Vascular canals are predominantly longitudinal canals that are circular in cross section, and their density is fairly uniform throughout the cortex. Osteocytes also are dispersed evenly throughout the bone tissue and do not seem to increase or decrease in density through the section. No LAGs are present.

Ribs

UMNH VP 12198. The circumference of this rib shaft at its point of sectioning is 58.0 mm. A cavity preserved in the center of the bone is filled with cancellous bone. Trabeculae are composed of primary bone rimmed with secondary tissue. The majority of the element (Fig. 15) consists of remodeled bone (i.e., secondary osteons), only 10% of the vascular canals are primary osteons. The vascular canals are entirely longitudinal and uniform in density throughout the bone. The trabeculae form a uniform network of primary bone tissue in the center, and the secondary osteons make up the bulk of the cortex. Because this bone is dominantly composed of secondary osteons, the collagen fiber orientation of primary bone tissue is undistinguishable. Osteocytes are uniformly dense throughout and there is no evidence of LAGs.

UMNH VP 20454.7. The circumference of this rib (Fig. 15) shaft is 75.0 mm.

Trabeculae comprise primary bone rimmed with secondary tissue, and make up an unordered web in the center of the cross section. Some fungal alteration is evident, but not enough to obscure the microstructure. The majority of vascular canals are longitudinally-oriented secondary osteons. Some primary osteons are present in the inner cortex, and their ratio with secondary osteons is 30:70. The diameter of the canals is larger in the interior of the bone, becoming smaller closer to the periosteum. The histology of this bone is uniform circumferentially. The preponderance of secondary osteons means that determining collagen fiber orientation of primary bone tissue is impossible. No LAGs are present.

Ossified tendons

UMNH VP 12198. The circumference of the sampled tendon fragment is 44.0 mm. It is composed entirely of remodeled bone (Fig. 15), and filled with compacted longitudinal canals, all circular in cross section, and no radial or circumferential canals. Because the tissue is composed of all secondary osteons, the orientation of primary tissue collagen fiber orientation is impossible to determine. No LAGs are present.

UMNH VP 20454.9. The circumference of this tendon (Fig. 15) fragment is 40 mm. The section itself measures 16.12 mm by 8.14 mm. Fungal alteration is evident, but is not as severe as in most of the limb bones from this same site. No cavity is present in the element's interior, but vascular spaces are larger towards the center of the cross section. The few visible trabeculae comprise primary bone rimmed with secondary tissue. Vascular canals are 90% secondary osteons, and all canals are longitudinally oriented, which decrease in diameter and increase in density towards the periosteum.

Because most of the tissue comprises secondary osteons, determining primary tissue collagen fiber orientation is impossible. There is no evidence of LAGs.

Kosmoceratops richardsoni Bone Histology

Femur

UMNH VP 17000. This femur (Fig. 12) was highly fragmented when recovered, and therefore the diaphyseal fragments used for this study may not have been from the exact mid-diaphysis. Based on the proportions of the femur and the sacrum of the specimen NHMUK R4948 of *Chasmosaurus belli* (Maidment and Barret, 2011), I estimate the femur length of UMNH VP 17000 to be approximately 100 cm, with a midshaft circumference of 45 cm. Two pieces were sectioned for study, both with incomplete cortex preservation, and thus their total circumference is unknown. The first fragment, UMNH VP 17000A with a maximum width of 72.2 mm, is dominated by cancellous bone that is fragmented by postmortem crystallization. This cancellous bone represents extensive trabeculae that underlie the cortex of the bone. The trabeculae are mainly composed of primary tissue, with some secondary osteons visible, and there is no apparent order to the trabecular organization. This bone's histology cannot be followed circumferentially because only one area preserves the original cortex. The cortex is almost entirely composed of secondary osteons with a concentrated rim of secondary osteons near the periosteum. The collagen fiber orientation of any primary tissue is hard to distinguish because of the abundance of secondary osteons, but the remodeled tissue is composed of woven fibered bone (Fig. 13). Both radial and longitudinal vascular canals are present, but the longitudinal canals dominate. There is no apparent order to the

occurrence of radial canals, and canal density also varies widely with no apparent pattern, ranging from 16 canals/mm^2 at 19 mm from center of the bone to 47 canals/mm^2 20 mm from the center of the bone. Osteocyte density also lacks any apparent pattern, ranging from 1315 osteocytes/mm^2 at 18 mm from the center of the bone to 2021 osteocytes/mm^2 at 22 mm from the center of the bone. These osteocytes densities represent remodeled tissue. No LAGs are present.

The second sectioned bone fragment from the femur, UMNH VP 17000B, has a preserved length of 80.9 mm (although this does not reflect the full dimensions of the femur) with a maximum width of 72.6 mm. The medullary cavity is infilled with matrix and cancellous bone that form extensive trabeculae; these have been fragmented by crystallization. The trabeculae are composed mostly of primary bone rimmed with secondary tissue. The trabeculae make up a reticular network of ellipses. The vascular canals, mostly longitudinal with some radial examples, are mostly secondary osteons, with some primary osteons present in the trabeculae. The secondary osteons are so dense that primary tissue collagen fiber orientation cannot bee seen. This vascular canal orientation is consistent across the thin section. Osteocytes are dense throughout the bone tissue. No LAGs are present.

UMNH VP 21339. The preserved length of this femur is 670 mm (with the distal end missing). This bone (Fig. 12) was sectioned at the midshaft of the femur, 44.0 cm from the proximal end. This bone was crushed dorsoventrally, preventing an accurate measurement of the midshaft circumference. Based on the preserved portion of this element, I estimate the circumference at ~400 mm. Trabeculae are not very extensive but are composed primarily of primary bone and form an unordered network. The original

collagen fiber orientation cannot be surmised because the bone tissue is dominated by secondary bone tissue. Although dominated by secondary osteons (Fig. 16), the cortex consists of ~5% primary tissue. All vascular canals are longitudinal with their density varying widely without any apparent pattern, ranging 22 canals/mm^2 at 5 mm from the center of the bone, 22 canals/mm^2 at 9 mm from the center of the bone, and 3 vascular canals/mm^2 at 18 mm from the center of the bone. Osteocyte density also varies in an unordered way, ranging from a density of 698 osteocytes/mm^2 at 4.0 mm from the center of the bone, to 2162 osteocytes/mm^2 at 14.5 mm from the center of the bone, and 1262 osteocytes/mm^2 at 18 mm from the center of the bone. However, these values largely represent the osteocytes densities of remodeled tissue. The histology of the bone is uniform circumferentially around the bone, with the larger vascular canals encircling the crushed medullary cavity and then decreasing in size further out towards the periosteum. No LAGs are apparent.

Indeterminate ceratopsid humeri

UMNH VP 16865.1. This element has a mid-diaphyseal circumference of 189 mm and has a complete length of 545 mm. This humerus (Fig. 10) was sectioned at the midshaft, 182 mm from the distal end. The medullary cavity internal to the cortex is 28.98 mm at the long axis by 24.97 mm, and is not crushed. Trabeculae are an extensive network with spaces between the trabeculae made of circles and ellipses that extend throughout the medullary cavity. The trabeculae are composed mainly of primary bone tissue. Where primary tissue still dominates, it appears to be made up of woven collagen fibers, but the abundance of secondary osteons makes this uncertain. The proportion of

simple canals versus primary osteons versus secondary osteons is 0:60:40. Most of the secondary osteons are located at or near the medullary cavity. Through the section, vascular canals change in size, starting larger closer to the inner cortex, and smaller towards the periosteum. Similarly, the shape of the longitudinal vascular canals change from circles to flattened ellipses that are more circumferential near the periosteum. In contrast, canal density does not follow this pattern, ranging from 8 canals/mm^2 at 18 mm from the center of the bone to 30 canals/mm^2 at 31 mm from the center of the bone. The density of the osteocytes does not follow a clear pattern either, averaging ~1456 osteocytes/mm^2, but varying from 254 osteocytes/mm^2 at 20 mm from the center of the bone to 2295 osteocytes/mm^2 at 22 mm from the center of the bone. Although no observable LAGs are present, a change in color is present, likely associated with a shift in microstructure. This change occurs 2 mm from the periosteum and is ~0.5 mm thick. In this zone, the osteocytes appear less dense, the vascular canals are more elliptical in shape, and vascular canal density decreases. The histology is uniform circumferentially with the secondary osteons encircling the medullary cavity and the rest of the bone comprising primary tissue.

UMNH VP 19490. This humerus (Fig. 10) has a mid-diaphyseal circumference of 204 mm and has a preserved length of 167.6 mm (the proximal and distal ends are not preserved) and was sectioned at the midshaft. The medullary cavity is 40.29 mm by 23.65 mm. There has been a little crushing on the anterior side but it has not skewed the shape of the medullary cavity. Trabeculae composed of primary bone but rimmed with secondary tissue form an unordered web that fills the entire medullary cavity. The cortex is dominated by secondary osteons so the collagen fiber orientation of the primary tissue

cannot be observed. A few primary osteons occur near the medullary cavity, but they comprise only ~10% of the vascular canals. The vascular canals are primarily longitudinal, mostly circular in cross section, with some radial canals adjacent to the periosteum. The vascular canals gradually increase in density towards the periosteum; 11 mm from the center of the bone has 22 canals/mm^2, whereas 21 mm from the center the bone has a density of 52 canals/mm^2 (Fig. 17). The variation in osteocyte density shows no apparent order, ranging from 1041 osteocytes/mm^2 at 13 mm from the center of the bone to 1938 osteocytes/mm^2 at 19 mm from the center of the bone. However, these values represent the osteocyte density of largely remodeled tissue. The bone histology is uniform circumferentially. No LAGs or abrupt changes in tissue type are present.

Summary of Histological Trends

The study sample of *Utahceratops* elements derived from the articulated individual at UMNH VP locality 945 (UMNH VP 20444.4 - femur, UMNH VP 20444.5 - tibia, UMNH VP 20444.1 - humerus, and UMNH VP 20444.2 - ulna) are dominated by primary osteons that are oriented longitudinally. Both the tibia and humerus display a few radial canals near the periosteum. Although almost all of the elements show significant color changes throughout the section, none exhibit orderly changes in vascular canal or osteocyte density. There is no evidence of LAGs or EFS in any of the bones from this animal. In all of the elements present, the collagen fibers are primarily woven. All bones from this individual are composed of mostly primary bone tissue and primary vascular canals. The collagen fiber orientation in all of the bones is woven. Therefore, I conclude that this animal was growing rapidly at the time of death. Because this animal appeared

to grow rapidly, there are no lines of arrested growth present, there is a low amount of remodeling, and the maximum preserved lengths of these bones are small relative to the largest examples of this taxon, I conclude that this animal is a juvenile individual.

The study elements from the disarticulated individual found at locality 945 (UMNH VP 20454.5 - femur, UMNH VP 20454.3 - tibia, UMNH VP 20454.8 - humerus, UMNH VP 20454.1 - ulna, UMNH VP 20454.7 - rib, and UMNH VP 20454.7 - tendon) are all dominated by longitudinal primary osteons. In all of these specimens, osteocyte density was consistent through the bone. The ribs consist of mostly secondary osteons, but this likely reflects a higher rate of remodeling for these elements relative to limb bones. Once again, although all of the limb bones show distinctive color changes, none of these bones contain LAGs. All of these limb bones are dominated by woven collagen fiber orientation. The femur, tibia and humerus all have trabeculae composed of primary bone. Because all of the bones from this animal are composed of primary bone tissue and primary vascular canals, and the collagen fiber orientation is woven, I conclude that this animal was growing rapidly at the time of death. Because of this rapid growth, the lack of remodeling, the absence of LAGs, and that the maximum preserved lengths of these bones are small relative to the largest examples of this taxon, I conclude that this animal was juvenile at the time of death.

UMNH VP locality 942 is a disarticulated bonebed that contains the remains of a minimum of three individuals of *Utahceratops*. Although the bones from this site cannot be assigned to particular individuals, they do share several microstructure characteristics. All of the elements in the study sample (UMNH VP 16860 - femur, UMNH VP 16681 - tibia, and UMNH VP 16861 – indeterminate limb shaft) possess trabeculae that are made

of unordered primary bone. All three bones express woven collagen fiber orientation and are dominated by secondary osteons. Most of the vascular canals are longitudinal, but they all contain some radial canals as well. No LAGs were observed. The femur (UMNH VP 16860) as well as the limb shaft (UMNH VP 16861) are from adult individuals based on the high degree of remodeling and large size. The tibia sectioned from this site (UMNH VP 16681) represents a smaller, subadult animal based on the presence of some simple and radial canals, and its smaller size, indicating that its was growing faster than the femur at time of death.

The elements sectioned from UMNH VP 12198 (femur, rib, and tendon) are from a single disarticulated individual of *Utahceratops*. All are dominated by secondary osteons with both the rib and the tendon being almost completely remodeled. Longitudinal vascular canals and dense osteocytes dominate all three elements. No LAGs are present. These characteristics, in addition to the large size of the femur, (complete length 874 mm and midshaft circumference 437 mm), suggests that this animal was an adult at the time of death.

The femur fragments from the holotype specimen of *Kosmoceratops* (UMNH VP 17000) share many similar histological attributes with UMNH VP 12198. In both sections, trabeculae are extensive and fill the medullary cavity. Both are dominated by longitudinally-oriented secondary osteons. No LAGs are present. These data suggest the individual was an adult. UMNH VP 21339 is a femur from a referred disarticulated specimen of *Kosmoceratops*. This bone is dominated by secondary osteons that are primarily longitudinally oriented. The osteocytes are dense throughout the bone, although these values represent remodeled tissue. This animal has not deposited LAGs or EFS.

These data, along with the large size of the femur, suggest the individual was an adult.

The indeterminate ceratopsid humerus (UMNH VP 16865.1) from UMNH VP locality 512 primarily consists of secondary osteons, but some primary osteons are present. The orientation of the canals changes from longitudinal to more circumferential moving nearer to the periosteum. No LAGs or EFS are present. Taken together, these data suggest the animal was still growing when it died. Perhaps this individual represents a subadult. This determination as a subadult is strengthened by the presence of more remodeling present in this bone than seen in the bones indicated as belonging to juvenile individuals. The second indeterminate ceratopsid humerus (UMNH VP 19490) possesses some similar histologic characteristics, but possesses a higher proportion secondary osteons, indicative of extensive remodeling. The vascular canals are predominantly longitudinal in orientation. This animal was most likely a subadult at the time of death based on the remodeling.

In sum, the bones sampled in this study represent a distribution of ontogenetic stages for *Utahceratops* and *Kosmoceratops*. The two *Utahceratops* from UMNH VP locality 945 (UMNH VP 20444 and UMNH VP 20454) are juvenile individuals of *Utahceratops* based on the high degree of vascularity, the low degree of remodeling, and the relatively short limb bone lengths. *Utahceratops* specimens representing a range of age classes were preserved at UMNH VP locality 942. The femur sampled (UMNH VP 16860) as well as the limb shaft (UMNH VP 16861) are from adult individuals, based on the high degree of remodeling (Fig. 18) and large size. The tibia sectioned from this site (UMNH VP 16681) pertains to a smaller, subadult animal, with a more moderate amount of remodelling. UMNH VP 12198 is an adult *Utahceratops*, based on the density of

secondary osteocytes present in the cortex of this element as well as its overall size. Both individuals of *Kosmoceratops* (UMNH VP 17000 and UMNH VP 21339) represent adult individuals with extensive remodeling, and compare well histologically with the *Utahceratops* inferred adults.

Figure 10: Cross sections of the humeri in this study. A. UMNH VP 20454.8; B. UMNH VP 20444.1; C. UMNH VP 19490; D. UMNH VP 16865.1. Arrow A indicates the anterior direction of the element and the L points to the lateral direction of the element.

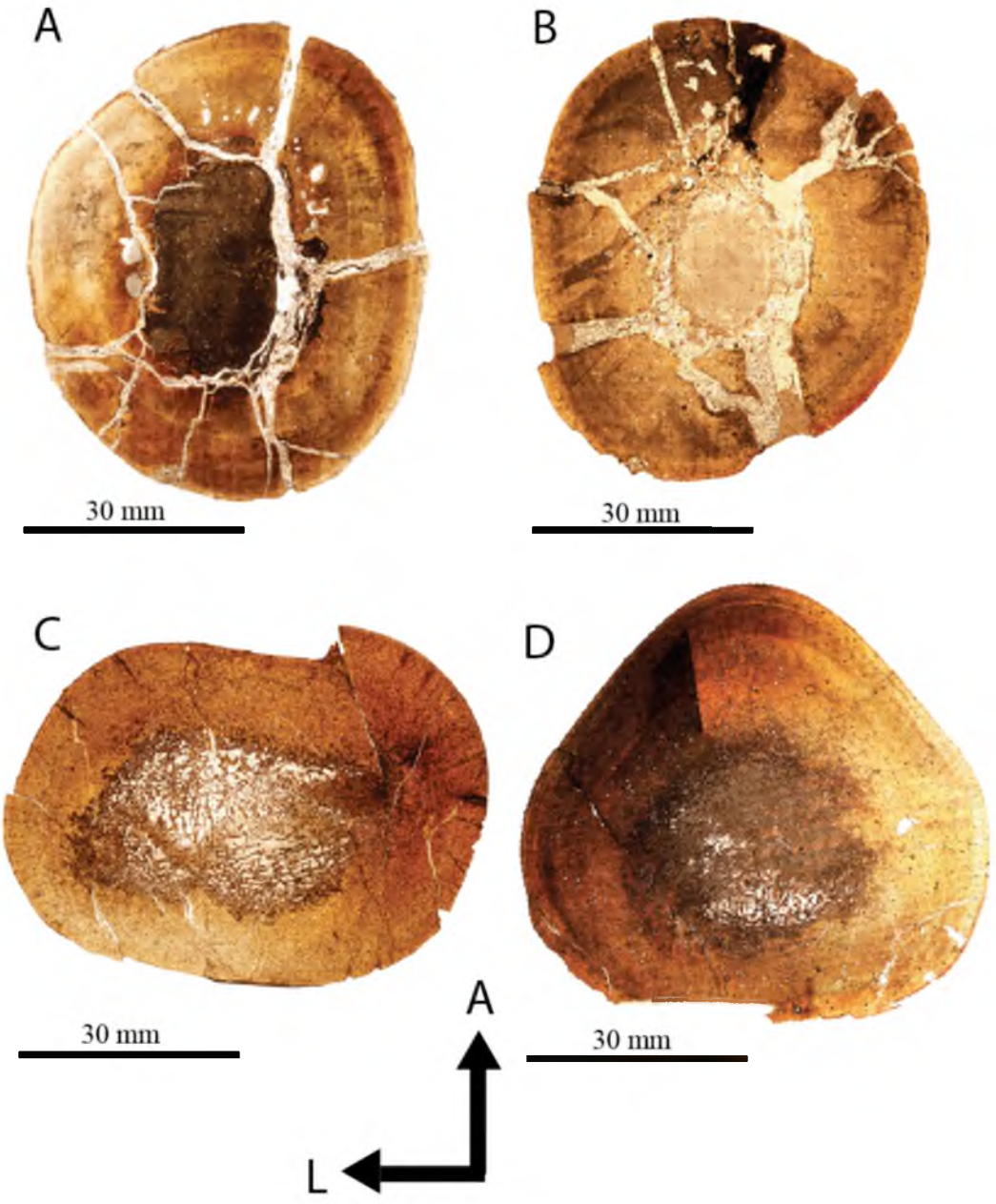
A
30 mm
B
30 mm
C
30 mm
D
30 mm
A
L

Figure 11. Cross sections of unlae sectioned for this study. A. Ulna UMNH VP 20454.1; B. Ulna UMNH VP 20444.2

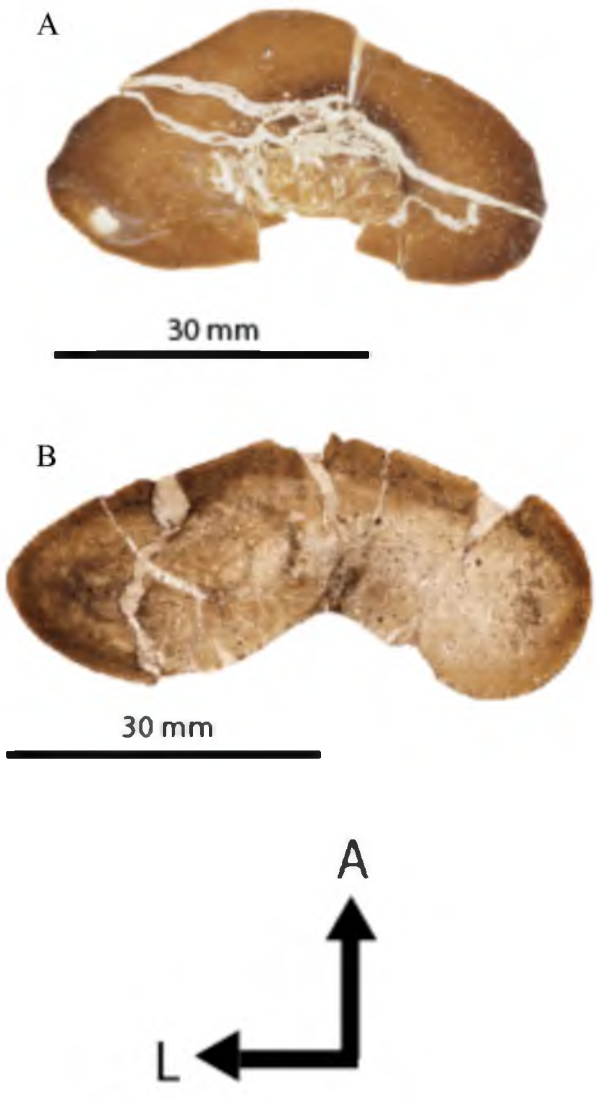
A
30 mm
B
30 mm
A
L

Figure 12. Cross sections of femora sectioned for this study. A. UMNH VP 20444.4; B. UMNH VP 20454.5; C. UMNH VP 16860; D. UMNH VP 21339; E. UMNH VP 12198; F. UMNH VP 17000. A points towards the anterior side of the element and L points laterally.

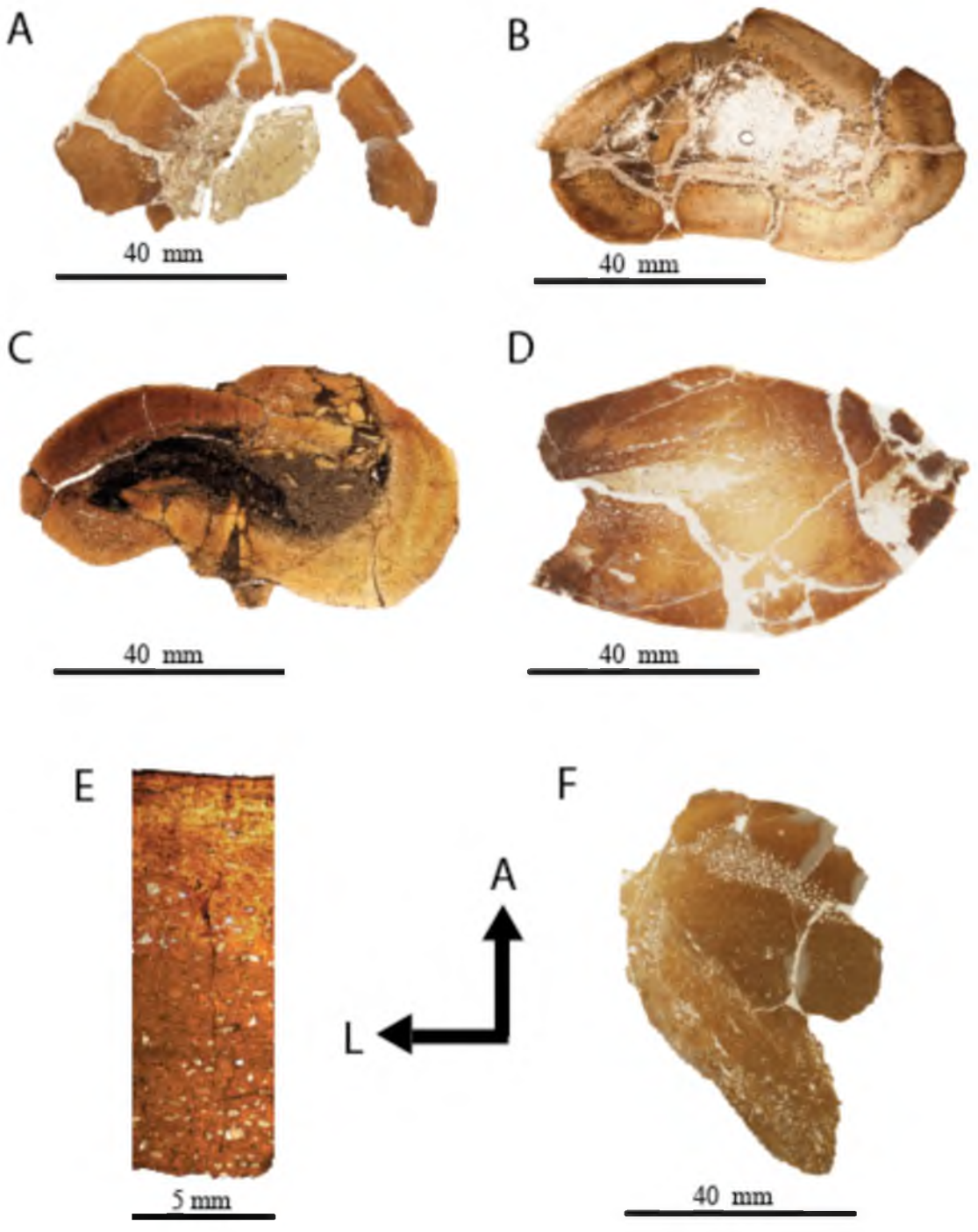
A
40 mm
B
40 mm
C
40 mm
D
40 mm
E
5 mm
A
L
F
40 mm

Figure 13. Close up images of the collagen fiber orientation of three representative bones. All bone tissue exhibits woven collagen fiber orientation. A. Left femur, UMNH VP 20454.5, of a juvenile animal *Utahceratops gettyi* from LOC 945. B. Right Femur, UMNH VP 16860, of an adult *Utahceratops gettyi* from LOC 942. C. Femur fragment from UMNH VP 17000 of an adult *Kosmoceratops richardsoni*.

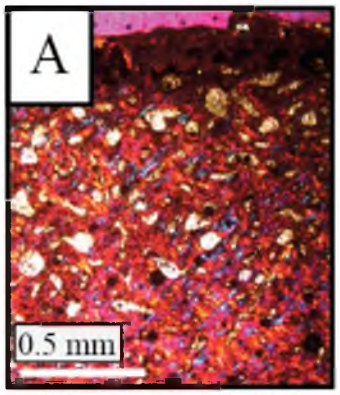

UMNH VP 20454.5

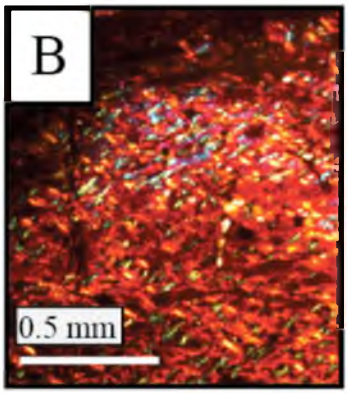

UMNH VP 16860

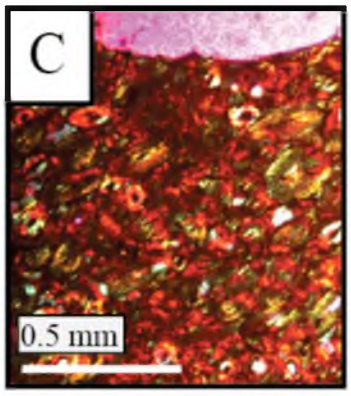

UMNH VP 17000

Figure 14. Cross sections of tibiae sectioned for this study. A. Tibia UMNH VP 20454.3; B. Tibia UMNH VP 20444.5; C. Tibia UMNH VP 16681. A points towards the anterior side of the element and L points laterally.

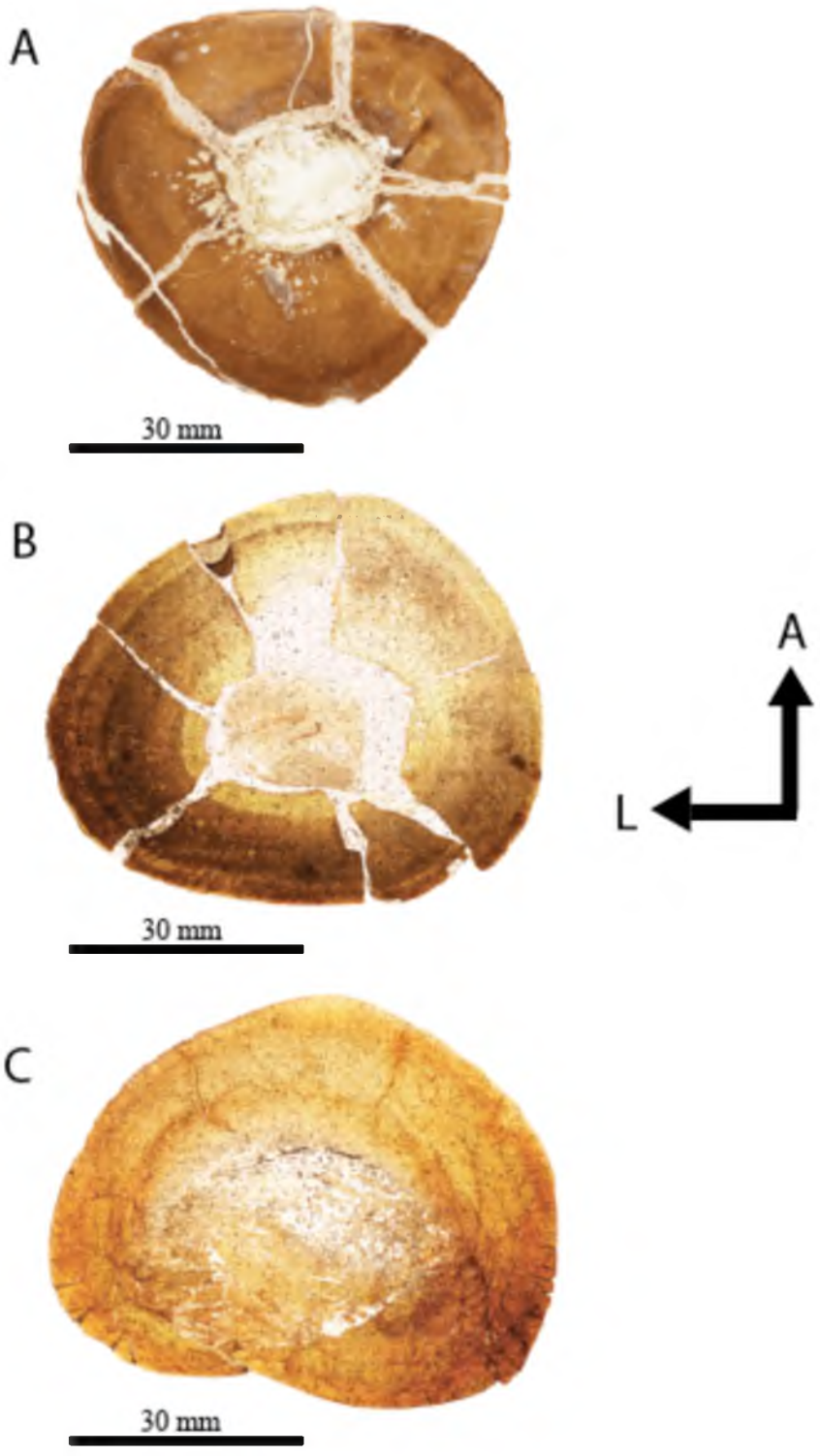
A
30 mm
B
30 mm
A
L
C
30 mm

Figure 15. Cross section of the ribs and ossified tendons sectioned for this study. Note the secondary canals that dominate these bones. A. A rib sectioned from UMNH VP 12198; B. An ossified tendon from UMNH VP 12198; C. A rib sectioned from UMNH VP 20454.7; D. An ossified tendon section from UMNH VP 20454.9. The arrow pointing at A indicates the anterior side of the element. The arrow pointing at L indicates the lateral side of the element.


A
10 mm
B
10 mm
C
10 mm
D
10 mm
A
L

Figure 16. A. A cross section of the femur UMNH VP 21339 from *Kosmoceratops richardsoni*. B. A view of the bone microstructure at the periosteum. Note the secondary osteons that make up the bone tissue.

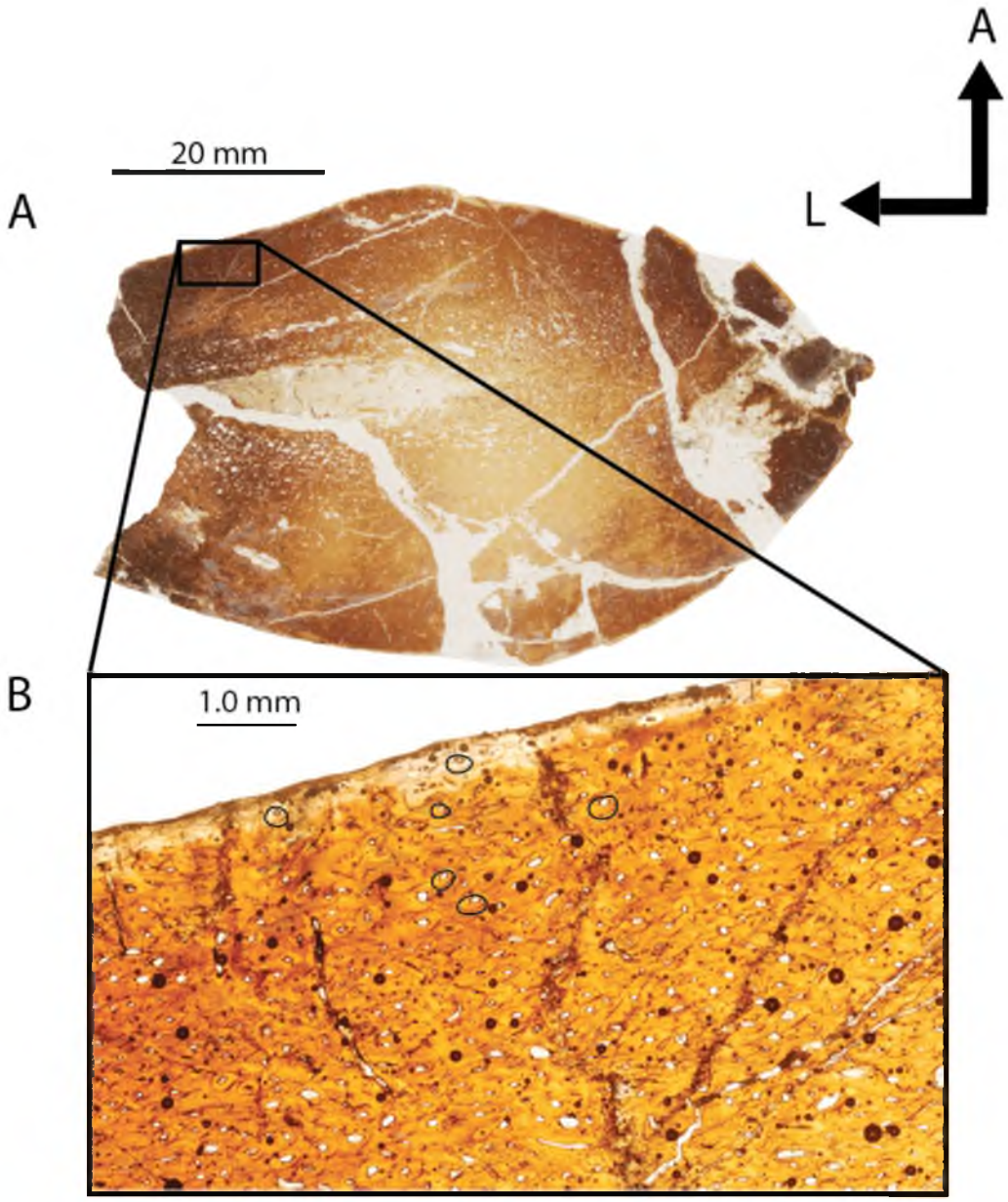
A
L
20 mm
A
B
1.0 mm

Figure 17. The change in vascularity in humerus UMNH VP 19490 from starting out large closer to the medullary cavity and becoming smaller and more dense near the periosteum.

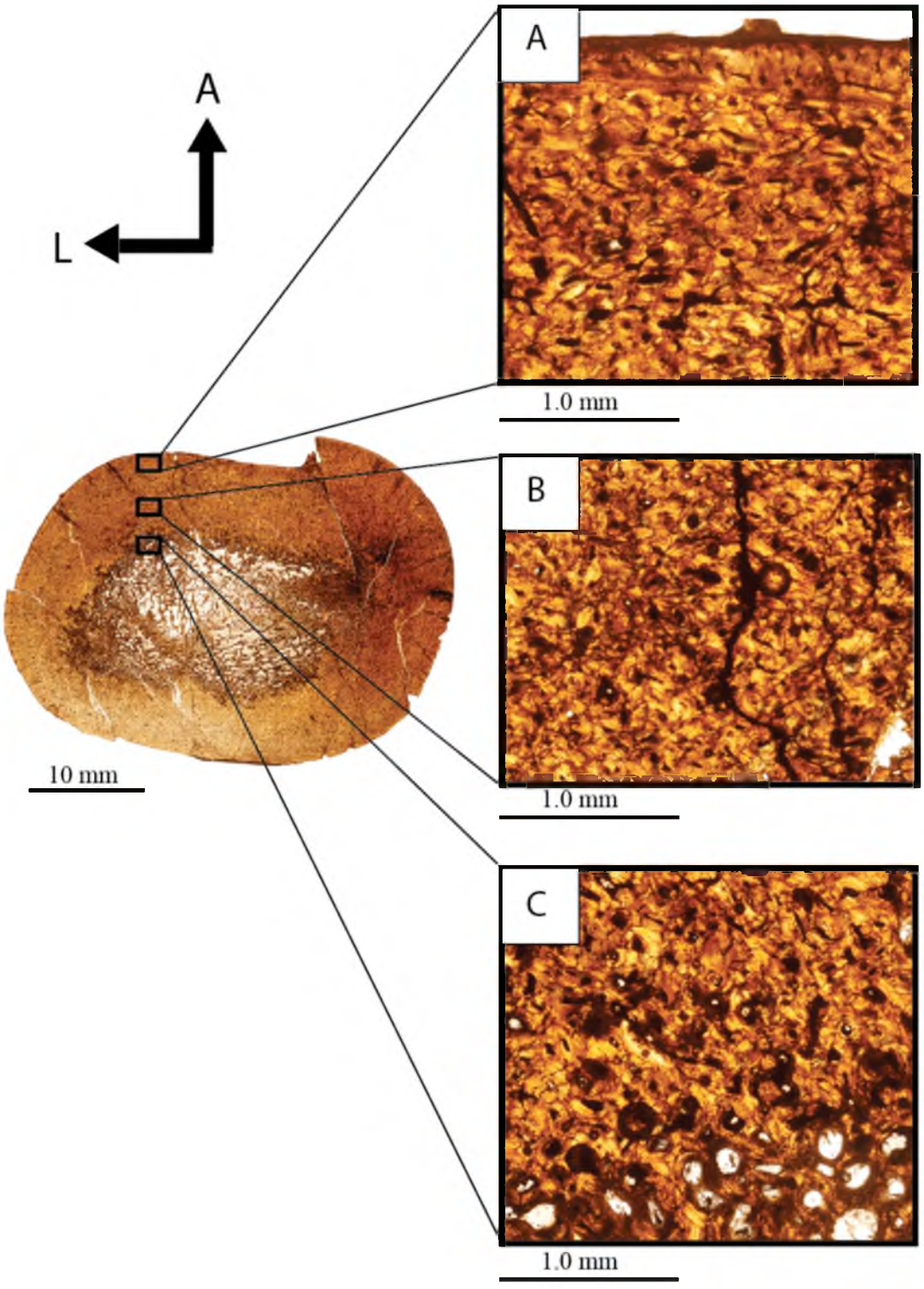
A
L
10 mm
A
1.0 mm
B
1.0 mm
C
1.0 mm

Figure 18. Comparison between the microstructure of a juvenile *Utahceratops gettyi*, an adult *Utahceratops*, and an adult *Kosmoceratops richardsoni*. A. A femur, UMNH VP 20444.4, from a juvenile of *Utahceratops gettyi* from LOC 945. Note that the microstructure is composed of primary osteons. B. A femur, UMNH VP 12198, from an adult of *Utahceratops*. Note that the microstructure is composed entirely of secondary osteons. C. A femur, UMNH VP 17000, from an adult *Kosmoceratops richardsoni*. Note that the microstructure is composed entirely of secondary osteons.

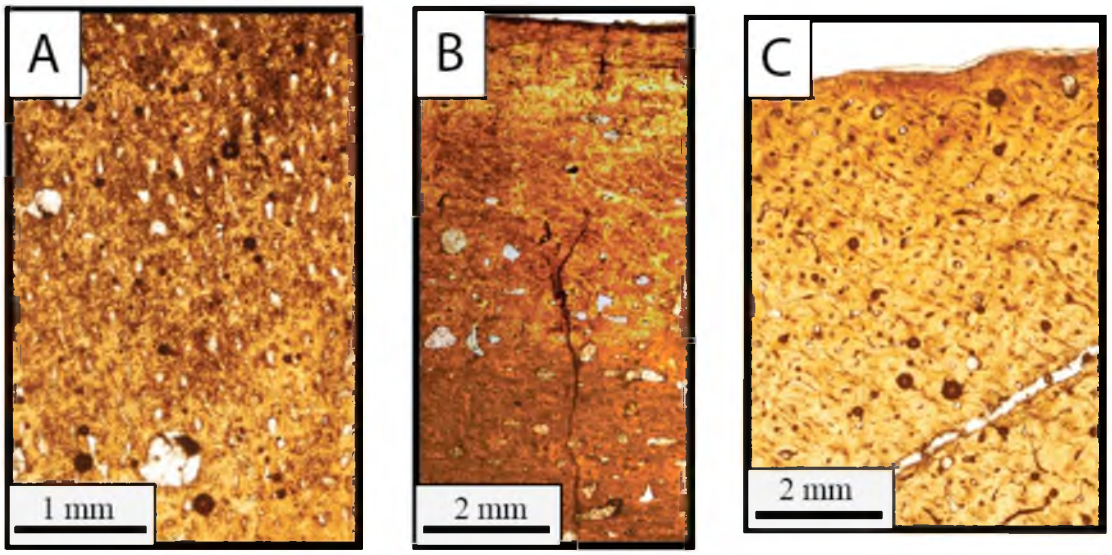
A
1 mm
B
2 mm
C
2 mm

DISCUSSION

Comparison With Other Ceratopsian Taxa

This study is the first to examine bone histology of chasmosaurine ceratopsid dinosaurs (*Utahceratops gettyi* and *Kosmoceratops richardsoni*), and therefore allows for the first time comparison with their sister clade Centrosaurinae (*Centrosaurus apertus*, *Pachyrhinosaurus pertoreum*, and *Einosaurus procurvicornis*), as well as with previously sampled smaller ceratopsians outside of Ceratopsidae (*Psittacosaurus* spp. and *Protoceratops andrewsi*).

I reexamined first-hand the microstructure of *Centrosaurus apertus* based on slides first analyzed by Lee (2006, 2007a & c). Two tibiae were quantitatively examined for this study. The trabeculae in these tibiae are composed of primary bone. Simple canals and primary osteons are both present but secondary osteons dominate in a 5:15:80 ratio for the tibia TMP 79.11.56. These canals are primarily longitudinally oriented, but radial canals are also present, though less abundant. The vascular canals seem to alternate between cycles of longitudinal and radial orientation, as first observed by Lee (2007a). Circumferentially oriented canals are also present but not nearly as abundant as longitudinal or radial canals. For the elements I examined, the osteocytes present do not have an increasing or decreasing density from the medullary cavity to the periosteum. At least two lines of arrested growth (LAGs) are visible in the tibia TMP 79.11.56 (at 20.65 mm and 21.91 mm from center of the medullary cavity), and at least five LAGs visible in

tibia TMP 66.10.36 (at 14.16, 15.67, 17.14, 18.88, and 19.94 mm from the medullary cavity). The bones sampled from *Utahceratops* and *Kosmoceratops* are similar in size to these bones sampled from *Centrosaurus*. Lee (2007a) observed a maximum of seven LAGs in *Centrosaurus* and concluded that *Centrosaurus* reached skeletal maturity in approximately 6 years. Vascular canal orientation and density, and osteocyte density of *Centrosaurus* match well with the condition in *Utahceratops* and *Kosmoceratops*. However, the repeated cycles of longitudinal and radial canals in *Centrosaurus* are not observed in either *Kosmoceratops* or *Utahceratops*. A major difference in the histology is the presence of multiple LAGs in *Centrosaurus*, and their absence in specimens of *Utahceratops* and *Kosmoceratops*, animals with the same or larger body size. Also, *Utahceratops* and *Kosmoceratops* possess more remodeling in the bone tissue of the adult animals then in *Centrosaurus*. In the adult specimens of *Utahceratops* (UMNH VP 12198 and UMNH VP 16861) and *Kosmoceratops* (UMNH VP 17000 and UMNH VP 21339), the secondary osteons permeate the entire bone tissue extending from the medullary cavity to the periosteum. In *Centrosaurus* (TMP 66.10.36, TMP 79.11.56, and TMP T-4) there is more primary bone throughout the bone tissue extending to near the periosteum.

An even greater contrast to the Utah taxa is provided by *Pachyrhinosaurus perotorum* (Fiorillo and Tykoski, 2012), a centrosaurine ceratopsid from the Maastrichtian Prince Creek Formation in the North Slope of Alaska. Erickson and Druckenmiller (2011) sampled a femur, UAMES 3551, estimated to be ~74 cm in length, that contains 18 LAGs, a total of 19 growth stages, and there are indications that the individual was still actively growing when it died because there are partially formed

vascular canals at the periosteal surface. The bone tissue of this femur of *Pachyrhinosaurus* was composed largely of reticularly oriented primary osteons, with longitudinally oriented primary osteons comprising the final five bands. Secondary osteons are present near the medullary cavity and lessen in density towards the periosteum (Erickson and Druckenmiller, 2011)). Chinsamy (1994) provided a figure from an unidentified species of Canadian *Pachyrhinosaurus*. She notes the presence of LAGs and the figure shows dense osteocytes. The overall histology of *Pachyrhinosaurus* differs slightly from *Utahceratops* and *Kosmoceratops* as it contains less remodeling, more reticular vascular canals and specimen contains numerous LAGs.

The only other histologically sampled centrosaurine is *Einosaurus procurvicornis* from the late Campanian of Montana; the study examined the tibiae of 16 individuals (Reizner, 2010). *Einiosaurus* contains highly vascularized bone tissue, predominantly longitudinally oriented canals, localized radial canals, and some circumferential canals present towards the periosteal surface (Reizner, 2010). No secondary osteons are present in the juveniles (average tibia circumference of 24.4 cm) but they are present in subadults (average tibia circumference 42.8 cm) (Reizner, 2010). This description of the animal's histology is very similar to that of *Utahceratops* and *Kosmoceratops* in that all three ceratopsians possess highly vascularized bone tissue, vascular canals that were predominantly longitudinally oriented, some radial canals, and dense secondary osteons throughout the bone tissue; however, no sampled *Utahceratops* and *Kosmoceratops* specimens contain LAGs.

These data from three centrosaurines and two chasmosaurines suggest that all ceratopsids share the presence of rapid growth indicators such as dense osteocytes and

reticular and radially oriented vascular canals. Based on the number and spacing of LAGs, growth slowed for *Einiosaurus* at around 3-5 years of age, and the oldest individual in this study is about 6 years old (Reizner, 2010). *Centrosaurus apertus* also reached skeletal maturity in about 6 years (Lee, 2007). Because *Utahceratops* and *Kosmoceratops* do not have LAGs, an estimate of the age cannot be made based on the histology. The amount of remodeling differs in the large ceratopsians. *Pachyrhinosaurus* has secondary osteons near the medullary cavity that lessen towards the periosteum, *Centrosaurus* has secondary osteons that do not dominate the bone tissue of the adult animals, *Einiosaurus* has secondary osteons that do dominate the bone tissue of older subadults individuals but not in the juveniles, and the *Utahceratops* and *Kosmoceratops* adult individuals have secondary osteons that dominate the bone tissue. The presence of LAGs and other growth marks varies considerably in these animals, from 18 in *Pachyrhinosaurus*, 7 in *Centrosaurus*, 5 in *Einiosaurus* to none in *Utahceratops* and *Kosmoceratops* (Fig. 19).

Only two nonceratopsid ceratopsians have been histologically sampled, *Protoceratops* and *Psittacosaurus*. Lee (2006, 2007a) and Makovicky et al. (2007) independently conducted histological studies of the basal neoceratopsian *Protoceratops andrewsi* from the Late Cretaceous of Mongolia, and I reexamined the specimens used in Lee's studies. Using LAGs observed in femora and fibulae, Makovicky et al. (2007) determined that *Protoceratops'* growth slowed around 9 to 10 years of age and ceased completely around 11-13 years; however, they did not provide detailed histological data on other microstructure (e.g., vascular canals and osteocytes). Lee (2006, 2007a) sectioned humeri, ulnae, femora, and tibiae and found that the circumferential bone

growth rate for *Protoceratops* ranged from 1-15 mm/yr (Lee, 2007a) and that the age of skeletal maturity for *Protoceratops* was ~7 years (Lee, 2006). The *Protoceratops* specimens that I reexamined display few trabeculae that are composed of primary bone and are sometimes rimmed with secondary bone tissue. The cortical bone tissue is predominantly comprised of primary osteons with some simple canals dispersed throughout the whole cross section. These vascular canals are almost entirely longitudinally-oriented; in femur MPC-D100/530, there is a 12:1 ratio of longitudinal to radially oriented canals. Vascular canal density does not increase or decrease appreciably throughout each section; however, osteocyte density does increase throughout the section from the medullary cavity to the periosteum. For example the femur from PIN uncatalogued "F-2" has the lowest density of 1384 osteocytes/mm^2 at 8.5 mm from the center of the medullary cavity, and 2769 osteocytes/mm^2 near the periosteum, 12 mm away from the center of the section. LAGs are present in all the thin sections that were quantitatively re-examined. For example, there were a total of 4 LAGs in femur MPC-D100/530 (0.5, 11.5, 12.2, and 12.5 mm away from the medullary cavity center). An EFS was not observed in any of the specimens. Trabeculae that are comprised of primary bone rimmed with secondary bone tissue are histological features shared with *Utahceratops* and *Kosmoceratops*. However, there are many differences between the larger taxa and the smaller taxon. The larger taxa possess an abundance of secondary osteons, no consistent osteocyte density increase from the medullary cavity to the periosteum, and they do not possess LAGs. The smaller taxon possesses a majority of primary osteons (not secondary osteons), has an osteocyte density increase and does possess LAGs.

Erickson and Tumanova (2000) investigated the bone histology of *Psittacosaurus mongoliensis*, a basal ceratopsian from the Late Cretaceous of Mongolia. Sampled individuals ranged from juvenile through adult developmental stages (Erickson and Tumanova, 2000), and I reexamined these specimens. No secondary osteons are present in any of the elements, with the tissue composed entirely of primary osteons. In the femur PIN 698/1977, radial canals dominate. Erickson and Tumanova (2000) observed a pattern of predominantly longitudinal canal orientation in juvenile individuals shifting to predominantly reticular canal orientation in the subadult and the adult specimens possessing dominantly reticular canal orientation near the medullary cavity with radial canals nearer to the periosteum. In these thin sections, vascular canal density increases from the medullary cavity to the periosteum (Erickson and Tumanova, 2000; this study). Radial canals dominate the *Psittacosaurus* femur I quantitatively examined, PIN 698/1977 (length ~20 cm and estimated to have been about 8 years old), and no secondary osteons were present. *Utahceratops* and *Kosmoceratops* are composed of both longitudinal canals and secondary canals with rare radial canals, unlike *Psittacosaurus*. Erickson and Tumanova (2000) concluded that the specimens ranged in age from 3 to 9 years and Lee (2007) concluded that the same specimens grew to be 11 years, but these data are not directly comparable to *Utahceratops* and *Kosmoceratops* because the Kaiparowits Fm. taxa lack LAGs or other growth marks.

Erickson et al. (2009) examined the bone microstructure of another species of *Psittacosaurus*, *P. lujiatunensis* from the Early Cretaceous Lujiatun bed of the Yixian Formation of Liaoning Province, China. In this study, fibulae from 26 specimens were sectioned (Erickson et al., 2009). The microstructure was not described in detail, but one

figured fibula (PKU VP 1056) (Erickson et al., 2009: fig. 3) appears to be highly vascularized. Lines of arrested growth are present but an EFS is not. According to Erickson et al. (2009), none of the specimens have an EFS, which indicates that these animals had not completely stopped growing. The specimens in this study were interpreted to range in age from neonates to 11 years old (Erickson et al., 2009). The lack of histological description and figures, as well as the sampling of different elements (e.g., fibulae vs. femur and tibia) make it difficult to compare with my data.

It appears that basal ceratopsians grew more slowly than large quadrupedal ceratopsids. This is evidenced by a generally higher number of definitive growth lines prevalent throughout development of the basal ceratopsians as well as the smaller distances between those LAGs. In contrast, the large ceratopsids possess larger distances between LAGs, which indicate a lot more bone grew in one year for the ceratopsids than the basal ceratopsians. The vascular canal orientation is predominantly longitudinal for all species studied other than *Psittacosaurus*, which was dominated by radial canals. *Utahceratops*, *Kosmoceratops*, *Protoceratops*, and *Psittacosaurus* all possessed more radial canals than circumferential canals, *Psittacosaurus* having the most radial canals than all of the other ceratopsians combined. The vascular canal density for the femora studied of the smaller ceratopsians is an average 33.46 canals/mm^2 for *Protoceratops* and 40.84 canals/mm^2 for *Psittacosaurus.* This compared with the average vascular canal density for femora of the larger ceratopsids sampled with 18.67 canals/mm^2 for *Utahceratops* and 18.68 canals/mm^2 for *Kosmoceratops*. The average osteocyte density for the femora studied of the smaller ceratopsians is 1853 osteocytes/mm^2 for *Protoceratops* and 2157.5 osteocytes/mm^2 for *Psittacosaurus*. The average osteocyte

density for the femora studied of the larger ceratopsids is 1437 osteocytes/mm^2 for *Utahceratops* and 1650.3 osteocytes/mm^2 for *Kosmoceratops*.

Comparison With Other Archosaurs

Extant crocodylians are poikilothermic ectotherms and grow significantly slower than birds (e.g., Case, 1978; Erickson et al., 2001; Padian et al., 2001). Crocodylian bones exhibit compact, dense tissue that contains sparse vascular canals and parallel-fibered collagen fiber orientation (Enlow and Brown, 1957, 1958), and numerous LAGs (Buffrénil, 1980; Ferguson et al., 1982). *Utahceratops* and *Kosmoceratops* did not grow in a similar way to extant or extinct crocodylians. Unlike most other reptiles, nonavian dinosaurs, including *Utahceratops* and *Kosmoceratops*, generally have complex, well-vascularized primary bone tissues and extensive secondary osteons, similar to birds and many large mammals today (Francillon-Vieillot et al., 1990; Padian et al., 2001).

Hadrosaurid ornithopod dinosaur histology is well documented (Horner et al., 1999; Horner et al., 2000; Cooper et al., 2008). *Maiasaura peeblesorum* and lambeosaurine *Hypacrosaurus stebingeri* from the late Campanian of Montana have limb bones that are predominantly composed of primary bone tissue and dense vascular canals (Horner et al., 1999; Horner et al., 2000; Cooper et al., 2008). These vascular canals are radial in orientation in younger individuals and change to longitudinal canals as the individuals get older. Trabeculae rimmed with secondary bone tissue, and the presence of LAGs and EFS in some animals, are all characteristics observed in both taxa (Horner et al., 1999; Horner et al., 2000; Cooper et al., 2008). *Utahceratops* and *Kosmoceratops* are similar in possessing dense vascularity, trabeculae rimmed with secondary tissue, and

rapid growth indicated by vascular canal density and orientation. However, sampled *Utahceratops* and *Kosmoceratops* differ in the absence of LAGs or an EFS.

Chinsamy et al. (2012) conducted bone histological analysis of polar *Edmontosaurus* from the Prince Creek Formation of the Alaskan North Slope and compared it with *Edmontosaurus* from the high-latitude temperate region of the Horseshoe Canyon Formation in Alberta, Canada. The polar *Edmontosaurus* would have lived in a cold-temperate climate, where there would be no sunlight for up to 6 months, and reduced overwintering foliage (Chinsamy et al., 2012). *Edmontosaurus* specimens from Alaska (humeri, femora, and tibiae) possessed dense vascularity and a change in vascular canal organization from reticular to more circumferential in the compacta. These periodic textural shifts comprise up to 8 cycles of alternating reticular and circumferential bone tissue (e.g., femur of DMNH 22557). This shift from quickly deposited reticular canals to slow forming circumferential canals was interpreted as consistent with polar winter darkness, subsequent periodic reductions in nutritional quality of forage, and shifts in energy balance (Chinsamy et al., 2012). True LAGs were absent in these animals. No such shifts from reticular to circumferential vascular canals were observed in either *Utahceratops* or *Kosmoceratops*. The dense vascularity as well as the lack of LAGs is consistent with the histology observed in both taxa.

These switches in vascular canal orientation were not consistently observed in the Horseshoe Canyon Formation sample of *Edmontosaurus* (Chinsamy et al., 2012). The cortical bone comprises reticular canals that switch to circumferential canals later in life; this is observed in all of the femora analyzed. In contrast, there are alternating cycles of circumferential and reticular vascular canals in the tibia, but they are not as numerous as

in the Alaskan sample. LAGs were also absent in these individuals. Chinsamy et al. (2012) propose that the variable histology observed in these animals reflect occasional difficulties in sourcing forage. *Utahceratops* and *Kosmoceratops* seem to grow more similarly to these temperate *Edmontosaurus* than to the polar dinosaurs, but lack this cycling of vascular canal orientation. Some of the bones of *Utahceratops* (femur of UMNH VP 16860, humerus and tibia of UMNH VP 20454, and femur of UMNH VP 12198) show a change in vascular orientation from longitudinal to somewhat reticular to circumferential near the periosteum, but this is a gradual transition rather than sudden in canal orientation. *Utahceratops*, *Kosmoceratops*, and *Edmontosaurus* all possess no LAGs.

A variety of other ornithopod ornithischian dinosaurs, including *Orodromeus makelai* (Horner et al., 2009), *Gasparinisaura cincosaltensis* (Cerda and Chinsamy, 2012), *Tenontosaurus tilletti* (Horner et al., 2009; Werning, 2012), *Dryosaurus altus* (Horner et al., 2009), *Dysalotosaurus lettowvorbecki* (Chinsamy, 1995; Hübner, 2012), and *Camptosaurus dispar* (Horner et al., 2009) have been histologically examined.

Orodromeus makelai possesses histologic characteristics and lower growth rates similar to other small dinosaurs (Horner et al., 2009). Femora and tibiae display vascular canals that are primarily longitudinally-oriented in both juveniles and adults. The bone tissue of juveniles is highly vascularized, and becomes slightly less dense in subadults, where the vascular canals are also slightly more reticulate. No secondary osteons are visible in the juvenile and subadult stages. At the adult stage, the outer 0.35 mm of the cortex is nearly avascular. Osteocytes are arranged circumferentially around the vascular spaces in the juvenile and subadult stages and osteocyte density decreases in the adult

stage. Sampled adults possess three LAGs with and EFS, and the first LAG appears at the 'late juvenile' stage (Horner et al., 2009). *Utahceratops* and *Kosmoceratops* are similar to *Orodromeus* in that longitudinal canals dominate all three animals, but *Utahceratops* and *Kosmoceratops* do not possess LAGs or an EFS and have a much higher rate of remodeling.

Cerda and Chinsamy (2012) sampled *Gasparinisaura cincosaltensis*, a basal ornithopod from the Late Cretaceous of Patagonia. Numerous postcranial elements were sectioned from 11 specimens. The bone tissue of the long bones of *Gasparinisaura cincosaltensis* is dominated by primary longitudinally-oriented vascular canals. Some radial canals are present. The long bones all possess a large medullary cavity surrounded by circumferential tissue with flattened osteocytes. Vascular canals are longitudinal in the inner cortex, and become laminar and less dense in the outer cortex (but never completely avascular). Some bones possess secondary osteons, but they are not abundant. Osteocyte density decreases towards the periosteum, and in some cases (tibia of MCS-Pv 002), osteocyte lacunae are spindle-shaped. There were several examples of elements where the bone tissue was woven-fibered in the inner and middle cortex, and then grade into parallel-fibered tissue in the outer cortex. In one case, the tibia of MCS-Pv 002 possesses highly vascularized bone tissue but with no true woven-fibered component. LAGs were present in some of the limb bones, with a maximum of 8 LAGs in the femur of MCS-Pv 110. *Utahceratops* and *Kosmoceratops* do not share a particularly similar histology with *Gasparinisaura*. Although all three taxa share a cortex dominated by longitudinally oriented canals with some radial canals present, *Gasparinisaura* has bone tissue that grades from woven collagen fibers to parallel oriented fibers, whereas *Utahceratops* and

Kosmoceratops limb bones comprise exclusively woven-fibered bone. Additionally, *Utahceratops* and *Kosmoceratops* have a higher proportion of secondary osteons then *Gasparinisaura*. The decrease of vascular canal and osteocyte density towards the periosteum, transition to parallel-fibered bone, lower amount of remodeling, and the presence of LAGs are all evidence that *Gasparinisaura* grows more slowly than *Utahceratops* and *Kosmoceratops*.

Among these histologically studied basal ornithopods, *Tenontosaurus tilletti* is much closer in body size to ceratopsids. The long-bone histology of *Tenontosaurus* is well studied (Horner et al., 2009; Werning, 2012). The bone tissue of juveniles is well vascularized by longitudinally-oriented primary canals, with some circumferential and radial canals also present. There is no difference in the degree of vascularity from the inner to the outer cortex in the juvenile stage, but the vascular canals become more circumferentially organized in later stages of growth (Horner et al., 2009). Some secondary osteons are present in subadults (Horner et al., 2009) and mostly primary tissue seen in the subadult samples studied by Werning (2012). Dense secondary osteons are present in the midcortex of the adults (Werning, 2012). Osteocytes are consistently dense throughout the cortex and well organized around the vascular canals (Horner et al., 2009; Werning, 2012). *Tenontosaurus* drastically slowed in growth as it reached skeletal maturity (Werning, 2012). LAGs first appear in subadults, and the oldest individuals possess multiple LAGs and an EFS (Horner et al., 2009; Werning, 2012). *Tenontosaurus*, *Utahceratops*, and *Kosmoceratops* appear to have grown similarly. They all possess bone tissues that are densely vascularized by predominatly longitudinally oriented primary canals, with some circumferential and radial canals, and dense osteocytes. All three taxa

have primary bone tissue that makes up the majority of the bone in juveniles and subadults and secondary bone tissue that make up the majority of the bone tissue in adults. *Tenontosaurus*, however, does display LAGs, and the oldest individuals have an EFS (Werning, 2012), characteristics that are not observed in sampled specimens of *Utahceratops* or *Kosmoceratops*. The lack of EFS in *Utahceratops* or *Kosmoceratops* could signify that these individuals are not as fully grown as the oldest individuals of *Tenontosaurus*.

Femora of *Dryosaurus altus* possess vascular canals whose orientation change from plexiform in the juvenile stage to more circumferential in the subadult stage (Horner et al., 2009). However, there is no change in density of vascular canals from the inner to the outer cortex nor is there a change in vascular density between juvenile and subadult stages. Secondary osteons are present in the larger subadult, but not observed in the juveniles (Horner et al., 2009). Osteocytes are abundant and well organized around the vascular spaces throughout ontogeny. The first LAG is observed at the subadult stage, and the largest sampled specimen, inferred to be a large subadult, possessed two LAGs (Horner et al., 2009).

A *Dysalotosaurus lettowvorbecki* femur (analyzed by Chinsamy, 1994, 1995) has an outer cortex that is well-vascularized and did not have an EFS. Secondary osteons are present but there are no LAGs observed in this individual. The bone histology of the subadults of *Dryosaurus* and *Dysalotosaurus* are similar to that of the histology of the adult animals of *Utahceratops* and *Kosmoceratops* in that these taxa possessed predominantly secondary osteons in the adult animals. In *Dryosaurus*, the primary osteons are oriented mainly longitudinally and circumferentially with occasional radial

canals (Chinsamy, 1994, 1995). The vascularization in *Dysalotosaurus* is most dense in areas where the primary bone wall is the thickest and less dense where the bone wall is the thinnest. The orientation of the canals is longitudinal where the bone wall is the thinnest and more plexiform to reticular in the thickest parts of the bone wall (Hübner, 2012). *Utahceratops* and *Kosmoceratops* have mostly longitudinally oriented canals, with rare radial and circumferential canals and are not more dense or less dense where the bone wall is thicker or thinner. *Utahceratops* and *Kosmoceratops* do not preserve any LAGs, whereas *Dryosaurus* and *Dysalotosaurus* do.

The single sampled specimen of a right femur of *Camptosaurus dispar* is well vascularized (Horner et al., 2009). The canals were primarily longitudinally-oriented with some reticular canals present. The femur possesses an abundance of secondary osteons that extend from the medullary cavity to the periosteum. This is similar to what is seen in the adult forms of *Utahceratops* and *Kosmoceratops*. No LAGs were observed in *Camptosaurus*, *Utahceratops* or *Kosmoceratops*.

Specimens of the basal ornithischians *Lesothosaurus diagnosticus* (Knoll et al., 2010) and the heterodontosaurid *Fruitadens haagarorum* (Butler et al., 2009) have also been histologically examined. Femora, tibiae, and fibulae were sectioned at the mid-diaphyses of specimens of *Lesothosaurus*. These juvenile elements reveal tissue that possesses dense vascularization that was oriented longitudinally, no secondary osteons, and no LAGs. These animals were considered to be rapidly and continuously growing (Knoll et al., 2010). A larger specimen of this animal was sectioned at the midshaft of the femur and has a cortex dominated by laminar bone with vascular canals oriented longitudinally and circumferentially with one or two LAGs present. The periphery of the

bone, however, is avascular, and there appears to be an EFS. *Utahceratops* and *Kosmoceratops* share more histological characteristics (dense vascularization, longitudinally oriented canals, no LAGs) with the juvenile *Lesothosaurus* because all taxa appear to be growing rapidly.

Butler et al. (2009) histologically examined two femora of the heterodontosaurid *Fruitadens*. LACM 120478 possesses both radial and longitudinally oriented vascular canals. No secondary osteons were present, and one LAG was present. The outer cortex comprises parallel-fibered bone. Butler et al. (2009) considered this a juvenile that was in the second year of its life when it died. Longitudinally oriented vascular canals dominate LACM 115727, and the entire cortex consist of parallel-fibered bone. There was a decrease in vascular canal density and size from the medullary cavity to the periosteum, with the bone closest to the periosteum being nearly avascular (Butler et al., 2009). Four LAGs, five growth zones were present, which means that this animal was four years old when it died and its growth was slowing (Butler et al., 2009). *Utahceratops* and *Kosmoceratops* did not grow similarly to the heterodontosaurid *Fruitadens*. The outer cortex of *Fruitadens* consist of parallel-fibered bone whereas *Utahceratops* and *Kosmoceratops* only consist of woven bone. A decrease in vascular density ending in bone tissue being nearly avascular is seen in *Fruitadens* whereas a decrease in density is not seen in any bone of *Utahceratops* and *Kosmoceratops* and none of the bone tissue was near to avascular.

Scutellosaurus lawleri, a small basal thyreophoran ornithichian dinosaur, appears to grow more similarly to that of a crocodylian than other ornithichian dinosaurs of similar size. Padian et al. (2004) sectioned a radius, a femur and a tibia from two

specimens of *Scutellosaurus*. All of the bones have tissue that is poorly vascularized. The vascular canals are predominantly longitudinally oriented and they decrease in density and size when approaching the outer cortex. In some of the bones (radius and tibia of UCMP 130580), the tissue becomes avascular near the periosteum. There were very few, if any, secondary osteons present. Osteocytes are not dense and flattened and organized into circumferential layers. The majority of the bones sectioned are dominated by parallel-fibered bone, and up to 7 LAGs are present. All of these lines of evidence suggest this dinosaur was growing very slow compared to other dinosaurs (Padian et al., 2004). These histological characteristics are very different from those in *Utahceratops* and *Kosmoceratops*, which are highly vascularized with dense osteocytes and highly remodeled. This evidence suggests that *Utahceratops* and *Kosmoceratops* grew much more rapidly than *Scutellosaurus*.

The long bones of *Stegosaurus* were histologically analyzed by Redelstorff and Sander (2009). Simple vascular canals and longitudinal primary osteons dominate the cortical tissue. There is a pattern of vascularization that begins as longitudinal primary osteons arranged in circular rows closer to the medullary cavity to being organized in a reticular pattern further out near the periosteum. In most specimens sampled, there is a decrease in vascularity in longitudinal canals when nearing the periosteum. The primary bone tissue is a mixture of predominantly woven and some parallel-fibered bone. Secondary osteons are present, sometimes dominating the entirety of the cortex. In younger specimens, secondary osteons are restricted to the inner cortex or just near the medullary cavity. In older specimens, there is a gradual slowing of growth with more avascular tissue near periosteum, and the outermost cortex consists of a parallel-fibered

bone without primary osteons. Up to 8 LAGs are present in sampled specimens, one of which possesses an EFS. Redelstorff and Sander (2009) hypothesize that *Stegosaurus* grew slower and perhaps had a lower metabolic rate than other dinosaurs of its size, as indicated by the lower vascularity and the presence of some parallel-fibered bone. *Stegosaurus* has some woven bone and some parallel-fibered bone, whereas *Utahceratops* and *Kosmoceratops* only posses woven bone. *Stegosaurus* has vascular canals that decrease in density towards the periosteum, whereas *Utahceratops* and *Kosmoceratops* did not exhibit a decrease in density. *Utahceratops* and *Kosmoceratops* do not have and LAGs whereas *Stegosaurus* has up to 8.

Early sauropodomorph saurischian dinosaurs, such as *Plateosaurus engelhardti*, have limb bones with a large medullary cavity, relatively thin bone walls, very little secondary cancellous bone, and rare resorption spaces. Vascularization comprises primarily circumferential vascular canals that become less dense towards the outer cortex, with up to 14 LAGs present (Sander and Klein, 2005; Klein and Sander, 2008). Among later sauropodomorphs, the larger neosauropods (e.g., *Apatosaurus*, *Diplodocus*, *Camarasaurus*, *Brachiosaurus*, and *Europasaurus*) initially deposit rapidly-growing bone tissue with large primarily longitudinally-oriented vascular canals radially oriented canals locally, such as in *Apatosaurus* (Klein and Sander, 2008). LAGs are not common among sauropods until late in ontogeny, although some show stratification of the cortex in the form of 'polish lines' (Sander 2000),'modulations', or 'cycles' (de Ricqlés, 1983; Rimblot-Baly et al., 1995; Curry, 1999; Curry Rogers and Erickson, 2005; Sander and Klein, 2005; Klein and Sander, 2007; Woodward, 2005). These polish lines are interpreted as growth line observed in polished section but not in thin-section (Sander,

2000), and are considered to be an intermediate stage between modulations and LAGs, as a slowing of growth not pronounced enough to arrest growth completely. Sauropods possess bone tissue that is extensively remodeled in the older individuals of *Alamosaurus* (Woodward and Lehman, 2009), and *Apatosaurus* (Curry, 1999; Klein and Sander, 2008) and they are near the inner cortex (Sander, 2000). Large resorption cavities are present in the interior of the bones in many sauropods (e.g., *Alamosaurus*; see Woodward and Lehman, 2009).

Sauropodomorph dinosaurs show some similarities to the growth strategies of *Utahceratops* and *Kosmoceratops*. Like sauropodomorphs, *Utahceratops* and *Kosmoceratops* seem to deposit bone tissue rapidly and do have large, dense predominantly longitudinal vascular canals closer to the medullary cavity. "Growth zones," lines seen in both polished and thin section, were observed in the tibia and ulnae of one specimen of *Utahceratops* (UMNH VP 20444) and these could indicate a momentary slowing of growth. These "growth zones" may be similar to those "polish lines" seen in sauropodomorph dinosaurs. However, *Utahceratops* and *Kosmoceratops* do not display any LAGs, Compared with *Plateosaurus*, the vascularity is primarily longitudinal rather than circumferential, and secondary osteons are abundant.

Large theropods (e.g., tyrannosaurids and *Allosaurus*) grew relatively quickly (Horner and Padian, 2004; Erickson et al., 2004; Bybee et al., 2006). Like many large dinosaurs, their limb bones are highly vascularized. The vascular canals are predominantly circumferential, with some radial and longitudinal canals present (Horner and Padian, 2004; Bybee et al., 2006). LAGs are ubiquitous, and indicate that adults grew to over 20 years in age (Horner and Padian, 2004; Erickson et al., 2004; Bybee et

al., 2006). High vascularity in the outermost cortical bone provides evidence that the animals were still actively growing at the time of death, though change in circumference between the exterior-most LAGs indicate that growth was slowing in the largest specimens (Horner and Padian, 2004; Bybee et al., 2006).

Utahceratops and *Kosmoceratops* grew relatively similarly to large theropods grew in that they all possess limb bones that are highly vascular; however, the vasculature differs in that *Utahceratops* and *Kosmoceratops* are dominated by longitudinal vascular canals with some radial and circumferential canals present, whereas *Tyrannosaurus rex* and *Allosaurus* are dominated by circumferential canals (Horner and Padian, 2004; Bybee et al., 2006). Furthermore, these theropods deposited significant numbers of LAGs, whereas *Utahceratops* and *Kosmoceratops* do not display any LAGs.

Evolution of Ceratopsian Body Size and Locomotion

Ceratopsian dinosaurs evolved from a small and bipedal form (such as *Psittacosaurus*), became quadrupedal when still small (e.g., *Protoceratops* and leptoceratopsids), and then grew to a large size within Ceratopsidae (e.g., *Utahceratops*, *Kosmoceratops*, *Centrosaurus apertus*, *Pachyrhinosaurus pertoreum*, and *Einosaurus*). Based on the histological evidence, *Utahceratops* and *Kosmoceratops* appear to have grown at a rapid rate, but an exact rate of growth cannot be predicted because no LAGs are present. *Utahceratops* and *Kosmoceratops* appear to be growing faster than the smaller taxa of *Protoceratops* and *Psittacosaurus* based on the lack of LAGs, the density of the secondary osteons, and the higher density of vascular canals per bone tissue area. There are two modes for how lineages evolve large size. One mode is to grow more

rapidly than your small bodied ancestors and the other is to grow for a longer period of time (Erickson and Brochu, 1999; Erickson et al., 2001; Padian et al., 2001). Based on the evidence provided above, all of the ceratopsids that have been histologically sectioned (e.g., *Utahceratops* and *Kosmoceratops*) appear to grow faster than *Protoceratops* and *Psittacosaurus*, thus exhibiting the first mode.

If an animal increases body size, the microstructure of the bones may be altered or affected in some way. Thick and dense trabeculae help support weight-bearing bones (Doube et al., 2011). Some of the weight-bearing bones in *Utahceratops* and *Kosmoceratops* have extensive trabeculae that would help support a large body. They also possess more than trabeculae than the smaller ceratopsians *Psittacosaurus* and *Protoceratops*. A similar trend is observed in extant mammals, where small animals have extremely reduced trabecular complexity compared with large mammals (Swartz et al., 1997). However, Swartz et al. (1997) also determined that there were no systematic differences in trabecular size or scaling patterns related to locomotor mode (Swartz et al., 1997). *Utahceratops* and *Kosmoceratops* possess more trabeculae than *Psittacosaurus* and *Protoceratops* but quadrupedal *Protoceratops* does not show more trabeculae than bipedal *Psittacosaurus*.

In the shift to quadrupedality during ceratopsian evolution, one might expect to see changes in the bone microstructure reflect this locomotor change, such as in bone wall thickness or abundance of trabeculae. When analyzing different archosaurs (specifically *Centrosaurus*, *Alligator*, and *Allosaurus*) with different locomotor modes, Lee (2007a) concluded that locomotor mode does not appear correlated to any growth pattern in bone wall thickness. Instead, how limb bones thickened during growth

appears to largely reflect differences in growth (Lee, 2007a). In bipedal non-avian dinosaurs, forelimb bones are released from locomotor and weight-bearing constraints and grow independently of them. However, in quadrupedal dinosaurs, both forelimb and hindlimb bones must grow while performing locomotor functions. Large, quadrupedal *Centrosaurus* and small, bipedal *Psittacosaurus* are characterized by negative allometry in bone wall thickness relative to bone girth (Lee, 2007a). This negative allometry observed in *Centrosaurus* and *Psittacosaurus* exhibit rapid periosteal growth relative to endosteal resorption and forms a thick-walled limb bone in juveniles. As the animal grows older, periosteal growth slows relative to endosteal resorption, making the walls of limb bones grow thinner (Lee, 2007a). This negative allometry is weakly observed in the femora of *Utahceratops*. Because negative allometry of bone wall thickness appears to be a characteristic of taxa that require active locomotion while growing quickly (Carrier, 1983; Carrier and Leon, 1990; Heinrich et al., 1999; Biewener, 2005; Main and Biewener, 2006) and because relatively rapid growth is a characteristic of dinosaurs (Erickson et al., 2001; Padian et al., 2001; Padian et al., 2004), it makes sense for the hindlimb bones of bipeds and both forelimb and hindlimb bones of quadrupeds to should show negative allometry in bone wall thickness (Lee, 2007a).

Metabolic Inferences

Although bone histology is not a direct consequence of thermal physiology, the two are intimately related. Specifically, bone growth rate varies directly with metabolic regime, and therefore indicators of fast growth rate are also indirect indicators of high metabolism (Montes et al. 2007). Metabolic rate is approximately one order of

magnitude higher in endothermic amniotes than in ectothermic taxa of similar body mass (Wieser, 1994; Montes et al., 2007). Bone tissue types reflect bone growth rates (de Margerie et al. 2002; de Margerie et al. 2004; Montes et al., 2007; Montes et al., 2010; Cubo et al. 2012), and therefore can inform us about metabolism of extinct organisms. For example, bone tissues with a highly vascular cortex, extensive remodeling, and some radial canals present are indicative of both a high growth rate and a high metabolism (de Margerie, 2004).

Modern crocodylians, which are poikilothermic ectotherms with a relatively slow metabolism, deposit compact bone tissue with low vascular density (Padian et al., 2004; Werning, 2012). This contrasts with the histological condition in *Utahceratops* and *Kosmoceratops*, which display high vascularity and both high vascular and osteocyte density. In contrast to crocodylians, birds, as homeothermic endotherms, grow rapidly (i.e., *Dromiceius novaehollandiae* and *Struthio camelus* increase their body mass by 50% per month [Castanet et al., 2000]). For example, the cortical tissue of *Dromiceius novaehollandiae* (emu), *Struthio camelus* (ostrich), and *Aptenodytes patagonicus* (king penguins) contain dense longitudinal, circumferential, and radial vascular canals (Castanet et al., 2000; de Margerie, 2004), and extensively remodeled trabeculae (de Margerie, 2004), very similar to the condition in *Utahceratops* and *Kosmoceratops*. Bird bone histology shows woven collagen fiber orientation (Castanet et al., 2000) (like Utahceratops and Kosmoceratops) while crocodylian bone histology exhibits parallel-fibered collagen fibered orientation (Werning, 2012).

Mammals have a rapid metabolism similar to that of birds (Castanet et al., 2000; Cubo et al., 2005). Many of the same histological features found in extant bird limb

bones and the Kaiparowits chasmosaurines are also seen in extant mammal bones (Enlow and Brown, 1958; Padian et al., 2001). These taxa share well-vascularized primarily longitudinal canals with some radial canals present, with significant remodeling in the form of secondary osteons (Enlow and Brown, 1958; de Ricqlés, 1991; Curry, 1999; Horner et al., 1999; Padian et al., 2001; Sander and Andrassy, 2006). Densely vascular bone tissue is correlated with an elevated metabolism able to support rapid, sustained growth (Schweitzer and Marshall, 2001; Montes et al., 2007). Woven-fibered collagen orientation, indicative of rapid growth, is seen in these Kaiparowits chasmosaurines as well as in mammals (Chinsamy and Hurum, 2006). Because *Utahceratops* and *Kosmoceratops* exhibit multiple histological characters (i.e. highly vascular cortex, remodeled trabeculae, etc.) that are also present in both extant birds and extant mammals, available evidence suggests that *Utahceratops* and *Kosmoceratops*, and indeed all sampled ceratopsians, are also homeothermic endotherms.

Although ceratopsids could have had their own unique "intermediate blooded" metabolism (Sampson, 2009), fully endothermic extant taxa show much in common histologically with these dinosaurs. The occurrence of such densely vascularized secondary Haversian bone in mammals and birds is partly attributed to their high metabolism, with their continual demands for calcium and phosphorus nutrients from bone mineral reservoirs (Enlow and Brown, 1957; Enlow, 1962; Bakker, 1972; de Ricqlés, 1974,1976; Ostrom, 1978), and this metabolically-influenced histological characteristic is clearly present in *Utahceratops* and *Kosmoceratops*. Also, comparisons of similarly sized dinosaurs and large mammals show that they grew at comparable rates (e.g., Case, 1978; Erickson et al., 2001; Horner and Padian, 2004; Lee and Werning,

2008), which supports an endothermic interpretation for large dinosaurs such as *Utahceratops* and *Kosmoceratops*.

Implications for Ceratopsid Ontogeny

Fowler et al. (2011) recently proposed that *Kosmoceratops* might represent an immature individual of *Vagaceratops irvinensis*, a chasmosaurine known only from the late Campanian Dinosaur Park Formation of Alberta. Such a synonomy is plausible given that *Kosmoceratops* and *Vagaceratops* are sister taxa (Sampson et al., 2010a) and of similar size. Because the bone histology of *Vagaceratops* has not been examined, I cannot directly compare growth records of these taxa to evaluate Fowler's hypothesis. However, based on the femoral histology of *Kosmoceratops*, I conclude that *Kosmoceratops* is not from an immature individual; both sectioned individuals (the holotype UMNH VP 17000 and UMNH VP 21339) represent subadult to adult individuals. Secondary osteons and extensive trabeculae dominate in these individuals, both of which are characteristics of older animals. If these specimens of *Kosmoceratops* were from young individuals, one would expect its bone microstructure to be composed primarily of simple canals and primary osteons with more radial canals (cf. Lee 2006, 2007; Reizner, 2010). The specimens of *Kosmoceratops* do not possess EFS, which indicates these animals had not fully stopped skeletal growth. However, not all adult dinosaur specimens show EFS (i.e. tyrannosaurids and *Allosaurus* (Horner and Padian, 2004; Erickson et al., 2004; Bybee et al., 2006)), and there appear to be indications that *Utahceratops* and *Kosmoceratops* did not lay down growth lines such as LAGs (see below). Therefore, all histological evidence leads to the conclusion that the specimens of

Kosmoceratops are not juveniles. A direct test of the *Kosmoceratops*/*Vagaceratops* synonymy hypothesis would require histological data from *Vagaceratops* specimens.

Recently there has been a debate over whether the sympatric chasmosaurine taxa *Torosaurus* and *Triceratops* are two distinct species, or whether *Torosaurus* is just an old adult of *Triceratops* (Scannella and Horner, 2010, 2011; Farke, 2011; Longrich and Field, 2012). *Kosmoceratops* and *Utahceratops* provide an example of two related species of large dinosaur that lived concurrently in the same place and that share the same ecological niche, analogous to the *Torosaurus*/*Triceratops* situation. My histological study of *Kosmoceratops* and *Utahceratops* demonstrates that the largest specimens both represent adults of the same ontogenetic stage. Thus, this confirms the two taxa are distinct species. If one species were a juvenile of the other, I would expect different histologic characteristics in the largest specimens of each taxon, and this is not the case. This confirmation that *Kosmoceratops* and *Utahceratops* are two distinct chasmosaurine species of similar sizes that overlap in time and space indicate that there is no a priori ecological reason that *Torosaurus* and *Triceratops* could not have also coexisted as separate taxa.

Latitudinal Variation in Growth

In my histological analysis, no LAGs or other growth marks were observed in the limb bones of *Utahceratops* and *Kosmoceratops*. This result was unexpected because all other sampled ceratopsians, including other large ceratopsids (e.g., *Centrosaurus*, *Pachyrhinosaurus*, *Einiosaurus*) do deposit LAGs in limb elements of similar size. When considering the geographic distribution of these late Campanian ceratopsid taxa, there

appears to be latitudinal pattern in number of LAGs in subadult/adult individuals (Figs. 20 & 21), with abundance decreasing towards lower latitudes. For example, *Pachyrhinosaurus* from Alaska preserves numerous (18) growth zones, *Centrosaurus* from Alberta preserves at most seven, *Einosaurus* from Montana possesses up to five LAGs, and the southern forms from Utah, *Utahceratops* and *Kosmoceratops*, display no LAGs.

In many samples of the adult animals of *Utahceratops* and *Kosmoceratops* (specimens UMNH VP 16860, UMNH VP 12198, UMNH VP 16861, UMNH VP 17000, and UMNH VP 21339), the cortical bone tissue is largely remodeled, dominated by secondary osteons. In these adult specimens, the remodeling extends to the periosteum that means that growth had slowed to a point where there was enough time for the periosteal tissue to be laid down and subsequently remodeled. In contrast, sampled specimens of *Centrosaurus* (e.g., TMP T-4, TMP 79.11.56, and TMP 66.10.36) of similar size all display LAGs, but the bone tissue is not composed entirely of secondary osteons, and the periosteal tissue is comprised of primary bone. This is evidence that these specimens of this northern taxon are not fully grown, yet are laying down LAGs during an ontogenetic stage when *Utahceratops* and *Kosmoceratops* are not.

Lines of arrested growth are laid down when an animal stops growing. The pauses that may form LAGs may be due to genetic rhythms that become coordinated with and reinforced by seasonal climatic change (Castanet et al., 1996; Chinsamy-Turan, 2005; Cerda and Chinsamy, 2012; Köhler et al. 2012) or formed in relation with photoperiod of the area where the animal lived (Castanet et al., 2004). If no lines of arrested growth are present, the animal might be younger than a year old. Alternatively, the animal might

have not slowed its growth enough for a line to be deposited. The presence of abundant remodeling in the cortex is good evidence for the latter option, in which case the animal grows rapidly early in life depositing primary tissue, dense primary osteons, dense osteocytes, and growth does not pause to form LAGs, and subsequently remodels this tissue as growth slows. This suggests that the potential latitudinal trend is not simply explained by differential sampling of ontogenetic stages across the different taxa.

There are several possible explanations for this observed latitudinal trend. First, because these taxa were largely endemic to their own basins (Lehman 1997; Sampson and Loewen, 2010; Sampson et al., 2010a; Gates et al., 2010), I could not sample the same species across the entire latitudinal range, so each species of ceratopsid could have a unique growth pattern that coincidentally matches latitudinal position. Second, these dinosaurs are found in penecontemporaneous, but not necessarily coeval strata (particularly *Pachyrhinosaurus* from the earliest Maastrichtian, which is ~3-5 million years younger), so these data could reflect temporal rather than geographic variation. Third, Campanian climate varied latitudinally across Laramidia (Wolfe and Upchurch, 1987; Lehman 1997), and this affected growth duration and/or growth rate. I cannot fully rule out the first two hypotheses, but the latitudinal climate hypothesis is most convincing. We know there was a latitudinal climate gradient throughout the Campanian (Wolfe and Upchurch, 1987; Lehman, 1997; Brinkman, 2003), and histological variation in ceratopsids appears to systematically follow this gradient. Furthermore, work with extant mammals indicates that the geographic range that the species occupies is directly correlated to the changes in climate and habitat associated with latitude (Emlen et al., 1986; Gates et al., 2010), and that these latitudinal changes are reflected in histology

(Klevezal, 1996; Köhler et al. 2012). More broadly, this hypothesis is consistent with recent evidence that Late Cretaceous dinosaur taxa were sorted by latitude (Mannion et al., 2012).

This interpretation is also consistent with a similar latitudinal signal described for the hadrosaurid ornithischian dinosaur *Edmontosaurus*, sampled from the Prince Creek Formation of the Alaskan North Slope and the Horseshoe Canyon Formation of Canada (Chinsamy et al., 2012). The polar samples showed many repeated growth cycles oscillating between reticular and circumferential canals, whereas these cycles were less numerous and more sporadic in the lower latitude sample from Canada (Chinsamy et al., 2012). In this case, both samples lacked LAGs. The LAGs observed in the Alaskan *Pachyrhinosaurus*, *Centrosaurus* from Alberta, and *Einosaurus* from Montana might reflect the responses of the bone reacting to environmental conditions, as proposed for the polar *Edmontosaurus*. An endotherm reacts to these extremes as resources are seasonally limited, and thus growth rate slows. The fact that *Utahceratops* and *Kosmoceratops* are from southern latitudes with a more equitable climate may cause the lack of LAGs because these taxa were able to sustain growth throughout the year.

An issue with this study is that I am comparing histology of centrosaurines from the north of Laramidia to the chasmosaurines from the south of Laramidia. To test the latitudinal climate hypothesis, chasmosaurines from the north, such as *Vagaceratops irvinensis*, the sister taxon of *Kosmoceratops*, or *Chasmosaurus* spp., as well as centrosaurines from the south, like the new Kaiparowits centrosaur (Getty et al., 2010; Lund, 2010), need to be histologically sampled. If the chasmosaurine from the north grows more similarly to the centrosaurines from the north (i.e., possessing LAGs) and the

centrosaurine from the south grows similarly to the chasmosaurines in the south (i.e., no LAGs present), then I can conclude that the latitudinal climate hypothesis for presence/absence and number of LAGs is well-supported.

Figure 19. A comparison of multiple species of ceratopsians analyzed histologically in this study. The first column illustrates possible growth marks in the bone tissue. The second column illustrates the difference in vascularity between the taxa studied. A. UMNH VP 16865.1 humerus from *Utahceratops gettyi*. Note the absence of true LAGs. B. Close up image of UMNH VP 16565.1. C. UMNH VP 17000 femur from *Kosmoceratops richardsoni*. Note the absence of true LAGs. D. Close up image of the microstructure of UMNH VP 17000. E. TMP 66.10.36 tibia from *Centrosaurus apertus*. Note the true LAGs, ~5. F. Close up image of TMP 66.10.36 tibia. G. "Un-numbered specimen" of the femur of *Protoceratops andrewsi*. Note the true LAGs present. H. Close up of "un-numbered specimen" of the femur of *Protoceratops andrewsi*. I. PIN 698/1977 femur of *Psittacosaurus mongoliensis*. Note the true LAGs present. J. Close up of PIN 698/1977 femur. Note the radially oriented vascular canals.

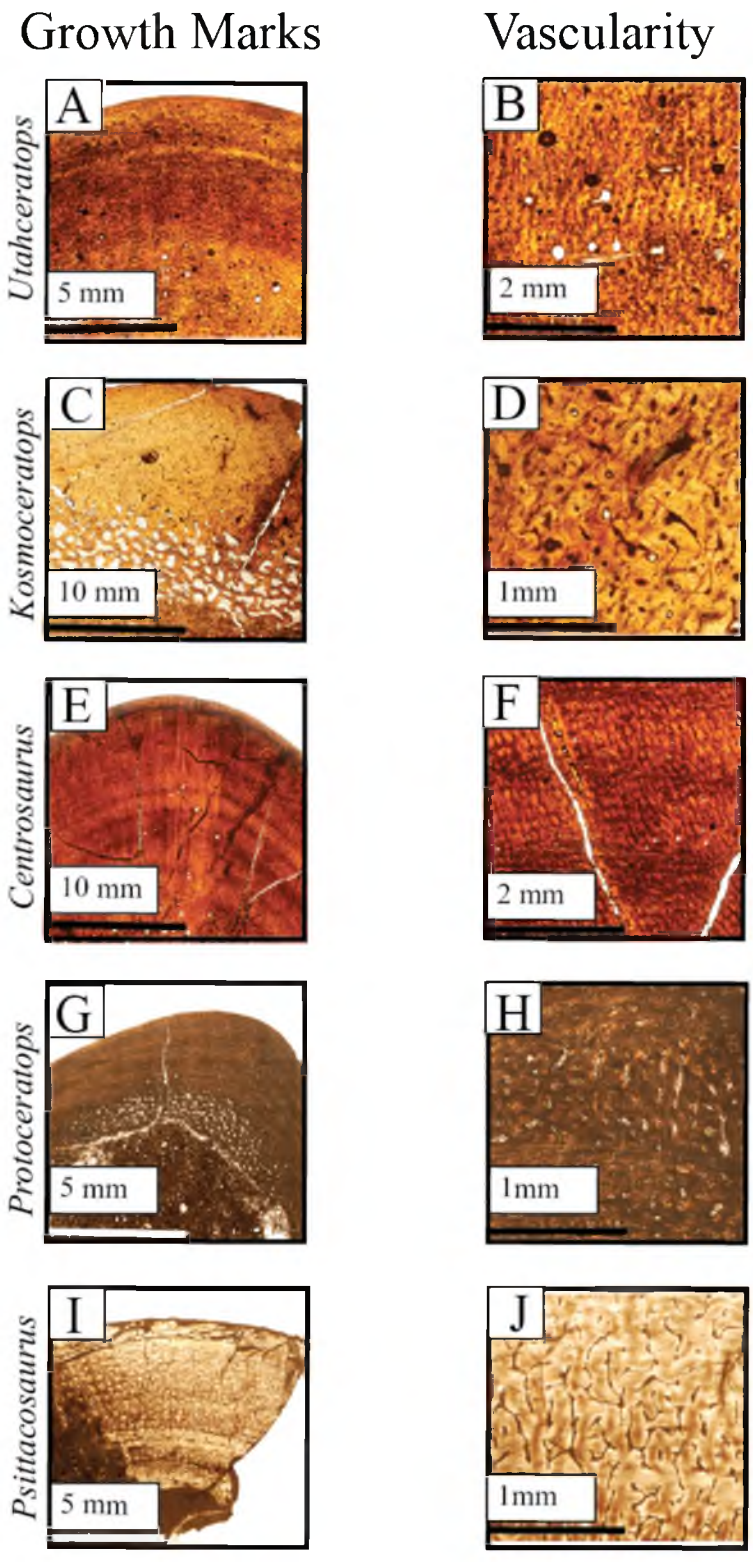
Growth Marks
Vascularity
Utahceratops
A
5 mm
B
2 mm
Kosmoceratops
C
10 mm
D
1mm
Centrosaurus
E
10 mm
F
2 mm
Protoceratops
G
5 mm
H
1mm
Psittacosaurus
I
5 mm
J
1mm

Figure 20. A paleogeographic map of Laramidia and Appalachia modified after Blakey, 2009. The orange star indicates the location of *Pachyrhinosaurus perotorum*, the red star indicates the location of *Centrosaurus apertus*, the green star indicated the location of *Einiosaurus procurvicornis* and the yellow star indicates the location of *Utahceratops gettyi* and *Kosmoceratops richardsoni.*


Pachyrhinosaurus perotorum
Maximum LAGs = 18
Centrosaurus apertus
Maximum LAGs = 7
Einiosaurus procurvicornis
Maximum LAGs = 5
LARAMIDIA
APPALACHIA
Utahceratops gettyi &
Kosmoceratops richardsoni
Maximum LAGs = 0

Figure 21. A. Graph of the femora of the ceratopsians that have been histologically sampled. The number of LAGs is plotted against the midshaft circumference. Note that the Utah taxa are on the x-axis having no LAGs. Note *Pachyrhinosaurus* is an outlier because of the 18 growth zones present. B. Graph of the tibiae of ceratopsians that have been histologically studied. Note the Utah forms are on the x-axis. Not that the small, basal ceratopsians *(Protoceratops* and *Psittacosaurus*) are closer to the y-axis than the larger ceratopsians are.

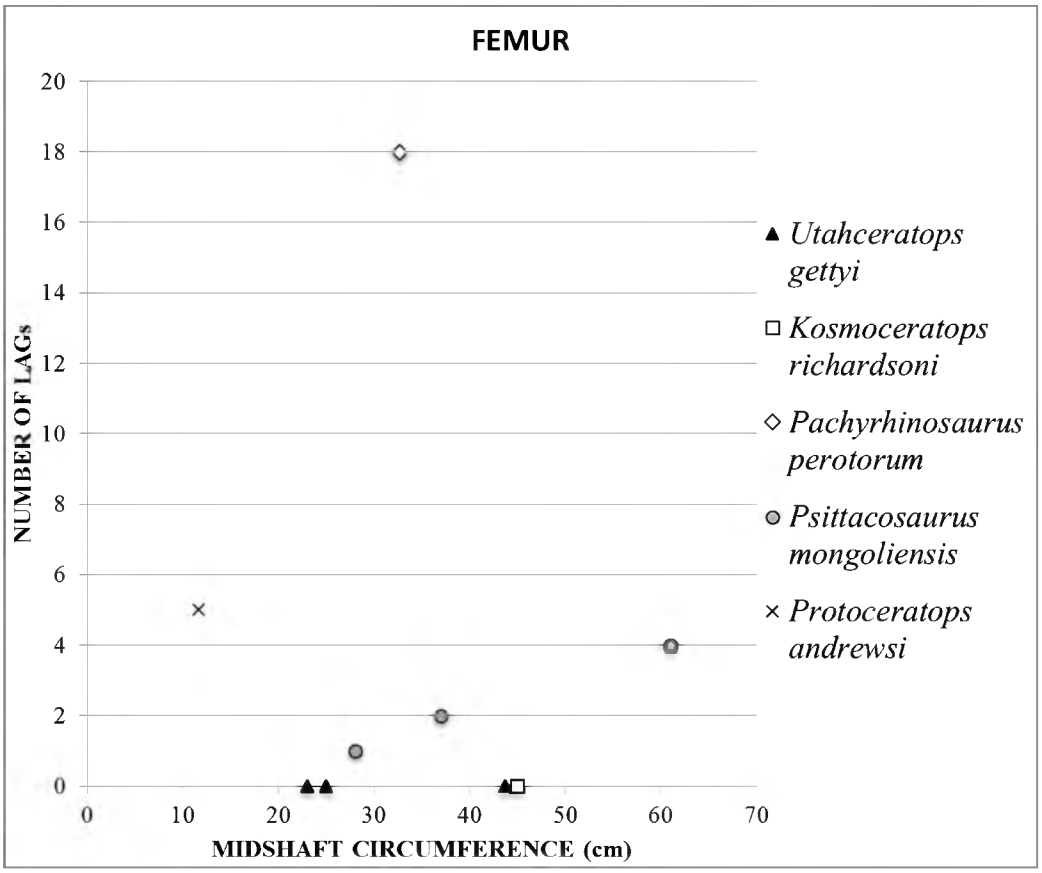
FEMUR
NUMBER OF LAGs
MIDSHAFT CIRCUMFERENCE (cm)
0
2
4
6
8
10
12
14
16
18
20
0
10
20
30
40
50
60
70
Utahceratops gettyi
Kosmoceratops richardsoni
Pachyrhinosaurus perotorum
Psittacosaurus mongoliensis
Protoceratops andrewsi

A

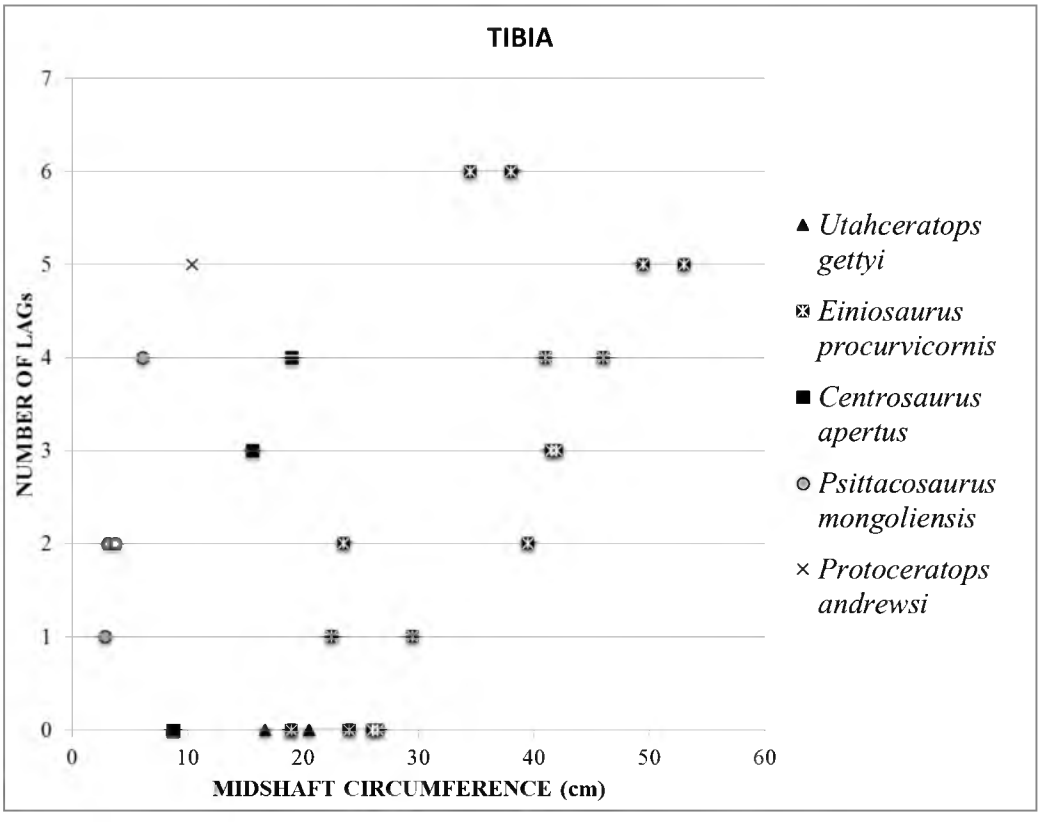
TIBIA
NUMBER OF LAGs
MIDSHAFT CIRCUMFERENCE (cm)
0
1
2
3
4
5
6
7
0
10
20
30
40
50
60
Utahceratops gettyi
Einiosaurus procurvicornis
Centrosaurus apertus
Psittacosaurus mongoliensis
Protoceratops andrewsi

B

CONCLUSIONS

The histology of the chasmosaurine ceratopsid dinosaurs *Utahceratops* and *Kosmoceratops* indicates that these chasmosaurs grew rapidly. All of the elements sampled (e.g. femora, tibiae, humeri, ulnae, ribs and tendons) from both species exhibited dense vascularity. The density of the vascularity did not increase or decrease moving from the medullary to the periosteum. The vascular canals had a tendency to be larger nearer to the medullary cavity and smaller towards the periosteum. The presence of radial canals in both species is also supportive of a high growth rate, as is the high of the osteocytes in both *Utahceratops* and *Kosmoceratops*.

The bones from the articulated individual of *Utahceratops* (UMNH VP 20444.4 - femur, UMNH VP 20444.5 - tibia, UMNH VP 20444.1 - humerus, and UMNH VP 20444.2 - ulna) from UMNH VP locality 945 represent bones from a juvenile animal based on the low amount of remodeling and the maximum preserved lengths of these bones. The study elements from the disarticulated *Utahceratops* individual found at locality 945 (UMNH VP 20454.5 - femur, UMNH VP 20454.3 - tibia, UMNH VP 20454.8 - humerus, UMNH VP 20454.1 - ulna, UMNH VP 20454.7 - rib, and UMNH VP 20454.7 - tendon) all represent bones from a juvenile animal based on the bone tissue being dominated by longitudinal primary osteons, the low amount of remodeling and the maximum preserved lengths of these bone. The femur (UMNH VP 16860) as well as the limb shaft (UMNH VP 16861) from UMNH VP locality 942 are from adult individuals

(of *Utahceratops*) based on the high degree of remodeling and large size. The tibia (UMNH VP 16681), from the same locality, represents a smaller, subadult *Utahceratops* individual based on the presence of some simple and radial canals, and its smaller size. The elements that were sectioned from *Utahceratops* UMNH VP 12198 (femur, rib, and tendon) represent elements from an adult animal based on the osteocyte density and the large size. Femur fragments that were histologically studied from the holotype specimen of *Kosmoceratops* (UMNH VP 17000) as well as from another individual of *Kosmoceratops* (UMNH VP 21339) come from two adult individuals based on the secondary osteons that dominate the bone tissue. The indeterminate ceratopsid humerus (UMNH VP 16865.1) from UMNH VP locality 512 represents a bone from an subadult animal based on the bone tissue primarily consisting of secondary osteons, but also some primary osteons. The second indeterminate ceratopsid humerus (UMNH VP 19490) is also from a subadult individual based on similar characteristics to UMNH VP 16865.1. In sum, the bones sampled in this study represent a distribution of ontogenetic stages for *Utahceratops* and *Kosmoceratops*.

Compared to other sampled ceratopsian dinosaurs, *Utahceratops* and *Kosmoceratops* grew most similar to the ceratopsids *Centrosaurus apertus*, *Pachyrhinosaurus perotorum*, and *Einosaurus procurvicornis*, indicating similar growth strategies for these groups of large quadrupedal ceratopsians. It seems that the presence of dense osteocytes, and reticular and radially oriented vascular canals are rapid growth indicators shared by all sampled large ceratopsids. None of these large ceratopsians possess dense, lamellar, avascular bone tissue which ectothermic reptiles like crocodilians have. Furthermore, these ceratopsids posses bone microstructure similar to

those of extant mammals and birds, which suggests that these animals share the characteristic of an elevated metabolism. The earlier ceratopsians *Psittacosaurus mongoliensis* and *Protoceratops andrewsi* also share indicators of rapid growth and elevated metabolism with *Centrosaurus apertus*, *Einosaurus procurvicornis*, *Pachyrhinosaurus perotorum*, *Utahceratops gettyi*, and *Kosmoceratops richardsoni*, but their higher numbers of lines of arrested growth (LAGs), smaller size, and lower vascularity suggest they grew more slowly than large quadrupedal ceratopsids. Based on histological comparisons other dinosaurs, *Utahceratops* and *Kosmoceratops* appear to grow more similarly to large ornithopods like hadrosaurs and large theropods, compared to sauropods, thyreophorans, or small ornithopods.

LAGs were not observed in any of the bones sampled from *Utahceratops* and *Kosmoceratops*. This result was unexpected because all other sampled ceratopsians do deposit LAGs in limb elements of similar and even smaller size. There appears to be latitudinal pattern in number of LAGs in subadult/adult individuals, with abundance decreasing towards lower latitudes. For example, *Pachyrhinosaurus* from Alaska preserves numerous (18) growth zones, *Centrosaurus* from Alberta preserves at most seven, *Einosaurus* from Montana possessing five and the southern forms from Utah, *Utahceratops* and *Kosmoceratops*, display no LAGs. This latitudinal trend may be due to the bone microstructure reflecting the latitudinal climate gradient known to exist during the Campanian.

REFERENCES

Amprino, R. 1967. Bone histophysiology. Guy's Hospital Report 116(2):51-69.

Bakker, R.T. 1972. Anatomical and ecological evidence of endothermy in dinosaurs. Nature, London 238:81-85.

Biewener, A. A. 2002. Future directions for the analysis of musculoskeletal design and locomotor performance. Journal of Morphology 252:38–51.

Brandau, D., and M. Getty. 2011. Discovery of a new chasmosaurine bonebed from the Kaiparowits Formation (Campanian) of southern Utah. Journal of Vertebrate Paleontology, Program and Abstracts, 2011, 76-77p.

Brandau, D., and R. Irmis. 2012. Comparative taphonomy of ceratopsid bonebeds: Implications of new data from southern Laramidia. Journal of Vertebrate Paleontology, Program and Abstracts, 2012 67-68p.

Brinkman, D.B. 2003. A review of nonmarine turtles from the Late Cretaceous of Alberta. Canadian Journal of Earth Science 40:557–571.

Brinkman, D.B., M.J. Ryan, and D.A. Eberth. 1998. The paleogeographic and stratigraphic distribution of ceratopsids (Ornithischia) in the upper Judith River Group of western Canada. Palaios 13:160-169.

Buffrénil, V. de. 1980. Mise en évidence de l'incidence des conditions de millieu sur la croissance de Crocodylus siamensis (Schneider, 1801) et valeur des marques de croissance squelettiques comme indicateur de l'age individuel. Archives de Zoologie Experimentale et Génerale 121:63-76.

Butler, R.J., P.M. Galton, L.B. Porro, L.M. Chiappe, D.M, Henderson, and G.M. Erickson. 2009. Lower limits of ornithischian dinosaur body size inferred from a new Upper Jurassic heterodontosaurid from North America. Proceedings of the Royal Society *B*: Biological Sciences.

Bybee, P.J., A.H. Lee. and E-T. Lamm. 2006. Sizing the Jurassic theropod dinosaur, *Allosaurus*: assessing growth strategy and evolution of ontogenetic scaling of limbs. Journal of Morphology 267:347-359.

Carrano, M. T. 2006. Body-size Evolution in the Dinosauria; Pp. 225-268 in M. T. Carrano, R. W. Blob, T. J. Gaudin and J. R. Wible (eds.), Amniote Paleobiology: Perspectives on the Evolution of Mammals, Birds, and Reptiles. University of Chicago Press, Chicago.

Carrier, D.R. 1983. Postnatal ontogeny of the musculoskeletal system in the black-tailed jack rabbit (Lepus californicus). Journal of Zoology 201:27–55.

Carrier, D.R. and L.R. Leon. 1990. Skeletal growth in the California gull (Larus californicus). Journal of Zoology 222:375–389.

Case, T.J. 1978. Speculations on the growth rate and reproduction of some dinosaurs. Paleobiology 4:320–328.

Castanet, J. 1978. Les marques de croissance osseuse comme indicateurs de l'age chez les lézards. Acta Zoologica Stockhom 59:35-48.

Castanet. J., F.J. Meunier, and A. de Ricqlès. 1977. L'enregistrement de la croissance cyclique par le tissu osseux chez les vertebres poïkilothermes: données comparatives et essai de synthèse. Bulletin biologique de la France et de la Belgique 61:183-202.

Castanet, J., H. Francillon-Vieillot, F.J. Meunier, and A. de Ricqlès.1993. Bone and Individual Aging; pp.245-283 in: B.K. Hall (ed.), Volume 7: Bone Growth - B. Boca Raton: CRC Press.

Castanet, J., K. Curry Rogers, J. Cubo, and J. Boisard. 2000. Periosteal bone growth rates in extant ratites (ostiche and emu). Implications for assessing growth in dinosaurs. Life Sciences 323:543-550.

Castanet, J., S. Croci, F. Aujard, M. Perret, J. Cubo, E. de Margerie. 2004. Lines of arrested growth in bone and age estimation in a small primate: *Microcebus murinus*. Journal of Zoology 263:31-39.

Cerda, I. A. and A. Chinsamy. 2012. Biological implications of the bone microstructure of the Late Cretaceous Ornithopod dinosaur *Gasparinisaura cincosaltensis*, Journal of Vertebrate Paleontology 31(2):355-386.

Chinsamy, A. 1990. Physiological implications of the bone histology of *Syntarsus rhodesiensis* (Saurischia: Theropoda). Palaeontologia Africana 27:77-82.

Chinsamy, A. 1993. Bone histology and growth trajectory of the prosauropod dinosaur *Massospondylus carinatus* Owen. Modern Geology 18:319-329.

Chinsamy, A. 1994. Dinosaur Bone Histology: Implications and Inferences; pp. 213-227 in G.D. Rosenberg and D. L. Wolberg (eds.), Dino Fest Proceedings of a Conference for the General Public. The Paleontological Society Special Publication No. 7.

Chinsamy, A. 1995. Ontogenetic changes in the bone histology of the Late Jurassic Ornithopod Dryosaurus lettowvorbecki. Journal of Vertebrate Paleontology, 15(1) :96-104.

Chinsamy-Turan, A. 2005. The Microstructure of Dinosaur Bone: Deciphering Biology with Fine-scale Techniques. Baltimore: The Johns Hopkins University Press, 195 pp.

Chinsamy, A. and J.H. Hurum. 2006. Bone microstructure and growth patterns of early mammals. Acta Paleontologica Polonica 51:325–338.

Chinsamy, A., D.B. Thomas, A.R. Tumarkin-Deratzian, and A.R. Fiorillo. 2012. Hadrosaurs were perennial polar residents. The Anatomical Record 295:610-614.

Cooper, L.N., A.H. Lee, M.L. Taper, and J.R. Horner. 2008. Relative growth rates of predator and pray dinosaurs reflect effects of predation. Proceedings of the Royal Society B 275, 2609-2615.

Cubo, J., F. Ponton, M. Laurin, E. de Margerie, and J. Castanet. 2005. Phylogenetic signal in bone microstructure of sauropsids. Systematic Biology 54(4):562-574.

Curry, K.A. 1999. Ontogenetic histology of *Apatosaurus* (Dinosauria: Sauropoda): new insights on growth rates and longevity. Journal of Vertebrate Paleontology 19:654-665.

Curry Rogers, K. and G.M. Erickson. 2005. Sauropod Histology; pp. 303-326 in K.A.C. Rogers and J.A. Wilson (eds), The Sauropods: Evolution and Paleobiology. University of California Press, Berkeley.

de Margerie, E., J. Cubo, and J. Castanet. 2002. Bone typology and growth rate: testing and quantifying 'Amprino's rule' in the mallard (*Anas platyrhynchos*). C.R. Biologies 325:221-230.

de Margerie, E., J-P. Robin, D. Verrier, J. Cubo, R. Groscolas, and J. Castanet. 2004. Assessing a relationship between bone microstructure and growth rate: a fluorescent labeling study in the king penguin chick (*Aptenodytes patagonicus*). Journal of Experimental Biology 207:869-879.

de Ricqlés, A.J. 1974. Evolution of endothermy: histological evidence. Evolutionary Theory 1:51-80.

de Ricqlés, A.J. 1976. On bone histology of fossil and living reptiles, with comments on its functional and evolutionary significance. A. d'A. Bellairs and C.B. Cox (eds.), Morphology and Biology of Reptiles. Linnean Soceity of London Symposium 3:123-150. Academic Press, London.

de Ricqlés, A.J. 1980. A Cold Look at the Warm-blooded Dinosaurs; pp.103-139 in R.D.K. Thomas and E.C. Olson (eds.), Boulder, Colo.: Published by Westview Press for the American Association for the Advancement of Science.

de Ricqlés, A.J. 1983. Cyclical growth in the long limb bones of a sauropod dinosaur. Acta Palaeontologica Polonica, 28:225.

de Ricqlés, A.J., F.J. Meunier, J. Castanet, and H. Francillon-Vieillot. 1991. Comparative Microstructure of Bone; pp. 1-78 in B.K. Hall (ed.),Volume 3: Bone Matrix and Bone Specific Products. Boston: CRC Press.

Dodson, P. 1993. Comparative craniology of the Ceratopsia. American Journal of Science 293A: 200–234.

Dodson, P., C.A. Forster, and S.D. Sampson. 2004. Ceratopsidae; pp. 494–513 in D.B.Weishampel, P. Dodson, and H. Osmólska (eds.), The Dinosauria. University of California Press, Berkeley.

Doube, M., M.M. Klosowski, Wiktorowicz-Conroy, A.M., Hutchinson, J.R. and Shefelbine, S.J. 2011. Trabecular bone scales allometrically in mammals and birds. Proceedings of the Royal Society *B*: Biological Sciences published online 9 March 2011.

Eaton, J.G. 1991. Biostratigraphic framework for Upper Cretaceous rocks of the Kaiparowits Plateau, southern Utah; pp. 47-63 in J. D. Nations and J. G. Eaton (eds.), Stratigraphy, Depositional Environments, and Sedimentary Tectonics of the Western Margin, Cretaceous Western Interior Seaway. Geological Society of America Special Publication 260.

Eaton, J.G., 1999. Vertebrate paleontology of the Paunsaugunt Plateau, upper Cretaceous, southwestern Utah. Utah Geological Survey.

Eberth, D.A., and A.P. Hamblin. 1993. Tectonic, stratigraphic and sedimentologic significance of a regional discontinuity in the upper Judith River Group (Belly River wedge) of southern Alberta, Saskatchewan, and northern Montana. Canadian Journal of Earth Sciences 30:174-200.

Emlen, J.T., M.J. DeJong, M.J. Jaeger, T.C. Moermond, K.A. Rusterholz, and R.P. White. 1986. Density trends and range boundary constraints of forest birds along a latitudinal gradient. Auk 103:791–803

Enlow, D. H. 1962. Functions of the Haversian systems. American Journal of Anatomy 110:268p.

Enlow, D.H. 1963. Principles of bone remodeling. An account of post-natal growth and remodeling processes in long bones and the mandible. Springfield: Charles C. Thomas. 131pp.

Enlow, D.H. and S.O. Brown. 1957. A comparative histological study of fossil and recent bone tissues. Part II. Texas Journal of Science 9:186-214.

Enlow, D.H. and S.O. Brown. 1958. A comparative histological study of fossil and recent bone tissues. Part III. Texas Journal of Science 10:212-217.

Erickson, G.M. and C.A. Brochu 1999. How the 'terror crocodile' grew so big. Nature 398:205-206.

Erickson, G.M. 2005. Assessing dinosaur growth patterns: a microscopic revolution. Trends in Ecology and Evolution 20:677-684.

Erickson, G.M., and T.A. Tumanova. 2000. Growth curve of *Psittacosaurus mongoliensis* Osborn (Ceratopsia: Psittacosauridae) inferred from long bone histology. Zoological Journal of the Linnean Society, v 130: 551-56.

Erickson, G.M. and P.S. Druckenmiller. 2011. Longevity and growth rate estimates for a polar dinosaur: a *Pachyrhinosaurus* (Dinosauria: Neoceratopsia) specimen from the North Slope of Alaska showing a complete developmental record. Historical Biology 1-8p.

Erickson, G. M., K. Curry-Rogers, and S.A.Yerby. 2001. Dinosaur growth patterns and rapid avian growth rates. Nature 412:429–433.

Erickson, G. M., P.J. Makovicky, P.J. Currie, M.A. Norell, S.A. Yerby, and C.A. Brochu. 2004. Gigantism and comparative life-history parameters of tyrannosaurid dinosaurs. Nature 430:772–775.

Erickson, G.M., P.J. Makovicky, B.D. Inouye, C. Zhou,and K. Gao. 2009. A life table for *Psittacosaurus lujiatunensis*: Initial insights into Ornithischian dinosaur population biology. The Anatomical Record 292:1514-1521.

Farke, A.A. 2011. Anatomy and taxonomic status of the chasmosaurine ceratopsian *Nedoceratops hateri* from the Upper Cretaceous Lance Formation of Wyoming, U.S.A. PLoS ONE January 2011 Volume 6 Issue 1 e16196.

Farlow, J.O. 1987. Speculations about the diet and digestive physiology of herbivorous dinosaurs. Paleobiology, Vol.13, No.1 (Winter, 1987), 60-72p.

Fassett, J.E., and M.B. Steiner. 1997. Precise age of C33N-C32R magnetic-polarity reversal, San Juan Basin, New Mexico and Colorado. New Mexico Geological Society Guidebook 48:239-247.

Ferguson, M.W.J., L.S. Honig, P. Bringas Jr., and H. C. Slavkin. 1982. In vivo and in vitro development of first branchial arch derivatives in Alligator mississippiensis; pp. 275-286 in A. D. Dixon and B. Sarnat (eds.), Factors and Mechanisms Influencing Bone Growth. Alan R. Liss Incorporated, New York.

Fiorillo, A.R. and R.S. Tykoski. 2012. A new species of the centrosaurine ceratopsid *Pachyrhinosaurus* from the North Slope (Prince Creek Formation: Maastrichtian) of Alaska. Acta Palaeontologica Polonica 57(3):561.

Foster, J. R., A. L. Titus, G. F. Winterfeld, M. C. Hayden, and A. H. Hamblin. 2001. Paleontological survey of the Grand Staircase-Escalante National Monument, Garfield and Kane counties, Utah. Utah Geological Survey Special Study 99:1-98.

Fowler, D. 2011. Reassessing ceratopsid diversity using unified frames of reference. Journal of Vertebrate Paleontology 31(3):111

Francillon-Vieillot, H., V. de Buffrénil, J. Castanet, J. Geraudie, F.J. Meunier, J.Y. Sire, L. Zylberberg, A.J. de Ricqlès. 1990. Microstructure and mineralization of vertebrate skeletal tissues; pp. 471-548 in J.G. Carter (ed.), Skeletal Biomineralization: Patterns, Processes and Evolutionary Trends. New York: Van Nostrand Reinhold.

Gates, T. A., S.D. Sampson, L.E. Zanno, E.M. Roberts, J.G. Eaton, R.L. Nydam, J.H. Hutchison, J.A. Smith, M.A. Loewen, and M.A. Getty. 2010. Biogeography of terrestrial and freshwater vertebrates from the Late Cretaceous (Campanian) Western Interior of North America. Palaeogeography, Palaeoclimatology, Palaeoecology 291:371-387.

Gates, T.A., and S.D. Sampson. 2007. A new species of Gryposaurus (Dinosauria: Hadrosauridae) from the Upper Campanian Kaiparowits Formation of Utah. Zoological Journal of the Linnean Society 151:351–376.

Getty, M. A., M.A. Loewen, E.M. Roberts, A.L. Titus, and S.D. Sampson. 2010. Taphonomy of horned dinosaurs (Ornithischia: Ceratopsidae) from the late Campanian Kaiparowits Formation, Grand Staircase-Escalante National Monument, Utah; pp. 478-494 in M. J. Ryan, B. J. Chinnery-Allgeier, and D. A. Eberth (eds.), New Perspectives on Horned Dinosaurs. Indiana University Press, Bloomington.

Goldstrand, P.M. 1990. Stratigraphy and paleogeography of Late Cretaceous and Early Tertiary rocks of southwest Utah: Utah Geological and Mineral Survey Miscellaneous Publication MP90-2:58p.

Goldstrand, P.M. 1991. Tectonostratigraphy, petrology, and paleogeography of Upper Cretaceous to Eocene rocks of southwest Utah. Ph.D dissertation, University of Nevada, Reno, Nevada, 205 pp.

Goldstrand, P.M. 1992. Evolution of the Late Cretaceous and Early Tertiary basins of southwest Utah based on clastic petrology. Journal of Sedimentary Petrology 62:495–507.

Goodwin, M.B., and A.L. Deino. 1989. The first radiometric ages from the Judith River Formation (Upper Cretaceous), Hill County, Montana. Canadian Journal of Earth Sciences 26:1384-1391.

Heinrich W-D. 1999. The taphonomy of dinosaurs from the Upper Jurassic of Tendaguru (Tanzania) based on field sketches of the German Tendaguru Expedition (1909–1913). Mitteilungen aus dem Museum für Naturkunde in Berlin, Geowissenschaftliche Reihe 2:25–61.

Horner, J.R., and M.B. Goodwin. 2008. Ontogeny of cranial epi-ossifications in *Triceratops*. Journal of Vertebrate Paleontology 28:134-144.

Horner, J.R., and K. Padian. 2004. Age and growth dynamics of *Tyrannosaurus rex*. Proceedings of the Royal Society London B 271:1875-1880.

Horner, J.R., A.J. de Ricqlés, and K. Padian. 1999. Variation in dinosaur skeletochronology indicators: implications for age assessment and physiology. Paleobiology 25:295–304.

Horner, J.R., A.J. de Ricqlés, and K. Padian. 2000. Long bone histology of the hadrosaurid dinosaur *Maiasaura peeblesorum*: Growth dynamics and physiology based on an ontogenic series of skeletal elements. Journal of Vertebrate Paleontology 20(1):115-129.

Horner, J.R. A.J. de Ricqlés, K. Padian, and R.D. Scheetz. 2009. Comparative long bone histology and growth of the "Hypsilophodontid" dinosaurs *Orodromerus makelai*, *Dryosaurus altus*, and *Tenontosaurus tillettii* (Ornythlschla: Euornithopoda). Journal of Vertebrate Paleontology 29(3):734-747.

Hübner, T.R. 2012. Bone histology in *Dysalotosaurus lettowvorbecki* (Ornithischia: Iguanodontia) - Variation, growth, and implications. PLoS ONE 7(1): e29958.

Irmis, R. B., J. H. Hutchison, J. J. W. Sertich, and A. L. Titus. In press. Crocodyliforms from the Late Cretaceous of Grand Staircase-Escalante National Monument and vicinity, southern Utah, U.S.A.; pp. in A. L. Titus and M. A. Loewen (eds.), At the Top of the Grand Staircase: The Late Cretaceous of Southern Utah. Indiana University Press, Bloomington.

Jinnah ZA, E.M. Roberts, A.L. Deino, J.S. Larsen, P.K. Link. 2009. New 40Ar-39Ar and detrital zircon U-Pb ages for the Upper Cretaceous Wahweap and Kaiparowits formations on the Kaiparowits Plateau, Utah: Implications for regional correlation, provenance, and biostratigraphy. Cretaceous Research 30 (2009) 287-299p.

Johnson, R. 1977. Size independent criteria for estimating relative age and the relationships among growth parameters in a group of fossil reptiles (Reptilia: Ichthyosauria). Canadian Journal of Earth Sciences 14:1916-1924.

Kauffman, E.G. 1984. Paleobiogeography and evolutionary response dynamic in the Cretaceous Western Interior Seaway of North America. Geological Association of Canada Special Paper 27:273-306.

Klein, N., and P.M. Sander. 2007. Bone histology and growth of the prosauropod dinosaur *Plateosaurus engelhardti* von Meyer, 1837 from the Norian bonebeds of Trossingen (Germany) and Frick (Switzerland). Special Papers in Palaeontology 77:169-206.

Klein, N. and P.M. Sander. 2008. Ontogenetic stages in the long bone histology of sauropod dinosaurs. Paleobiology, 34(2):247-263.

Klevezal, G.A. 1996. Recording structures of mammals: Determination of age and reconstruction of life history. A.A Balkema/Rotterday/Brookfield.

Knoll, F., K. Padian, and A. de Ricqlés. 2010. Ontogenetic change and adult body size of the early ornithischian dinosaur *Lesothosaurus diagnosticus*: Implications for basal ornithischian taxonomy. Gondwana Research 17:171-179.

Köhler, M., N. Marin-Moratalla, X. Jordana, and R. Aanes. 2012. Seasonal bone growth and physiology in endotherms shed light on dinosaur physiology. Doi:10.1038/nature11264.

Lambe, L.M. 1915. On *Eoceratops canadensis*, gen. nov., with remarks on other genera of Cretaceous horned dinosaurs. Canadian Geological Survey, Museum Bulletin No. 12., Geology Series No. 24:1-49.

Lawton, T.F., S.L. Pollock, and R.A.J. Robinson. 2003. Integrating sandstone petrology and nonmarine sequence stratigraphy: Application to the Late Cretaceous fluvial systems of southwestern Utah, U.S.A. Journal of Sedimentary Research 73:389–406.

Lee, A.H. 2006. Evolution of rapid limb growth and vascular canal organization in ceratopsian dinosaurs. Journal of Vertebrate Paleontology 26(3):89A.

Lee, A.H. 2007a. Interplay between growth and mechanics in the evolution of bone microstructure in dinosaurs. Ph.D. dissertation, University of California, Berkeley, Berkeley, California, 210 pp.

Lee, A.H. 2007b. Bone microstructure reflects evolution of large size in horned dinosaurs. Microscopy Society of America 13(Suppl 2).

Lee, A.H. 2007c. How Centrosaurus (and other ceratopsians) grew to large size. Paper presented at: Ceratopsian symposium, Royal Tyrrell Museum of Palaeontology. Abstracts Volume; Drumheller, AB.

Lee, A. H., and S. Werning. 2008. Sexual maturity in growing dinosaurs does not fit reptilian growth models. PNAS V 105, no. 2,582-587p.

Lehman, T. M. 1997. Late Campanian dinosaur biogeography in the western interior of North America; pp. 223-240 in D. L. Wolberg, E. Stump, and G. D. Rosenburg (eds.), Dinofest International Proceedings. Academy of Natural Sciences, Philadelphia.

Lehman, T. M. 2001. Late Cretaceous dinosaur provinciality; pp. 310-328 in D. H. Tanke, K. Carpenter, and M. W. Skrepnick (eds.), Mesozoic Vertebrate Life: New Research Inspired by the Paleontology of Philip J. Currie. Indiana University Press, Bloomington.

Levitt, C.G. 2011. Bone histology and growth of chasmosaurine ceratopsid dinosaurs from the Campanian Kaiparowits Formation, southern Utah. Journal of Vertebrate Paleontology, Program and Abstract, 2011 143pp.

Little, W.W. 1995. The influence of tectonics and eustacy on alluvial architecture, middle Coniacian through Campanian strata of the Kaiparowits Basin, Utah. Ph.D. dissertation, University of Colorado, Boulder, 328 pp.

Loewen, M.A., S.D. Sampson, E.K. Lund, A.A. Farke, M.C. Aguillón-Martínez, C.A. De Leon, R.A. Rodríguez-de la rosa, M.A. Getty, and D.A. Eberth. 2010. Horned dinosaurs (Ornithischia: Ceratopsidae) from the Upper Cretaceous (Campanian) Cerro del Pueblo Formation, Coahuila, Mexico. pp. 99-116 in M.J. Ryan, B.J. Chinnery-Allgeier, and D.A. Eberth (eds.), New Perspectives on Horned Dinosaurs. Indiana University Press, Bloomington and Indianapolis.

Longrich, N.R., and D.J. Field. 2012. *Torosaurus* is not *Triceratops*: Ontogeny in chasmosaurine ceratopsids as a case study in dinosaur taxonomy. PLoS ONE February 2012 Volume 7 Issue 2 e32623.

Lund, E.K. 2010. *Nasutuceratops titusi*, A new basal centrosaurine dinosaur (Ornithischia: Ceratopsidae) from the upper cretaceous Kaiparowits Formation, Southern Utah. M.S. thesis, University of Utah, Salt Lake City, Utah, 172pp.

Maidment, S.C.R., and P.M. Barrett. 2011. A new specimen of *Chasmosaurus belli* (Ornithischia: Ceratopsidae), a revision of the genus, and the utility of postcrania in the taxonomy and systematics of ceratopsid dinosaurs. Zootaxa 2963:1-47p.

Main, R.P., and A.A. Biewener. 2006. *In vivo* bone strain and ontogenetic growth patterns in relation to life-history strategies and performance in two vertebrate taxa: goats and emu. Physiological and Biochemical Zoology 79:57-72.

Makovicky, P.J., R.W. Sadleir, P. Dodson, G.M. Erickson, and M.A. Norell. 2007. Life history of *Protoceratops andrewsi* from Bayn Zag, Mongolia. Journal of Vertebrate Paleontology 27:109A.

Mannion, P., O. Upchurch, R. Mateus, N. Barnes, and M.E.H. Jones. 2012. New information on the anatomy and systematic position of Dinheirosaurus lourinhanensis (Sauropoda: Diplodocoidea) from the Late Jurassic of Portugal, with a review of European diplodocoids. Journal of Systematic Palaeontology 10(3):521-551

Ostrom, J.H. 1978. The evidence for endothermy in dinosaurs; pp. 15-54 in R.D.K Thomas and E.C. Olson (eds.), A cold look at the warm-blooded dinosaurs. Westview Press.

Padian, K., A.J. de Ricqlès, and J.R. Horner. 2001. Dinosaurian growth rates and bird origins. Nature 412:405-408.

Padian, K., J. R. Horner, and A. J. de Ricqlés. 2004. Growth in small dinosaurs and pterosaurs: the evolution of archosaurian growth strategies. Journal of Vertebrate Paleontology 24:555–571.

Pascal, M. and J. Castanet. 1978. Methodes de détermination de l/age chez le chat Haret des iles Kerguelen. Terre et Vie 32: 529-555.

Peabody, F.E. 1961. Annual growth zones in living and fossil vertebrates. Journal of Morphology 108:11-62.

Redelstorff, R. and P.M. Sander.2009. Long and gridle bone histology of *Stegosaurus*: Implications for growth and life history. Journal of Vertebrate Paleontology 29(4):1087-1099.

Reizner, J.A. 2010. An ontogenetic series and population histology of the ceratopsid dinosaur *Einiosaurus procurvicornis*. M.S. thesis, Montana State University, Bozeman, Montana, 109 pp.

Rimblot-Baly, E., A. de Ricqlés, and L. Zylberberg. 1995. Analyse paléohistologique d'une serie de croissance partielle chez Lapparen-tosaurus madagascariensis (Jurassique Moyen): Essai sur la dynamique de croissance d'un dinosaure sauropode. Annales de Paléontologie 81:49-86. Sanchez-Herraiz, M. J., M. Est

Roberts, E.M., M.A. Chan, and S.D. Sampson. 2003. Taphonomic analysis of the Late Cretaceous Kaiparowits Formation in the Grand Staircase-Escalante National Monument, southern Utah. Geological Society of America Abstracts with Programs, 35(6):591A.

Roberts, E.M. 2007. Facies architecture and depositional environments of the Upper Cretaceous Kaiparowits Formation, southern Utah, Sedimentary Geology, 197:207-233.

Roberts, E.M., A.D. Deino, and M.A. Chan. 2005. 40Ar/39Ar age of the Kaiparowits Formation, southern Utah, and correlation of coeval strata and faunas along the margin of the Western Interior Basin: Cretaceous Research, 26:307-318.

Roberts, E. M., S. D. Sampson, A. Deino, and S. Bowring. In press. The Kaiparowits Formation: a remarkable record of Late Cretaceous terrestrial environments, ecosystems and evolution in western North America; pp. in A. L. Titus and M. A. Loewen (eds.), At the Top of the Grand Staircase: The Late Cretaceous of Southern Utah. Indiana University Press, Bloomington.

Roberts, L. N. R., and M.A. Kirschbaum.1995. Paleogeography of the Late Cretaceous of the Western Interior of middle North America - coal distribution and sediment accumulation. U.S. Geological Survey Professional Paper 1561:1-115.

Rogers, R.R., 1994. Nature and origin of through-going discontinuities in nonmarine foreland basin strata, Upper Cretaceous, Montana: implications for sequence analysis. Geology 22:1119-1122.

Rogers, R.R., C.C. Swisher III, J.R. Horner. 1993. 40Ar/39Ar age correlation of the nonmarine Two Medicine Formation (Upper Cretaceous), northwestern Montana, U.S.A. Canadian Journal of Earth Sciences 30:1066-1075.

Ryan, M. J., and A.P. Russell. 2001. The dinosaurs of Alberata (exclusive of Aves); pp. 279-297 in D. Tanke and K. Carpenter (eds.), Mesozoic Vertebrate Life: New Research Inspired by Paleontology of Philip J. Currie. Indiana University Press, Bloomington.

Sampson, S. D. 1997. Dinosaur combat and courtship; pp. 383–393 in J. O. Farlow and M. K. Brett-Surman (eds.), The Complete Dinosaur. Indiana University Press, Bloomington.

Sampson, S. D. 2009. Dinosaur Odyssey: Fossil Threads in a Web of Life. University of California Press.

Sampson, S.D., and M.A. Loewen. 2010. Unraveling a Radiation: A review of the diversity, stratigraphic distribution, biogeography, and evolution of horned dinosaurs (Ornithischia: Ceratopsidae); pp. 405-427 in M.J. Ryan, B.J. Chinnery-Allgeier, and D.A. Eberth (eds.), New Perspectives on Horned Dinosaurs. Indiana University Press, Bloomington and Indianapolis.

Sampson, S.D., M.A. Loewen, A.A. Farke, E.M. Roberts, C.A. Forster, J.A. Smith, and A.L. Titus. 2010. New horned dinosaurs from Utah provide evidence for intracontinental dinosaur endemism. PLoS One.

Sampson, S. D., T.A. Gates, E.M. Roberts, M.A. Getty, L. Zanno, A.L. Titus, M. A. Loewen, J.A. Smith, E.K. Lund, and J. Sertich. 2010. Grand Staircase-Escalante National Monument: a new and critical window into the world of dinosaurs; pp. 141-158, Learning from the Land: Grand Staircase-Escalante National Monument Science Symposium Proceedings. Bureau of Land Management, Cedar City.

Sander, P.M. 2000. Long bone histology of the Tendaguru sauropods: Implications for growth and biology. Paleobiology 26:466-488.

Sander, P. M., and N. Klein. 2005. Unexpected developmental plasticity in the life history of an early dinosaur. Science 310: 1800–1802.

Sander, P.M., and P. Andrássy. 2006. Lines of arrested growth and long bone histology in Pleistocene large mammals from Germany: What do they tell us about dinosaur physiology? Palaeontographica Abt. A, 277, Lfg. 1-6, 143-159.

Scannella, J.B., and J.R. Horner. 2010. *Torosaurus* Marsh, 1891, is *Triceratops* Marsh, 1889 (Ceratopsidae: Chasmosaurinae): Synonymy through ontogeny. Journal of Vertebrate Paleontology 30(4):1157-1168.

Scannella, J.B., and J.R. Horner. 2011. *'Nedoceratops'*: An example of a transitional morphology. PLoS ONE December 2011, Volume 6 Issue 12 e28705.

Schweitzer, M.H, and C.L. Marshall. 2001. A molecular model for the evolution of endothermy in the theropod-bird lineage. Journal of Experimental Zoology 291:317–338.

Swartz, S.M., A. Parker, and C. Huo. 1998. Theoretical and empirical scaling patterns and topological homology in bone trabeculae. The Journal of Experimental Biology 201:573-590.

Trueman, C. N., and D. M. Martill. 2002. The long-term survival of bone: The role of bioerosion. Archaeometry 44:371–382.

Werning, S. 2012. The ontogenetic osteohistology of *Tenontosaurus tilletti*. PLoS ONE 7(3): e33539.

White, P.D., D.E. Fastovsky, and P.M. Sheehan. 1998. Taphonomy and suggested structure of the dinosaurian assemblage of the Hell Creek Formation (Maastrichtian), eastern Montana and western North Dakota. Palaios 13:41-51.

Wieser W. 1994. Cost of growth in cells and organisms: general rules and comparative aspects. Biological Reviews 68**:**1–33.

Wolfe, J.A., and G.R. Upchurch Jr. 1987. North American nonmarine climates and vegetation during the Late Cretaceous. Palaeogeography, Palaeoclimatology, Palaeoecology 61:33–77.

Woodward, H.N. 2005. Bone histology of the sauropod dinosaur *Alamosaurus sanjuanensis* from the Javelina Formation, Big Bend National Park, Texas. M.S. thesis, Texas Tech University, Texas, 239 pp.

Woodward, H.N. and T.M. Lehman. 2009. Bone histology and microanatomy of *Alamosaurus sanjuanensis* (Sauropoda: Titanosauria) from the Maastrichtian of Big Bend National Park, Texas. Journal of Vertebrate Paleontology 29(3):807-821.

You, H.L. and P. Dodson. 2004. Basal Ceratopsia; pp. 478-493 in D. Weishampel, P. Dodson, and H. Osmólska (eds.), The Dinosauria, Second Edition. University of California Press, Berkeley.

Zanno, L.E., and S.D. Sampson. 2005. A new caenagnathid from the Upper Cretaceous Kaiparowits Formation, Grand Staircase-Escalante National Monument, Utah. Journal of Vertebrate Paleontology 25:897–904.